



**T.C.**  
**KAHRAMANMARAŞ SÜTÇÜ İMAM UNIVERSITY**  
**GRADUATE SCHOOL OF NATURAL AND APPLIED SCIENCES**

**SYNTHESIS, ANALYTICAL AND SPECTROSCOPIC  
CHARACTERIZATION OF NOVEL NANOPARTICLES  
/NANOPIGMENTS USING A MICROWAVE ASSISTED  
METHOD**

**Othman Abdulrahman HAMAD**

**MASTER THESIS**  
**DEPARTMENT OF BIOENGINEERING AND SCIENCES**

**KAHRAMANMARAŞ-TURKEY 2014**

**T.C.  
KAHRAMANMARAŞ SÜTÇÜ İMAM UNIVERSITY  
GRADUATE SCHOOL OF NATURAL AND APPLIED SCIENCES**

**SYNTHESIS, ANALYTICAL AND SPECTROSCOPIC  
CHARACTERIZATION OF NOVEL NANOPARTICLES  
/NANOPIGMENTS USING A MICROWAVE ASSISTED  
METHOD**

**Othman Abdulrahman HAMAD**

**MASTER THESIS  
DEPARTMENT OF BIOENGINEERING AND SCIENCES**

**KAHRAMANMARAŞ-TURKEY 2014**

M.Sc thesis entitled “SYNTHESIS, ANALYTICAL AND SPECTROSCOPIC CHARACTERIZATION OF NOVEL NANOPARTICLES /NANOPIGMENTS USING A MICROWAVE ASSISTED METHOD” and prepared by Othman Abdulrahman HAMAD, who is a student at Bioengineering and Sciences Department, Graduate School of Natural and Applied Sciences, Kahramanmaraş Sütçü İmam University, was certified by all the majority jury members, whose signatures are given below.

Assoc. Prof. Dr. Hüseyin KÖKSAL (Supervisor) .....

Department of Chemistry  
Kahramanmaraş Sütçü İmam University

Prof. Dr. Mehmet TÜMER (Member) .....

Department of Chemistry  
Kahramanmaraş Sütçü İmam University

Assoc. Prof. Dr. Mehmet Said BOZGEYİK (Member) .....

Department of Physics  
Kahramanmaraş Sütçü İmam University

I approve that the above signatures related to the members.

Prof. Dr. M. Hakkı ALMA .....

Director of Graduate School

## **DECLARATION**

I hereby declare that all information in the thesis has been obtained and presented in accordance with academic rules and ethical conduct. I also declare that, as required by these rules and conduct, I have fully cited and referenced all the material and results that are not original to this work.

Othman Abdulrahman HAMAD

Note: the original and other sources used in this thesis, the Declaration, tables, figures and photographs showing the use of resources, subject to the provisions of Law No. 5846 on Intellectual and Artistic Works.

**SYNTHESIS, ANALYTICAL AND SPECTROSCOPIC CHARACTERIZATION  
OF NOVEL NANOPARTICLES /NANOPIGMENTS USING A MICROWAVE  
ASSISTED METHOD**

**(YÜKSEK LİSANS TEZİ)**

**Othman Abdulrahman HAMAD**

**ÖZ**

Bu tez çalışmamızda, yapısında üç metal bulunan nanoyapılar basit ve hızlı olan mikrodalga-yardımlı metod ile sentezlendi. Bu sentezlerde tiyoüre yakıt gibi kullanırken, etilen glikol (EG) yüzey gerilimini düşürücü ve indirgen olarak kullanıldı Bilinen eski yöntemlerle kıyaslandığında bu yöntem reaksiyon sürelerini kısaltmıştır. Oksitlerin morfolojisi, parça büyüklüğü ve mikroyapısı SEM ve XRD ile analiz edildi. Mikrodalga radyasyonuna maruz kalan  $Ru_{0.62}In_{0.38}Al_2O_3$  ve  $Ru_{0.77}Co_{0.23}In_2O_3$  parçacıkları, nano büyüklükte ve kübik fazda elde edildi. Nanoparçacıkların ortalama büyüklükleri 100 nm'den düşüktür. FT-IR çalışmaları, metal-oksijen ve metal-oksijen-metal bağlarının oluşumunu doğrulamaktadır.  $Ru_{0.77}Co_{0.23}In_2O_3$  oksidinin XRD ve SEM sonuçları bu bileşiğin nano olduğunu ve yüksek kristalin ve küre-benzer yapıda olduğunu göstermektedir.  $Ru_{0.63}Co_{0.37}Al_2O_3$ ,  $Ru_{0.93}Ni_{0.07}Al_2O_3$  ve  $Ru_{0.54}Cu_{0.46}Al_2O_3$  parçacıklarının çiçek-tipli yapısı elde edildi. Genel olarak, elde edilen ortalama kristal büyüklükleri 41-94 nm arasındadır. Sentezlenen  $Ru_xM_{1-x}In_2O_3$  (M: Co, Ni, Pd, Pt, Cu) yapısındaki nanoparçacıkların yapısı polykristalin ve küre olarak gözlenmiştir. EDX spektrumlarında üründe beklendiği gibi Ru, Fe, Co, Ni, Cu, Pd, Pt, In ve Al elementlerine rastlandı. Yüzey örtücülüğünde kullanılan ve yük etkilerini yok etmek amaçlı kullanılan altın EDX spektumlarında gözlemlendi. Öte yandan, N, S, P, Cl, vb. elementlere rastlanmayışı, sentezlenen nanoparçacıkların saf yapıda olduğunu göstermektedir.

**Key Words:** Nanoparçacıklar, nanopigmentler, mikrodalga-yardımlı, metal oksit

Kahramanmaraş Sütçü İmam Üniversitesi

Fen Bilimleri Enstitüsü

Biyomühendislik ve Bilimleri, Aralık, 2014

Danışman: Doç. Dr. Hüseyin KÖKSAL

Sayfa sayısı: 101

# SYNTHESIS, ANALYTICAL AND SPECTROSCOPIC CHARACTERIZATION OF NOVEL NANOPARTICLES /NANOPIGMENTS USING A MICROWAVE ASSISTED METHOD

(M.Sc. THESIS)

Othman Abdulrahman HAMAD

## ABSTRACT

In this thesis, three metal composed of nanostructures have been successfully synthesized by a simple and rapid microwave-assisted method using thiourea as the fuel and ethylene glycol (EG) as the surfactant. In comparison with conventional heating, microwave-assisted method shortens the reaction time. The morphology, particle size and microstructure were analyzed using SEM and XRD. Microwave irradiation has yielded nanosized cubic phase  $\text{Ru}_{0.62}\text{In}_{0.38}\text{Al}_2\text{O}_3$  and  $\text{Ru}_{0.77}\text{Co}_{0.23}\text{In}_2\text{O}_3$  particles. The mean grain size of the nanoparticles less than 100 nm FT-IR studies confirms the presence of metal–oxygen and metal-oxygen-metal bond. XRD and SEM of the synthesized nanoparticles show that the as prepared  $\text{Ru}_{0.77}\text{Co}_{0.23}\text{In}_2\text{O}_3$  has high crystallinity and sphere-like shape. Flower shape  $\text{Ru}_{0.63}\text{Co}_{0.37}\text{Al}_2\text{O}_3$ ,  $\text{Ru}_{0.93}\text{Ni}_{0.07}\text{Al}_2\text{O}_3$  and  $\text{Ru}_{0.54}\text{Cu}_{0.46}\text{Al}_2\text{O}_3$  particles were obtained. Generally, the crystallite sizes were found in the range of 41-94 nm. The synthesized  $\text{Ru}_x\text{M}_{1-x}\text{In}_2\text{O}_3$  architectures (M: Co, Ni, Pd, Pt, Cu) were found to be polycrystalline and spherical in shape. The EDX analysis indicated that the elements of Ru, Fe, Co, Ni, Cu, Pd, Pt, In and Al existed in the products. The surface treatment of spray gold for elimination of charged effects were responsible for the signals of gold in the EDX analysis of the products. In other words, no impurities like N, S, P, Cl, etc. were detected except for Ru, Fe, Co, Ni, Cu, Pd, Pt, In and Al elements, indicating the nanoparticles were pure.

**Key Words:** Nanoparticles, nanopigments, microwave-assisted, metal oxide

Kahramanmaraş Sütçü İmam University  
Graduate School of Natural and Applied Sciences  
Department of Bioengineering and Sciences, December, 2014

Supervisor: Assoc. Prof. Dr. Hüseyin KÖKSAL  
Page number: 101

# SYNTHESIS, ANALYTICAL AND SPECTROSCOPIC CHARACTERIZATION OF NOVEL NANOPARTICLES /NANOPIGMENTS USING A MICROWAVE ASSISTED METHOD

(YÜKSEK LİSANS TEZİ)

## ÖZET

Küresel ve çiçek tipli  $Ru_xM_{1-x}Al_2O_3$  (M: Fe, Co, Ni, Cu, In) ve  $Ru_xM_{1-x}In_2O_3$  (M: Co, Ni, Pd, Pt, Cu) nanoparçacıklar/nanopigmentler, mikrodalga-yardımlı yöntemle sentezlendi. Kullanılan ham maddeler, analitik dereceli reaktifler olup ilave saflaştırma yapmadan kullanıldı. Bir özgün deney olan bu yöntemde,  $Ru_xM_{1-x}Al_2O_3$  genel formülündeki bileşik, 1 mmol  $RuCl_3.3H_2O$ , 2 mmol of metal tuzları (M), 4 mmol alüminyum ve indiyum tuzları azar miktarlardaki deiyonize sularda çözülerek, teflon kapaklı 50 ml'lik tüpte el ile sallanarak karıştırıldı, bu çözeltinin üzerine 1 mmol tiyoüre ve 10 ml su ilave edilerek karıştırıldı. Çözeltinin rengi siyaha döndü. Tübün kalan kısmı üzerine 10 ml etilen glikol ilave edildi ve teflon kapak ile ağzı kapatıldı. Tüb mikrodalga içine yerleştirilerek, 600 W güçde, 1 saat radyasyona maruz bırakıldı. Ortam sıcaklığı 200 °C olarak ayarlandı. Reaksiyon süresi dolduktan sonra, tube oda sıcaklığında soğutuldu, siyah toz ürünler süzüldü. Defalarca kez deiyonize su ile yıkandıktan sonra bir kaç defada mutlak etanol ile safsızlıkları gidermek için yıkandı. Elde edilen toz ürün 10 saat boyunca 75 °C'de vakumlu etüvde kurutuldu. Elde edilen son ürünler  $Ru_xM_{1-x}Al_2O_3$  (M:Fe, Co, Ni, Cu, In) ve  $Ru_xM_{1-x}In_2O_3$  (M: , Co, Ni, Pd, Pt, Cu) nanoparçacıklar olarak elde edildi ve X-Işını Kırınımı (XRD, dalga boyu 0.154 nm Cu-K $\alpha$  radyasyonlu, 10-70 arasında değişen 2 $\theta$  açılı). Nanoparçacıkların morfolojisi Taramalı Elektron Mikroskobu (SEM) ile incelendi. Bileşiklerin içeriği ve safsızlığı Enerji Dağılımlı X-ışını spektroskopisi (EDX, 15 kV) tayin edildi. SEM ve EDX analizleri ZEISS Marker and EVO/LS10 Model adındaki cihazla gerçekleştirildi. Oksitlerin band titreşimleri Fourier Dönüşümlü İnfrared spaektrumu (FT-IR) ile kayd edildi. Bu cihaz Perkin Elmer Marker, Spectrum 400 Model, FT-IR spectrometre'dir.

# **SYNTHESIS, ANALYTICAL AND SPECTROSCOPIC CHARACTERIZATION OF NOVEL NANOPARTICLES /NANOPIGMENTS USING A MICROWAVE ASSISTED METHOD**

## **SUMMARY**

Spherical and flower type  $\text{Ru}_x\text{M}_{1-x}\text{Al}_2\text{O}_3$  (M: Fe, Co, Ni, Cu, In) and  $\text{Ru}_x\text{M}_{1-x}\text{In}_2\text{O}_3$  (M: Co, Ni, Pd, Pt, Cu) nanoparticles/nanopigments were prepared by a microwave-assisted process. All of the raw materials were of analytical grade reagents and were used without further purification. In a typical experimental procedure,  $\text{Ru}_x\text{M}_{1-x}\text{Al}_2\text{O}_3$  was prepared from a mixture including 1 mmol of  $\text{RuCl}_3 \cdot 3\text{H}_2\text{O}$ , 2 mmol of Metal salts (M), 4 mmol of Aluminum acetylacetonate ( $\text{Al}(\text{C}_5\text{H}_7\text{O}_2)_3$ ) and  $\text{InCl}_3$ , each substance dissolved in small amount of deionized water with vigorous stirring in microwave Teflon container tube (50 ml) and then thiourea (0.5 g, 1 mmol) was added to metal solution mixture and dissolved in addition of 10 ml deionized water to form a black-blue solution. At the end tube was filled with 10 ml of ethylene glycol (EG) and closed with teflon closer. The obtained mixture was located at the center of a microwave system and irradiated in constant power (600 W). The exposure time was 60 min at 200 °C. After the reaction was terminated, the product was allowed to cool to room temperature, the resulting dark black powders were rinsed and washed with deionized water and absolute ethanol several time until free from impurities. The precipitate was dried at 75 °C in a vacuum oven for 10 h to get the sample of type  $\text{Ru}_x\text{M}_{1-x}\text{Al}_2\text{O}_3$  (M: Fe, Co, Ni, Cu, In) and  $\text{Ru}_x\text{M}_{1-x}\text{In}_2\text{O}_3$  (M: , Co, Ni, Pd, Pt, Cu). Pure nanoparticles could be obtained and analyzed by X-ray Diffraction (XRD) using the Cu-K $\alpha$  radiation with 0.154 nm wavelength at 2 $\theta$  angle range from 10 to 70. The morphologies of the samples were observed by Scanning Electron Microscopy (SEM), using a Scanning electron microscopy (SEM) and Energy Dispersive X-Ray spectroscopy (EDX) employing an accelerating voltage of 15 Kv, same machine but different result characterizations (ZEISS Marker and EVO/LS10 Model). The Fourier Transform Infrared spectra (FT-IR) of the samples were recorded using a Perkin Elmer Marker, Spectrum 400 Model, FT-IR spectrometer.



## **ACKNOWLEDGEMENTS**

Of all, I want to express my best thanks to merciful Allah who have been giving me enough strength to perform and complete my scientific project successfully.

A special gratitude my Supervisor, Assoc. Prof. Dr. Hüseyin KÖKSAL, a true guide who supported and encouraged me during the entire tenure of the project. He inspired me to drive this thesis towards the path of glory and success.

I also express my thanks to head of department Prof.Dr. Mehmet TUMER, Assist. Prof. Dr. Serhan URUS and USKIM colleagues for their co-operation and valuable advice during the course work and my project work.

I would like to express my deepest appreciation to all those who provided me the possibility to complete this research.

Finally, special thanks to my mom and all my friends for their help.

Othman Abdulrahman HAMAD

## LIST OF CONTENTS

	<u>Page No</u>
ÖZ.....	I
ABSTRACT.....	Ii
ÖZET.....	Iii
SUMMARY.....	Iv
ACKNOWLEDGEMENTS.....	V
LIST OF CONTENTS.....	Vi
LIST OF ABBREVIATIONS.....	xi
LIST OF FIGURES.....	Xiii
LIST OF TABLES.....	Xv
1. INTRODUCTION.....	1
1.1. Overview.....	2
1.2. Historically nanoparticales/nanopigments.....	2
1.3. Methods of Nanoparticle Synthesis.....	3
1.4. Nanoparticles in Various Fields.....	6
1.5. Some words about NPs/nanopigments.....	7
1.5.1. Properties of nanoparticles.....	7
1.5.2. Motivation for Development of Nano.....	7
1.5.3. Size of Nanoparticles.....	7
1.5.4. Shape of Nanoparticles.....	8
1.5.5. Structure of Nanoparticles.....	9
1.6. Define Pigments.....	10
1.7. Overview pigments.....	11
1.8. Overview nanopigments.....	12
1.9. Define Microwave.....	13
1.10. Microwaves employer.....	13
1.11. Microwave utilize for organic and in organic materials.....	13
1.12. Some advantages of MW.....	15
2. LITERATURE REVIEW.....	17

2.1. Microwave-assisted synthesis of Ru nanoparticles .....	17
2.2. Microwave-assisted preparation of FeTiO <sub>3</sub> powders.....	17
2.3. Microwave assisted synthesis of Co <sub>3</sub> O <sub>4</sub> nanoparticles .....	18
2.4. Nano-crystalline Sm <sub>0.5</sub> Sr <sub>0.5</sub> Co(Fe)O <sub>3-δ</sub> perovskite oxides.....	19
2.5. NiFe <sub>2</sub> O <sub>4</sub> Nanoparticles Produced with Microwave-Assisted Combustion Method.....	20
2.6. Microwave-assisted rapid synthesis of alumina nanoparticles .....	21
2.7. Cerium zinc molybdate nano pigment by innovative ultrasound assisted approach.....	21
2.8.Synthesis of Zn <sub>0.7</sub> Ni <sub>0.3</sub> Fe <sub>2</sub> O <sub>4</sub> nanoparticles via microwave-assisted method.....	22
2.9. Microwave-assisted synthesis of CdS intercalated .....	23
2.10. Ni <sub>0.6</sub> Zn <sub>0.4</sub> Fe <sub>2</sub> O <sub>4</sub> nano-particles prepared by conventional hydrothermal method.....	24
2.11.Microwave-assisted synthesis of Ti <sub>1-x</sub> V <sub>x</sub> O <sub>2</sub> (x = 0.0 – 0.10) nanopowders.....	25
2.12. Zinc oxide nanostructures synthesized by rapid microwave irradiation methods.....	25
2.13. Flower-like Bi <sub>2</sub> WO <sub>6</sub> and Bi <sub>2</sub> O <sub>3</sub> -Bi <sub>2</sub> WO <sub>6</sub> composite by Microwave-assisted.....	26
2.14. Nanoparticles obtained by microwave-assisted oxidation technique.....	27
2.15 Synthesis of cadmium-doped copper oxide nanoparticles.....	29
3. MATERIAL AND METHOD.....	30
3.1. Chemical substance .....	30
3.2. Overview our work .....	33
3.3. Experimental .....	35
3.3.1. Synthesis of Ru <sub>0.4</sub> Fe <sub>0.6</sub> Al <sub>2</sub> O <sub>3</sub> nanoparticles.....	35
3.3.2. Synthesis of Ru <sub>0.63</sub> Co <sub>0.37</sub> Al <sub>2</sub> O <sub>3</sub> nanoparticles.....	36
3.3.3. Synthesis of Ru <sub>0.93</sub> Ni <sub>0.07</sub> Al <sub>2</sub> O <sub>3</sub> nanoparticles.....	36
3.3.4. Synthesis of Ru <sub>0.54</sub> Cu <sub>0.46</sub> Al <sub>2</sub> O <sub>3</sub> nanoparticles.....	37

3.3.5. Synthesis of $\text{Ru}_{0.62}\text{In}_{0.38}\text{Al}_2\text{O}_3$ nanoparticles.....	38
3.3.6. Synthesis of $\text{Ru}_{0.77}\text{Co}_{0.23}\text{In}_2\text{O}_3$ nanoparticles.....	38
3.3.7. Synthesis of $\text{Ru}_{0.65}\text{Ni}_{0.35}\text{In}_2\text{O}_3$ nanoparticles.....	39
3.3.8. Synthesis of $\text{Ru}_{0.92}\text{Pd}_{0.08}\text{In}_2\text{O}_3$ nanoparticles.....	40
3.3.9. Synthesis of $\text{Ru}_{0.54}\text{Pt}_{0.46}\text{In}_2\text{O}_3$ nanoparticles.....	40
3.3.10. Synthesis of $\text{Ru}_{0.56}\text{Cu}_{0.44}\text{In}_2\text{O}_3$ nanoparticles.....	41
4. RESULTS AND DISCUSSION.....	42
4.1. NPs of $\text{Ru}_{0.4}\text{Fe}_{0.6}\text{Al}_2\text{O}_3$ .....	42
4.1.1 SEM analysis of $\text{Ru}_{0.4}\text{Fe}_{0.6}\text{Al}_2\text{O}_3$ .....	42
4.1.2. EDX analysis of $\text{Ru}_{0.4}\text{Fe}_{0.6}\text{Al}_2\text{O}_3$ .....	44
4.1.3. XRD analysis of $\text{Ru}_{0.4}\text{Fe}_{0.6}\text{Al}_2\text{O}_3$ .....	45
4.1.4. FT-IR analysis of $\text{Ru}_{0.4}\text{Fe}_{0.6}\text{Al}_2\text{O}_3$ .....	45
4.2. NPs of $\text{Ru}_{0.63}\text{Co}_{0.37}\text{Al}_2\text{O}_3$ .....	47
4.2.1 SEM analysis of $\text{Ru}_{0.63}\text{Co}_{0.37}\text{Al}_2\text{O}_3$ .....	47
4.2.2. EDX analysis of $\text{Ru}_{0.63}\text{Co}_{0.37}\text{Al}_2\text{O}_3$ .....	49
4.2.3. XRD analysis of $\text{Ru}_{0.63}\text{Co}_{0.37}\text{Al}_2\text{O}_3$ .....	49
4.2.4. FT-IR analysis of $\text{Ru}_{0.63}\text{Co}_{0.37}\text{Al}_2\text{O}_3$ .....	50
4.3. NPs of $\text{Ru}_{0.93}\text{Ni}_{0.07}\text{Al}_2\text{O}_3$ .....	52
4.3.1. SEM analysis of $\text{Ru}_{0.93}\text{Ni}_{0.07}\text{Al}_2\text{O}_3$ .....	52
4.3.2. EDX analysis of $\text{Ru}_{0.93}\text{Ni}_{0.07}\text{Al}_2\text{O}_3$ .....	54
4.3.3. XRD analysis of $\text{Ru}_{0.93}\text{Ni}_{0.07}\text{Al}_2\text{O}_3$ .....	54
4.3.4. FT-IR analysis of $\text{Ru}_{0.93}\text{Ni}_{0.07}\text{Al}_2\text{O}_3$ .....	55
4.4. NPs of $\text{Ru}_{0.54}\text{Cu}_{0.46}\text{Al}_2\text{O}_3$ .....	57
4.4.1. SEM analysis of $\text{Ru}_{0.54}\text{Cu}_{0.46}\text{Al}_2\text{O}_3$ .....	57
4.4.2. EDX analysis of $\text{Ru}_{0.54}\text{Cu}_{0.46}\text{Al}_2\text{O}_3$ .....	59

4.4.3. XRD analysis of $\text{Ru}_{0.54}\text{Cu}_{0.46}\text{Al}_2\text{O}_3$ .....	59
4.4.4. FT-IR analysis of $\text{Ru}_{0.54}\text{Cu}_{0.46}\text{Al}_2\text{O}_3$ .....	60
4.5. NPs of $\text{Ru}_{0.62}\text{In}_{0.38}\text{Al}_2\text{O}_3$ .....	62
4.5.1. SEM analysis of $\text{Ru}_{0.62}\text{In}_{0.38}\text{Al}_2\text{O}_3$ .....	62
4.5.2. EDX analysis of $\text{Ru}_{0.62}\text{In}_{0.38}\text{Al}_2\text{O}_3$ .....	63
4.5.3. XRD analysis of $\text{Ru}_{0.62}\text{In}_{0.38}\text{Al}_2\text{O}_3$ .....	63
4.5.4. FT-IR analysis of $\text{Ru}_{0.62}\text{In}_{0.38}\text{Al}_2\text{O}_3$ .....	64
4.6. NPs of $\text{Ru}_{0.77}\text{Co}_{0.23}\text{In}_2\text{O}_3$ .....	66
4.6.1. SEM analysis of $\text{Ru}_{0.77}\text{Co}_{0.23}\text{In}_2\text{O}_3$ .....	66
4.6.2. EDX analysis of $\text{Ru}_{0.77}\text{Co}_{0.23}\text{In}_2\text{O}_3$ .....	67
4.6.3. XRD analysis of $\text{Ru}_{0.77}\text{Co}_{0.23}\text{In}_2\text{O}_3$ .....	68
4.6.4. FT-IR analysis of $\text{Ru}_{0.77}\text{Co}_{0.23}\text{In}_2\text{O}_3$ .....	69
4.7. NPs of $\text{Ru}_{0.65}\text{Ni}_{0.35}\text{In}_2\text{O}_3$ .....	71
4.7.1. SEM analysis of $\text{Ru}_{0.65}\text{Ni}_{0.35}\text{In}_2\text{O}_3$ .....	71
4.7.2. EDX analysis of $\text{Ru}_{0.65}\text{Ni}_{0.35}\text{In}_2\text{O}_3$ .....	72
4.7.3. XRD analysis of $\text{Ru}_{0.65}\text{Ni}_{0.35}\text{In}_2\text{O}_3$ .....	72
4.7.4. FT-IR analysis of $\text{Ru}_{0.65}\text{Ni}_{0.35}\text{In}_2\text{O}_3$ .....	73
4.8. NPs of $\text{Ru}_{0.92}\text{Pd}_{0.08}\text{In}_2\text{O}_3$ .....	74
4.8.1. SEM analysis of $\text{Ru}_{0.92}\text{Pd}_{0.08}\text{In}_2\text{O}_3$ .....	74
4.8.2. EDX analysis of $\text{Ru}_{0.92}\text{Pd}_{0.08}\text{In}_2\text{O}_3$ .....	76
4.8.3. XRD analysis of $\text{Ru}_{0.92}\text{Pd}_{0.08}\text{In}_2\text{O}_3$ .....	77
4.8.4. FT-IR analysis of $\text{Ru}_{0.92}\text{Pd}_{0.08}\text{In}_2\text{O}_3$ .....	78
4.9. NPs of $\text{Ru}_{0.54}\text{Pt}_{0.46}\text{In}_2\text{O}_3$ .....	80
4.9.1. SEM analysis of $\text{Ru}_{0.54}\text{Pt}_{0.46}\text{In}_2\text{O}_3$ .....	80

4.9.2. EDX analysis of $\text{Ru}_{0.54}\text{Pt}_{0.46}\text{In}_2\text{O}_3$ .....	81
4.9.3. XRD analysis of $\text{Ru}_{0.54}\text{Pt}_{0.46}\text{In}_2\text{O}_3$ .....	82
4.9.4. FT-IR analysis of $\text{Ru}_{0.54}\text{Pt}_{0.46}\text{In}_2\text{O}_3$ .....	83
4.10. NPs of $\text{Ru}_{0.54}\text{Pt}_{0.46}\text{In}_2\text{O}_3$ .....	85
4.10.1. SEM analysis of $\text{Ru}_{0.54}\text{Pt}_{0.46}\text{In}_2\text{O}_3$ .....	85
4.10.2. EDX analysis of $\text{Ru}_{0.54}\text{Pt}_{0.46}\text{In}_2\text{O}_3$ .....	86
4.10.3. XRD analysis of $\text{Ru}_{0.54}\text{Pt}_{0.46}\text{In}_2\text{O}_3$ .....	87
4.10.4. FT-IR analysis of $\text{Ru}_{0.54}\text{Pt}_{0.46}\text{In}_2\text{O}_3$ .....	88
5. CONCLUSION.....	90
REFERENCES.....	93
CURRICULUM VITAE.....	101

## LIST OF ABBREVIATIONS

<b>NPs:</b>	Nanoparticles.
<b>NPgs:</b>	Nanopigments.
<b>MW:</b>	Microwave.
<b>XRD:</b>	X-Ray Diffraction.
<b>SEM:</b>	Scanning Electron Microscopy.
<b>FTIR:</b>	Fourier Transform Infrared Spectroscopy.
<b>EDX</b>	Energy Dispersive X-Ray spectroscopy
<b>M:</b>	Metal.
<b>Ru:</b>	Ruthenium.
<b>Ni:</b>	Nickel.
<b>Co:</b>	Cobalt.
<b>Fe:</b>	Ferric or Ferrate.
<b>Cu:</b>	Copper.
<b>Y:</b>	Yttrium.
<b>Pt:</b>	Platinum.
<b>Pd:</b>	Palladium.
<b>In:</b>	Indium.
<b>Etc:</b>	Etcetera.
<b>H:</b>	Hour.
<b>°C:</b>	Degree Centigrade.
<b>NM:</b>	Nano Meter.
<b>NNI:</b>	National Nanotechnology Initiative.
<b>US</b>	United States
<b>AD:</b>	Architectural Digest.
<b>CVD:</b>	Chemical Vapour Deposition.
<b>S:</b>	Surface.
<b>V:</b>	Volume.
<b>Au:</b>	Gold
<b>Cl:</b>	Chloride
<b>K:</b>	Kelvin
<b>Fig:</b>	Figure
<b>PC:</b>	Phthalocyanine

<b>LED:</b>	Light Emitting Diodes
<b>Me:</b>	Meter
<b>GHz:</b>	Gigahertz
<b>MHz:</b>	Megahertz
<b>PEG:</b>	Poly Ethylene Glycol
<b>W:</b>	Watt
<b>TEG:</b>	Tetra Ethylene Glycol
<b>PVP:</b>	Poly Vinyl Pyrrolidone
<b>CATB:</b>	Cetyl Trimethyl Ammonium Bromide
<b>EG:</b>	Ethylene Glycol
<b>Min:</b>	Minute
<b>MA:</b>	Milli Ammeter
$\lambda$ :	Lambda
<b>CM:</b>	Centimeter
<b>%:</b>	Percentage
<b>W:</b>	Weight
<b>G:</b>	Gram
<b>M Mol:</b>	Milli Mole
<b>MI:</b>	Milli Liter
<b>P</b>	page



## LIST OF FIGURES

	<u>Page No</u>
Figure 1.1. Photographs of the famous Lycurgus cup which displays a different color.....	3
Figure 1.2 Typical synthetic methods for nanoparticles for the top-down and bottom-up approaches.....	4
Figure 1.3. Nanoparticles in a wide variety of different shapes and sizes.....	8
Figure 1.4. Schematic images of bimetal nanoparticles: alloy structure, core–shell structure, and heterojunction structure, of complex metal nanoparticles.....	10
Figure 1.5. Show world Consumption of Inorganic Color pigments.....	11
Figure 2.1. XRD pattern of the synthesized Ru NPs.....	17
Figure 2.2. SEM micrographs of FeTiO <sub>3</sub> samples.....	18
Figure 2.3. FT-IR spectrums of FeTiO <sub>3</sub> samples.....	18
Figure 2.4. (a) XRD pattern of Co <sub>3</sub> O <sub>4</sub> sample, (b) FTIR spectrum of Co <sub>3</sub> O <sub>4</sub> .....	19
Figure 2.5. Morphology of the SSC oxide precursor and the calcined powders.....	19
Figure 2.6. SEM images of NiFe <sub>2</sub> O <sub>4</sub> nanoparticles.....	20
Figure 2.7. X-ray diffraction pattern of NiFe <sub>2</sub> O <sub>4</sub> nanoparticles.....	20
Figure 2.8. SEM images of Al NP using tea leaves extract.....	21
Figure 2.9. FT-IR of Al NP using tea leaves extract.....	21
Figure 2.10. FT-IR pattern of the synthesized Ce <sub>2</sub> Zn <sub>3</sub> (MoO <sub>4</sub> ) <sub>6</sub> nanoparticles.....	22
Figure 2.11. XRD and line profile fitting of ferrite powder by microwave method.....	23
Figure 2.12. FT-IR spectrum of Zn <sub>0.7</sub> Ni <sub>0.3</sub> Fe <sub>2</sub> O <sub>4</sub> .....	23
Figure 2.13. SEM of (a) K <sub>4</sub> Nb <sub>6</sub> O <sub>17</sub> (b) mm-K <sub>4</sub> Nb <sub>6</sub> O <sub>17</sub> /CdS (c) CdS (d) M-K <sub>4</sub> Nb <sub>6</sub> O <sub>17</sub> .....	24
Figure 2.14. FT-IR spectra of Ni <sub>0.6</sub> Zn <sub>0.4</sub> Fe <sub>2</sub> O <sub>4</sub> ferrites.....	24
Figure 2.15. SEM graphs of Ni <sub>0.6</sub> Zn <sub>0.4</sub> Fe <sub>2</sub> O <sub>4</sub> ferrites.....	25
Figure 2.16. SEM images of TiO <sub>2</sub> .....	25
Figure 2.17. SEM images of synthesized ZnO nanostructures.....	26

Figure 2.18. XRD patterns of the synthesized ZnO nanostructures.....	26
Figure 2.19. SEM of products (a) 140 °C, (b) 150 °C, (c) 160 °C and (d) 170 °C .....	27
Figure 2.20. SEM images of NiO nanoparticles.....	28
Figure 2.21. XRD patterns of NiO nanoparticles.....	28
Figure 2.22. (a) FT-IR spectrum of $\beta$ -Ni(OH) <sub>2</sub> precursor and (c) final product (NiO).....	28
Figure 2.23. XRD spectrum of both pure and cadmium-doped CuO nanoparticles.....	29
Figure 2.24. SEM of pure CuO nanoparticles (1), cadmium-doped CuO NPs(2).....	29
Figure 3.1. Microwave used in synthesized.....	31
Figure 3.2. This FT-IR used for analysis.....	32
Figure 3.3. This XRD used for analysis.....	32
Figure 3.4. This SEM and EDX used for analysis.....	33
Figure 4.1a. SEM image of Ru <sub>0.4</sub> Fe <sub>0.6</sub> Al <sub>2</sub> O <sub>3</sub> nanoparticles prepared.....	43
Figure 4.1b. SEM image of Ru <sub>0.4</sub> Fe <sub>0.6</sub> Al <sub>2</sub> O <sub>3</sub> nanoparticles prepared.....	43
Figure 4.2. EDX spectrum of Ru <sub>0.4</sub> Fe <sub>0.6</sub> Al <sub>2</sub> O <sub>3</sub> nanoparticles.....	44
Figure 4.3. X-ray diffraction patterns of the Ru <sub>0.4</sub> Fe <sub>0.6</sub> Al <sub>2</sub> O <sub>3</sub> nanoparticles.....	45
Figure 4.4. The FT-IR spectra of Ru <sub>0.4</sub> Fe <sub>0.6</sub> Al <sub>2</sub> O <sub>3</sub> nanoparticles.....	46
Figure 4.5 a. SEM images of Ru <sub>0.63</sub> Co <sub>0.37</sub> Al <sub>2</sub> O <sub>3</sub> nanoparticles prepared.....	48
Figure 4.5 b. SEM images of Ru <sub>0.63</sub> Co <sub>0.37</sub> Al <sub>2</sub> O <sub>3</sub> nanoparticles prepared.....	48
Figure 4.6. EDAX spectrum of Ru <sub>0.63</sub> Co <sub>0.37</sub> Al <sub>2</sub> O <sub>3</sub> nanoparticles.....	49
Figure 4.7. X-ray diffraction patterns of the Ru <sub>0.63</sub> Co <sub>0.37</sub> Al <sub>2</sub> O <sub>3</sub> nano particles.....	50
Figure 4.8. The FT-IR spectra of Ru <sub>0.63</sub> Co <sub>0.37</sub> Al <sub>2</sub> O <sub>3</sub> nanoparticles.....	51
Figure 4.9a. SEM images of Ru <sub>0.63</sub> Co <sub>0.37</sub> Al <sub>2</sub> O <sub>3</sub> nanoparticles prepared.....	53
Figure 4.9b. SEM images of Ru <sub>0.93</sub> Ni <sub>0.07</sub> Al <sub>2</sub> O <sub>3</sub> nanoparticles prepared.....	53
Figure 4.10. EDX spectrum of Ru <sub>0.93</sub> Ni <sub>0.07</sub> Al <sub>2</sub> O <sub>3</sub> nanoparticles.....	54
Figure 4.11. X-ray diffraction patterns of the Ru <sub>0.93</sub> Ni <sub>0.07</sub> Al <sub>2</sub> O <sub>3</sub> nano- particles.....	55

Figure 4.12. The FT-IR spectra of $\text{Ru}_{0.93}\text{Ni}_{0.07}\text{Al}_2\text{O}_3$ nanoparticles.....	56
Figure 4.13a. SEM images of $\text{Ru}_{0.54}\text{Cu}_{0.46}\text{Al}_2\text{O}_3$ nanoparticles prepared.....	58
Figure 4.13b. SEM images of $\text{Ru}_{0.54}\text{Cu}_{0.46}\text{Al}_2\text{O}_3$ nanoparticles prepared.....	58
Figure 4.14. EDX spectrum of $\text{Ru}_{0.54}\text{Cu}_{0.46}\text{Al}_2\text{O}_3$ nanoparticles.....	59
Figure 4.15. X-ray diffraction patterns of the $\text{Ru}_{0.54}\text{Cu}_{0.46}\text{Al}_2\text{O}_3$ nano particles.....	60
Figure 4.16. The FT-IR spectra of $\text{Ru}_{0.54}\text{Cu}_{0.46}\text{Al}_2\text{O}_3$ nanoparticles.....	61
Figure 4.17. SEM images of $\text{Ru}_{0.62}\text{In}_{0.38}\text{Al}_2\text{O}_3$ nanoparticles prepared.....	62
Figure 4.18. EDX spectrum of $\text{Ru}_{0.62}\text{In}_{0.38}\text{Al}_2\text{O}_3$ nanoparticles.....	63
Figure 4.19. X-ray diffraction patterns of the $\text{Ru}_{0.62}\text{In}_{0.38}\text{Al}_2\text{O}_3$ nano particles.....	64
Figure 4.20. The FT-IR spectra of $\text{Ru}_{0.62}\text{In}_{0.38}\text{Al}_2\text{O}_3$ nanoparticles.....	65
Figure 4.21a. SEM images of $\text{Ru}_{0.77}\text{Co}_{0.23}\text{In}_2\text{O}_3$ nanoparticles prepared.....	66
Figure 4.21b. SEM images of $\text{Ru}_{0.77}\text{Co}_{0.23}\text{In}_2\text{O}_3$ nanoparticles prepared.....	67
Figure 4.22. EDAX spectrum of $\text{Ru}_{0.77}\text{Co}_{0.23}\text{In}_2\text{O}_3$ nanoparticles.....	68
Figure 4.23. X-ray diffraction patterns of the $\text{Ru}_{0.77}\text{Co}_{0.23}\text{In}_2\text{O}_3$ nano- particles.....	69
Figure 4.24. The FT-IR spectra of $\text{Ru}_{0.77}\text{Co}_{0.23}\text{In}_2\text{O}_3$ nanoparticles.....	70
Figure 4.25. SEM images of $\text{Ru}_{0.65}\text{Ni}_{0.35}\text{In}_2\text{O}_3$ nanoparticles prepared.....	71
Figure 4.26. EDX spectrum of $\text{Ru}_{0.65}\text{Ni}_{0.35}\text{In}_2\text{O}_3$ nanoparticles.....	72
Figure 4.27. X-ray diffraction patterns of the $\text{Ru}_{0.65}\text{Ni}_{0.35}\text{In}_2\text{O}_3$ nanoparticles.....	73
Figure 4.28. The FT-IR spectra of $\text{Ru}_{0.65}\text{Ni}_{0.35}\text{In}_2\text{O}_3$ nanoparticles.....	74
Figure 4.29a. SEM images of $\text{Ru}_{0.92}\text{Pd}_{0.08}\text{In}_2\text{O}_3$ nanoparticles prepared.....	75
Figure 4.29b. SEM images of $\text{Ru}_{0.92}\text{Pd}_{0.08}\text{In}_2\text{O}_3$ nanoparticles prepared.....	76
Figure 4.30. EDX spectrum of $\text{Ru}_{0.92}\text{Pd}_{0.08}\text{In}_2\text{O}_3$ nanoparticles.....	77
Figure 4.31. X-ray diffraction patterns of the $\text{Ru}_{0.92}\text{Pd}_{0.08}\text{In}_2\text{O}_3$ nanoparticles.....	78
Figure 4.32. The FT-IR spectra of $\text{Ru}_{0.92}\text{Pd}_{0.08}\text{In}_2\text{O}_3$ nanoparticles.....	79
Figure 4.33a. SEM images of $\text{Ru}_{0.54}\text{Pt}_{0.46}\text{In}_2\text{O}_3$ nanoparticles prepared.....	80

Figure 4.33b. SEM images of Ru <sub>0.54</sub> Pt <sub>0.46</sub> In <sub>2</sub> O <sub>3</sub> nanoparticles prepared.....	81
Figure 4.34. EDAX spectrum of Ru <sub>0.54</sub> Pt <sub>0.46</sub> In <sub>2</sub> O <sub>3</sub> nanoparticles.....	82
Figure 4.35. X-ray diffraction patterns of the Ru <sub>0.54</sub> Pt <sub>0.46</sub> In <sub>2</sub> O <sub>3</sub> nanoparticles.....	83
Figure 4.36. The FT-IR spectra of Ru <sub>0.54</sub> Pt <sub>0.46</sub> In <sub>2</sub> O <sub>3</sub> nanoparticles.....	84
Figure 4.37a. SEM images of Ru <sub>0.56</sub> Cu <sub>0.44</sub> In <sub>2</sub> O <sub>3</sub> nanoparticles prepared.....	85
Figure 4.37b. SEM images of Ru <sub>0.56</sub> Cu <sub>0.44</sub> In <sub>2</sub> O <sub>3</sub> nanoparticles prepared.....	86
Figure 4.38. EDAX spectrum of Ru <sub>0.56</sub> Cu <sub>0.44</sub> In <sub>2</sub> O <sub>3</sub> nanoparticles.....	87
Figure 4.39. X-ray diffraction patterns of the Ru <sub>0.56</sub> Cu <sub>0.44</sub> In <sub>2</sub> O <sub>3</sub> nanoparticles.....	88
Figure 4.40. The FT-IR spectra of Ru <sub>0.56</sub> Cu <sub>0.44</sub> In <sub>2</sub> O <sub>3</sub> nanoparticles.....	89

## 1. INTRODUCTION

Nanotechnology is the science that deals with matter at the scale of 1 billionth of a meter (i.e.,  $10^{-9}$  m = 1 nm), and is also the study of manipulating matter at the atomic and molecular scale. In general, the size of nanoparticles (NPs) spans the range between 1 and 100 nm. A nanoparticle is the most fundamental component in the fabrication of a nanostructure, and is far smaller than the world of everyday objects that are described by Newton's laws of motion, but bigger than an atom or a simple molecule that are governed by quantum mechanics. The United States (US) instituted the National Nanotechnology Initiative (NNI) back in 2000, which was soon followed (2001) by a plethora of projects in nanotechnology in nearly most of the US Departments and Agencies [1].

The term NP refers to particles with sizes between 1 and 100 nm that show extraordinary properties compared to the corresponding bulk materials. This is because nanoparticles have a large surface area, a greater fraction of surface atoms and a high surface to volume ratio in contrast to their bulk counterparts. As the size of a nanoparticle decreases, the fraction of surface atoms increases, consequently it increases the reactivity and makes them highly reactive catalysts [2].

Nanotechnology refers to the use of matter with at least one dimension below 100 nanometers. Such materials can exhibit unique properties for various applications. It also requires understanding the size and shape dependence of physical properties in design, fabrication and assembly of nanomaterials and devices with predictable behavior. Currently, significant progress has been made in the ability to produce shape-controlled nanoparticles, such as nanorods and nanowires, particularly using chemical synthesis methods. The overall goal is to improve the performance and utilization of nanomaterials for various applications, ranging from sensing devices to photonic materials, molecular electronics and advanced oxidation techniques.

Nanomaterials form a recent area of intense scientific interest because nanoscale materials exhibit unique properties and have a wide variety of applications in the development of magnetic materials for data storage, optoelectronics, medical diagnostics, photocatalysts, sensors, and alternative energy. Potential applications of nanotechnologies have been investigated in some important sectors, such as energy, communications, water purification, pollution reduction and environmental progress, medical and biomedical

applications. This technology allows significant reduction of resource consumption and pollution via improving the sustainability of energy utilization, recycling and detoxification technology [3].

### **1.1. Overview**

The history of the nanoparticle from ancient times to the Middle Ages has been summarized by Daniel and Astruc. The first book on colloidal gold was published in 1618 by the philosopher and medical doctor Francisci Antonii. This book includes considerable information on the formation of colloidal gold solutions and their medical uses, including successful practical cases. A complete treatise on colloidal gold was published in 1718 by Helcher. In the treatise, this philosopher and doctor stated that the use of boiled starch in its drinkable gold preparation noticeably enhanced its stability. In 1818, Jeremias Benjamin Richters suggested an explanation for the differences in color shown by various preparations of drinkable pink or purple gold solutions in that these solutions contained gold in the finest degree of subdivision, whereas yellow solutions were found when the fine particles had aggregated [4].

In 1909, Hansa Yellow was introduced to the market as the first monoazo yellow pigment. Phthalocyanine blue pigments also appeared in 1935. The rapid advances in pigment chemistry led to such important classes of pigments as disazo condensation pigments in 1954, quinacridones in 1955, azo pigments of the benzimidazolone series in 1960, the isoindolinone pigments in 1964, and the diketopyrrolo pyrrole pigments in 1986 [5].

### **1.2. Historically nanoparticules/nanopigments**

Of particular importance, the optical property is one of the fundamental attractions and a characteristic of a nanoparticle. For example, a 20 nm gold nanoparticle has a characteristic wine red color. A silver nanoparticle is yellowish gray. Platinum and palladium nanoparticles are black. Not surprisingly, the optical characteristics of nanoparticles have been used from time immemorial in sculptures and paintings even before the 4th century Architectural Digest (AD). The most famous example is the Lycurgus cup (fourth century AD) illustrated in Figure 1.1.

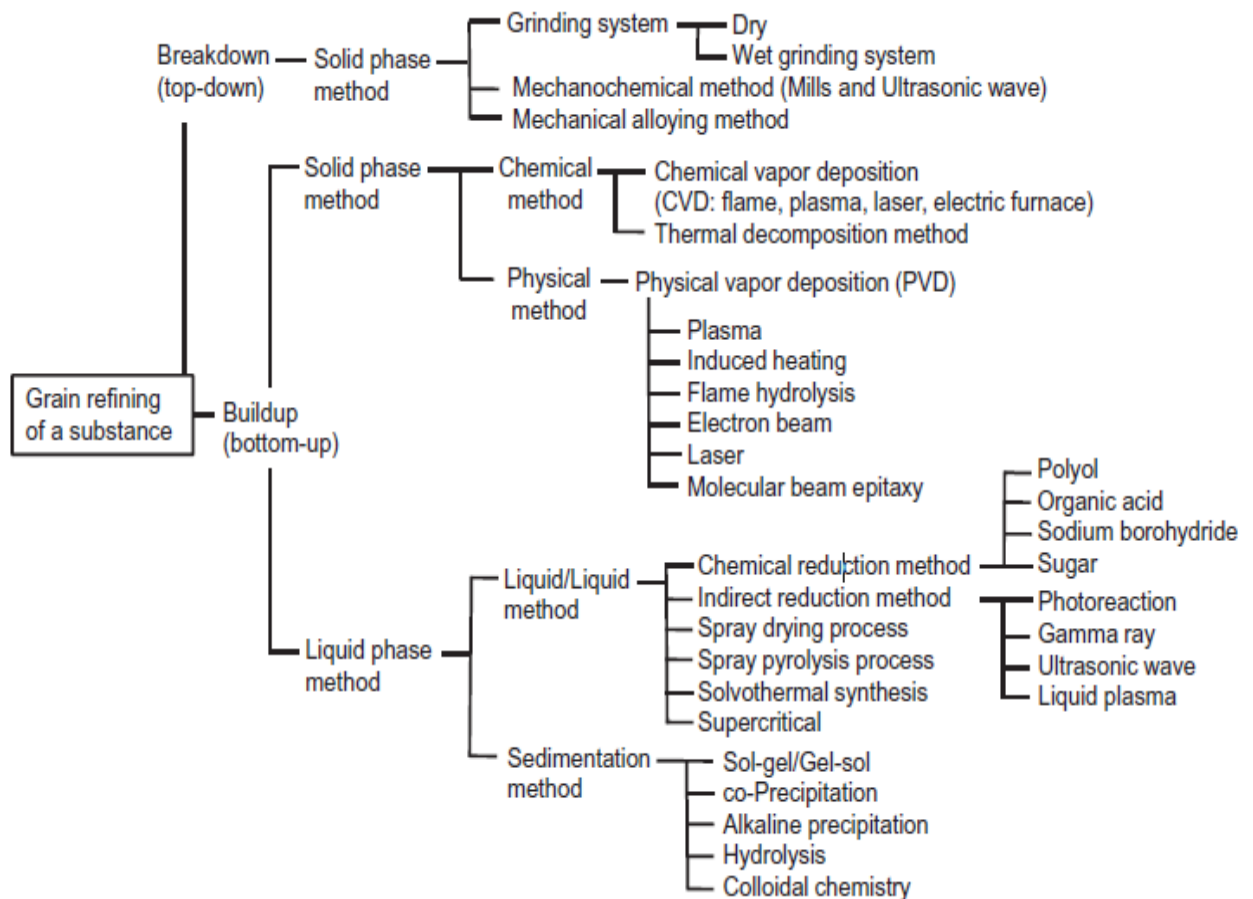


Figure 1.1. Photographs of the famous Lycurgus cup which displays a different color depending on whether it is illuminated externally (a) or internally (b).

This extraordinary cup is the only complete historic example of a very special type of glass, known as dichroic glass, that changes color when held up to the light. The opaque green cup turns to a glowing translucent red when light is shone through it internally (i.e., light is incident on the cup at  $90^\circ$  to the viewing direction). Analysis of the glass revealed that it contains a very small quantity of tiny ( $\sim 70$  nm) metal crystals of Ag and Au in an approximate molar ratio of 14: 1, which give it these unusual optical properties. It is the presence of these nanocrystals that gives the Lycurgus Cup its special color display. The reader can marvel at the cup now in the British Museum [6].

### 1.3. Methods of Nanoparticle Synthesis

Various preparation techniques for nanoparticles (nonmaterial's) are summarized in Figure 1.4. Two approaches have been known in the preparation of ultrafine particles from ancient times. The first is the breakdown (top-down) method by which an external force is applied to a solid that leads to its break-up into smaller particles. The second is the build-up (bottom-up) method that produces nanoparticles starting from atoms of gas or liquids based on atomic transformations or molecular condensations.



**Figure 1.2** Typical synthetic methods for nanoparticles for the top-down and bottom-up approaches.

The top-down method is the method of breaking up a solid substance; it can be subdivided into dry and wet grinding. A characteristic of particles in grain refining processes is that their surface energy increases, which causes the aggregation of particles to increase also. The manufacture of nanoparticles of 10 to 100 nm is possible by careful control of the reaction. Performing the high temperature chemical reaction in the CVD method requires heat sources such as a chemical flame, a plasma process, a laser, or an electric furnace.

The chemical reduction the process uses non-complicated equipment or instruments, and can yield large quantities of nanoparticles at a low cost in a short time. Of particular interest in this regard is the use of microwave radiation as the heat source that can produce high quality nanoparticles in a short time period besides the chemical reduction method which adds a reducing agent (direct reduction method).

Although various techniques have been summarized in Figure 1.2, there are some features to consider that are common to all the methods. That is, the synthesis of



nanoparticles requires the use of a device or processes that fulfills the following conditions:

- Control of particle size, size distribution, shape, crystal structure and composition distribution
- Improvement of the purity of nanoparticles (lower impurities)
- Control of aggregation
- Stabilization of physical properties, structures and reactants
- Higher reproducibility
- Higher mass production, scale-up and lower costs [1]

There are several methods for producing nanoparticles. However, microwave assisted synthesis of nanomaterials is gaining much interest among researchers owing to its unique features such as environmental friendly...ect.[7] Different kinds of nanostructures could be prepared by thermal methods, hydrothermal method, electrochemical methods, sol-gel methods, solid-state reactions, chemical reduction and decomposition route, sonochemical methods and photochemical methods [8].

**Microwave-assisted synthesis:** rapid heating has received considerable attention as a new promising method for the one-pot synthesis of metallic nanostructures in solutions.

**Hydrothermal method:** defined hydrothermal synthesis as the heterogeneous reactions in aqueous media above 100 °C and 1 bar in a closed system.

**Sol-gel methods:** formation of an oxide network through polycondensation reactions of a molecular precursor in a liquid.

**Solid-state reactions:** a chemical reaction between solids, the occurrence of which is detected by a characteristic color, also includes reactions that result in the precipitation or dissolution of a colored deposit.

**Chemical reduction:** chemical reactions in which the number of electrons associated with an atom or a group of atoms is increased. The electrons taken up by the substance reduced are supplied by another substance, which is thereby oxidized.

**Photochemical methods:** Photochemistry is the scientific study of chemical changes that are caused by light.

### **Top Down Approach**

- Mechanical Milling.
- Lithography (hybrid technology).

- Electro-explosion (thermal / chemical).
- Laser Ablation (Thermal).
- Spark Erosion (Electric Arc Discharge).

### **Bottom up Approach**

- Sol-gel technique.
- Aerosol based process.
- Chemical vapour deposition (CVD).
- Molecular condensation.
- Electrospinning.
- Self Assembly.

### **1.4. Nanoparticles in Various Fields**

**Electronics:** Displays, High density data storage, Non-volatile RAMs, Interconnections, EMI shieldings, Small multilayer Capacitors, optoelectronics devices, and optical fibers joining coating.

**Power/Energy:** Solar cells, Fuel cells, Batteries, Automotive catalysts, H<sub>2</sub> storage using metal hydrides.

**Health care /Medical:** Cancer treatments, Virus detection, Drug delivery, Inhalable insulin, Bone growth promoters, Antioxidant drugs based on fullerenes, Anti-bacterial wound dressing & fungicide.

**Environmental:** Environmental friendly antifouling paints & coatings, more sensitive sensors, Alumina fibers for water treatment, Self cleaning glass, Pollution destroying paints.

**Consumer goods:** Anticounterfeit device, Water/stain repellent textiles, adhesives for cardboard packaging, Ski wax, Antiglare/antimisting glass mirrors, Tennis balls/Rackets using nanoclays.

**Engineering:** Thermal barrier coatings, Spark plug, Chemical sensors, Moisture barrier films for packaging, Pigments & scratch resistant coatings, Structural enhancement of polymers & coatings, Inks conducting & magnetic, cutting tool bits [9].

## **1.5. Some words about NPs/nanopigments**

### **1.5.1. Properties of nanoparticles**

Several factors can affect the properties of nanoparticles. Among these, size (diameter, length, width, etc), surface (surface chemistry, surface charge, surface morphology, surface roughness, and surface contamination), and structure of the nanoparticles (crystal structure, shape, porosity, chemical composition, aggregation, etc) are the major characteristics that determine their fundamental properties such as color, melting temperature, conductivity, and reactivity. For example, the melting temperature for gold nanoparticles with a diameter of 6 nm 1150 Kelvin (K) is about twice the melting temperature for gold particles with a diameter of 2 nm (650 K) [10].

### **1.5.2. Motivation for Development of Nano**

- Unique properties of materials in nano-scale
  - Large surface area per unit volume
  - Large surface energy
  - Low melting point (difference can be as large as 100 °C)
- Motivation for Development of NPs
  - Reduce processing temperature
  - Reduce thermal stresses during processing
- Increased strength of solder alloys
  - Finer microstructure
  - Less prone to grain coarsening
  - Restriction of dislocation movement and grain boundary sliding
- Interconnection miniaturization
  - Very small pitch applications
  - Increase fine pitch interconnection reliability [9].

### **1.5.3. Size of Nanoparticles**

The physical and chemical properties of nonmaterials depend not only on their composition but also on the particle size and shape. The size distribution of the particles becomes a very important factor, provides rapid and uniform heating of reagents, solvents

intermediates and products. Fast heating accelerates the reduction of metal precursors and the nucleation of the metal cluster, resulting in nanostructures with smaller sizes, narrower size distributions and a higher degree of crystallization [11]. When the size of the catalyst reaches the NPs, the probability of recombination of photo-generated electron–hole pair diminishes owing to their fast arrival at reaction sites on the surface, If the size of the nanoparticles decreases (i.e., increase in specific surface area), then the increase in the surface energy of such nanoparticles will facilitate their aggregation [12]. One can control the size of synthesized materials which could lead in change of the physical and chemical properties of the synthesized materials [13]. The size of particles decreased with increasing MW power and decreasing irradiation time (keeping input energy constant) [14].

In chemical sciences, as the metal particles are reduced in size, bulk properties of the particles disappear to be decrease in the crystal size; NPs metal oxides may exhibit unique properties which can be significantly different from those of their bulk counterparts, for example, the large interfacial areas, homogeneity and highly reactive surfaces, unusual optical, electrical, and catalytic properties, etc [15].



Figure1.3. Nanoparticles in a wide variety of different shapes and sizes [16]

#### 1.5.4. Shape of Nanoparticles

The shape of nanoparticles is an important factor that determines the nature of the surface plasmon resonance band just as the size of the NPs. The catalytic activity as well

as chemical properties depends on their size and shape. MW synthesis has been increasingly applied in various fields of chemistry and in material science due to its generally simple, rapid volumetric heating and the consequent dramatic increase in reaction rate. Their applications in the preparation of nano-sized materials have been reported [17].

However, in many cases MNPs are unstable due to their high surface energy because of the high surface-to-volume (S/V) ratio [18]. It is known that, the specific surface area and surface-to-volume ratio increase dramatically as the size of a material decreases. The high surface area brought about by nanoparticle size is beneficial to many based devices [19]. The surface of the crushed pigment particles can also be chemically treated to enable the individual particles to stay in a stable dispersed state. However, when stored for an extended period of time the pigment particles can again agglomerate and adversely affect the color [20]. In addition to the race for completely novel materials with improved performance, however, optimizing existing materials with respect to morphology and size as well as development [21].

#### **1.5.5. Structure of Nanoparticles**

The electronic, mechanical and magnetic properties of particles on the nanoscale are often dramatically different from their bulk counterparts. Relaxations of the atomic positions and defects are some of the causes for this behavior. The precise determination of the structure of nanoparticles demands a modification of the methods being used for bulk material. We are trying to determine through the use of model systems which methods in structure research are best suited to reveal particular phenomena that occur in nanoparticles [22].

Utilized different metals prepared different of nanostructures could be oxides nonmaterials have attracted a great deal of attention different fields because of their various technological applications [23]. Nanoparticles that are composed of two or more metals differ in their catalytic, magnetic, and optical characteristics from nanoparticles that consist of a single metal. Such nanoparticles can be sub-divided into three kinds of structures: (i) The alloy structure that exists randomly in a crystal (ii) the core-shell structure in which the metal at the center differs from the peripheral metal; and (iii) the twinned hemisphere structure wherein two sorts of hemispheres are joined. The latter heterojunction structure facilitates phase separation. Nanostructures consisting of complex metal nanoparticles tend

to hide the various new features. The core-shell structure is comparatively easy to fabricate in complex metal nanoparticles with effective functional control, which has led to several studies and reports in the literature [24]. Inorganic or organic surfactants or assisting molecules are used as templates or structure-directing agents which can control both the growth and morphologies of final products [25], different synthesis methods have been investigated for the preparation of different results [26].

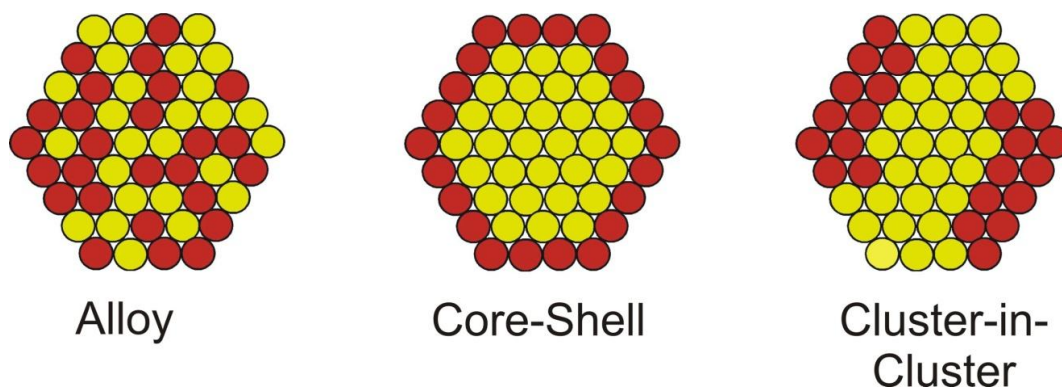


Figure 1.4. Schematic images of bimetal nanoparticles: alloy structure, core-shell structure, and heterojunction structure, of complex metal nanoparticles [27].

## 1.6. Define Pigments

Pigments can be defined as color, black, white or fluorescent particulate organic or inorganic solids that are usually insoluble in and essentially physically and chemically unaffected by the vehicle or substrate in which they are incorporated. They alter appearance by selective absorption and/or by scattering of light [28]. Pigments are inorganic or organic, colored, white or black materials which are practically insoluble in the medium in which they are incorporated [5]. Nano-pigments are organic or inorganic substances; insoluble, chemically and physically inert into the substrate or binders, with a particle small size [29].

-A substance used as coloring.

-Dry coloring matter, usually an insoluble powder, to be mixed with water, oil, or another base to produce paint and similar products.

-Pigments are chemical compounds which reflect only certain wavelengths of visible light. This makes them appear "colorful". Flowers, corals, and even animal skin contain pigments which give them their colors. More important than their reflection of light is the ability of pigments to absorb certain wavelengths.

## 1.7. Overview pigments

Dyes and pigments are among the most widespread products applied in human life. We cannot even imagine our life without colors and colored materials. The important influence of color on humans was determined a long time ago. Nowadays, there are no places in our lives without the application of dyes and pigments. At the same time, their application has caused various ecological problems. In spite of this, no one proposed their prohibition, because the most important principle in modern ecology is the principle of prevention but not of prohibition [30].

In general, a pigment is defined as being any solid, organic/inorganic, white, black, colored or fluorescent that is insoluble in the matrix into which it is incorporated and which does not react chemically or physically with it. The textile industry uses large amounts of water in its dyeing processes. Due to environmental problems the supercritical dyeing process has been developed. In this process supercritical carbon dioxide is used as the solvent for dyes. On the other hand, pigments, used in the formulation of paints, inks, toners and photographic emulsions can be micronized by supercritical antisolvent process [30].

Pigments are usually dispersed in vehicles or substrates for application and retain a crystal or particulate structure throughout the coloration process. The largest volume inorganic color pigment is synthetic iron oxide.

The following pie chart shows world consumption of inorganic color pigments:

**World Consumption of Inorganic Color Pigments—2010**

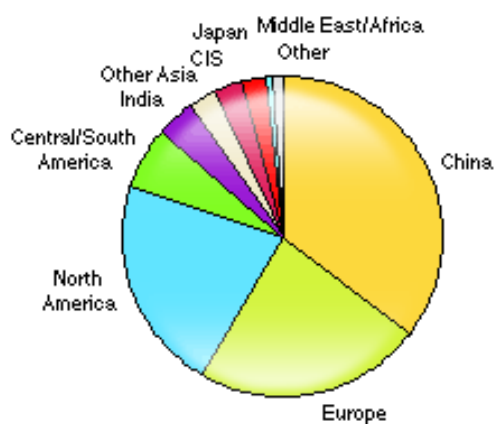


Figure 1.5. Show world Consumption of Inorganic Color pigments.

## 1.8. Overview nanopigments

Nano-pigments are inorganic or organic material, insoluble, chemically and physically inert into the substrate or binders with particle size less than 100 nm. The ceramic pigments with particle size in the nano scale have massive potential market, because of their high surface area, which assures higher surface coverage, higher number reflectance points and hence improved scattering. Ceramic pigments are basically a white or colored material, having high thermal stability and chemical resistance in order to be used at high temperature. Recently the development of a new ceramic pigment has fostered the research and application of pigments stable over 1200 °C. Blue pigments are widely used in industry to bring color to plastics, paints, fibers, papers, rubbers, glass, cement, glazes, ceramics, and porcelain enamels [31]. Inorganic nanopigments are extensively used in a variety of applications such as paints, plastics, and glasses [32]. There are many different pigments for the different paper and process types. The coating pigments have usually smaller particle size and their color is whiter the size and shape of pigment particles can be measured by different analyses [33].

Inorganic pigments are widely used as cool materials for building roofs and facades.  $\text{TiO}_2$ , a white pigment with a high solar reflectance of about 87%, is currently regarded as the best pigment for coating materials. However, non-white pigments are often preferred for esthetic reasons, and they can serve as a glare control remedy for avoiding “white blight”. Nickel titanate ( $\text{NiTiO}_3$ ) is a traditional yellow pigment [34].

The most important industrial application of phthalocyanines is the formation of color complexes with metal cations that are used as highly stable pigments and dyes. In addition, they can find commercial applications as: photovoltaic materials in solar cells, systems for fabrication of light emitting diodes (LED)...etc [35]. Pigments with excellent spreading properties, brilliant colors, high color intensity, gloss and stability, most effect pigments are titania coated mica pigments, and they depict excellent brilliant colors. The combination of two pigments can exhibit satisfactory spreading properties, high color effect, and good color saturation [20]. A literature survey indicates that based techniques have been used in the production of a wide variety of nano-materials suitable for different applications materials pigment and nanopigments [36].



## 1.9. Define Microwave

Microwaves are an electromagnetic radiation with wavelengths between 0.01 and 1 m and occupy the electromagnetic spectrum between infrared and radio waves. They occupy the frequency range between 0.3 and 30 GHz; however for commercial microwaves, narrower ranges around 2.5 GHz is typically employed [37].

**-Microwave** an electromagnetic wave with a wavelength in the range 0.001-0.3 m, shorter than that of a normal radio wave but longer than those of infrared radiation. Microwaves are used in radar, in communications, and for heating in microwave ovens and in various industrial processes.

**-Microwave oven** an oven that uses microwaves to cook or heat food [38].

## 1.10. Microwaves employer

Microwaves were employed in organic synthesis, but their application in inorganic synthesis remained infrequent because microwave heating can affect mechanical properties. Microwaves utilize electromagnetic energy which, like all electromagnetic radiation, has an electrical as well as a magnetic component in the 300–300,000 megahertz (MHz) range, though only the electrical field transfers energy in order to heat a substance.

There are two specific mechanisms of interaction between materials and microwaves:

(i) dipole rotation and (ii) ionic conduction. Both mechanisms require effective coupling between the components of the target material and the rapidly oscillating electrical field of the microwaves [39]. Recently, pointed out that microwave or ultrasonic wave could be used to assist material preparation, by which the reaction could be promoted by microwave sintering or ultrasonic cavitations, and this is an environment-friendly technique [40].

## 1.11. Microwave utilize for organic and inorganic materials

Microwave technology which firstly were used in studies on the design and production of military equipment during the Second World War, has been developed in time and continued to be used in different areas. These areas; food processing (heating, defrosting, quality control, and etc.), drying of industrial products (paper, wood, etc.), acceleration of chemical reactions (micro-reaction control), the melting of industrial

products (glass, rubber, slurries), sintering (ceramic, metal powder), plasma production, mineral processes (rock breaking, crushing), waste treatment and recycling processes [41].

Microwave-assisted processing methods, as good examples, have been developed for a variety of applications in organic and inorganic synthesis and transformations. There are many examples of the successful application of MW assisted green chemistry for synthesis of micro/nanostructured materials in the literature. This special issue addresses rapid methods for synthesis of organic and inorganic micro/nonmaterial to maximize the efficient use of safer raw materials and to reduce waste for fabrication of various micro/nanostructured materials. With MW synthesis, the yield of product increases from 60% up to 85% as compared to conventional method, which reduced the time, waste, and formation of by product. In addition, the reaction time is reduced from 4–8 hrs to 5-10 minutes [42]. Many reactions that do not occur under classical methods of heating can be carried out with high yields under microwave irradiation. Microwaves have the potential for large scale applications specifically in biodiesel production due to their ability to interact with a variety of reagents. [43].

Although many successful examples of the application of MW heating in organic chemistry have been reported, the expansion of MW synthesis in inorganic chemistry has been much slower. MW method is quite fast, simple and very energy efficient. MW heating is achieved through the interaction between the electric field of MW radiation and water or other solvents of high dielectric constant or solvent molecules with large dipole moment [33], MW radiations has provided a new, efficient and environmentally benign methodology for the synthesis of various metal oxide nanoparticles of diverse morphologies and size [44]. In contrast with the conventional technology to sinter materials, where they are heated by conduction, convection and radiation, the material processed in a microwave oven is heated through the interactions of the material with the microwave radiation. When the main factors are controlled, it is possible to have a final product in shorter time, with higher cleaning environment [45].

Microwave techniques have been successfully used in syntheses and have been confirmed to be more environmental friendly than the conventional processes. MW assisted nanoparticle synthesis is relatively a new strategy for producing various kinds of nanoparticles. The nanostructures are influenced by microwave irradiation time; reagent concentration and molar ratio of the precursors [46]. In microwave heating, dipolar

molecules tend to align themselves with the alternating field of microwave [47]. Microwave irradiation technique has been used for the rapid synthesis of a variety of compounds, and microwave-accelerated solvent-free organic reactions have received special attention [48]. At these reactor sizes microwaves, acting as a volumetric heating source, do not suffer from heat-transfer resistance [49].

### **1.12. Some advantages of MW**

Microwave dielectric heating has many advantages compared with conventional heating, such as prompt start up, uniform heating, very short heating time, easy heat control (on and off), low cost. It has been extensively applied to the synthesis of metallic nanostructures [50].

Microwave-assisted heating synthesis has some advantages such as short heating time, homogeneous thermal transmission, and the ability to produce narrow particles [51], has unique effects and significant merits such as easy workup, rapid volumetric heating, high reaction rate, short reaction time [52], change of the association between the species within the reaction mixture, creation of hot spots and enhancement of the dissolution of the precursor low energy budget, distribution and increased phase purity, with reduced time of exposure to microwaves, we could obtain better specific capacitance and better stability against cycling, higher reaction rates, higher selectivity and higher yields of products, determined by its specific heat, thermal conductivity, density and viscosity, high reaction rate [53], high purity and non toxic products [54], energy saving and production of inorganic nanoparticles with narrow size distribution as compared with other methods, have been synthesized using microwave irradiation technique for different applications [52], volumetric and selective heating, compactness of equipment, speed of on-off switching and is pollution free as there are no combustion products [47], fast, simple and efficient in energy, has been developed and is widely used in various fields such as molecular sieve preparation, radiopharmaceuticals, the preparation of inorganic complexes and oxide, organic reactions, plasma chemistry, analytical chemistry and catalysis. Approach (both solid and wet) has been recently used for the preparation of wide range of materials [44].

Microwave energy has the potential to be used in metal recovery operations, such as heating, drying, leaching, roasting/smelting and waste management fast wet dissolution of

various types of solids are some of the most well-known microwave applications [55]. Generally, in the absence of any protective agent, very large particle sizes (of the order of a few hundred nanometers) were obtained with relevant agglomeration [56] specialized instruments MW use of toxic reagents, long reaction time, and need of calcinations and requirement of external additives during the reaction [57], Possibility of forming new metallic stable structure [58]. The ability to work under high pressure conditions for relatively short times make reactions faster from days and hours to minutes and seconds has motivated research areas such as combinatorial chemistry and drug discovery [59]. However, energy transfer from the microwaves to the materials is achieved through the interaction of microwave radiation with water or other solvents with high dielectric constant or solvents molecules with large dipole moments [60]. Such materials have been widely used in some fields, such as paints, cosmetics, coatings, adhesives, biochemistry...ect[61].

## 2. LITERATURE REVIEW

### 2.1. Microwave-assisted synthesis of Ru nanoparticles

Polyethylene glycol (PEG) stabilized Ru NPs were synthesized by MW method in presence of glucose as reducing agent. The MW reaction for different amounts of added glucose and PEG was monitored Small sized NPs. The size of particles decreased with increasing MW power and decreasing irradiation time (keeping input energy constant). This is first report where Ru NPs were employed in catalytic decolorization of an azo dye, which is an important application in waste water treatment. The reaction products were characterized by XRD. The Bragg reflections ( $2\theta = 38.0, 43.8, 57.7, 68.8$  and  $77.8$ ) correspond to the indexed planes of the Ru.

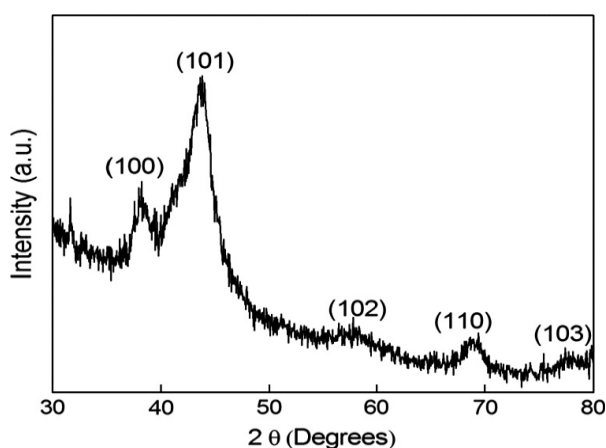


Figure 2.1. XRD pattern of the synthesized Ru NPs [14]

### 2.2. Microwave-assisted preparation of FeTiO<sub>3</sub> powders

FeTiO<sub>3</sub> powders were prepared from (Fe+Ti) mixed carbonate precursor by the MW assisted calcinations method. It is demonstrated that the calcinations process can be divided in to three different stages: the removal of water, the decomposition of precursor and the formation of FeTiO<sub>3</sub>. A variety of techniques, such as FT-IR, and SEM were utilized to characterize the samples. The results indicated that FeTiO<sub>3</sub> powders can be prepared by MW assisted calcinations for 120 min at 600°C; powders prepared and have a mean particle size of 400–500 nm.

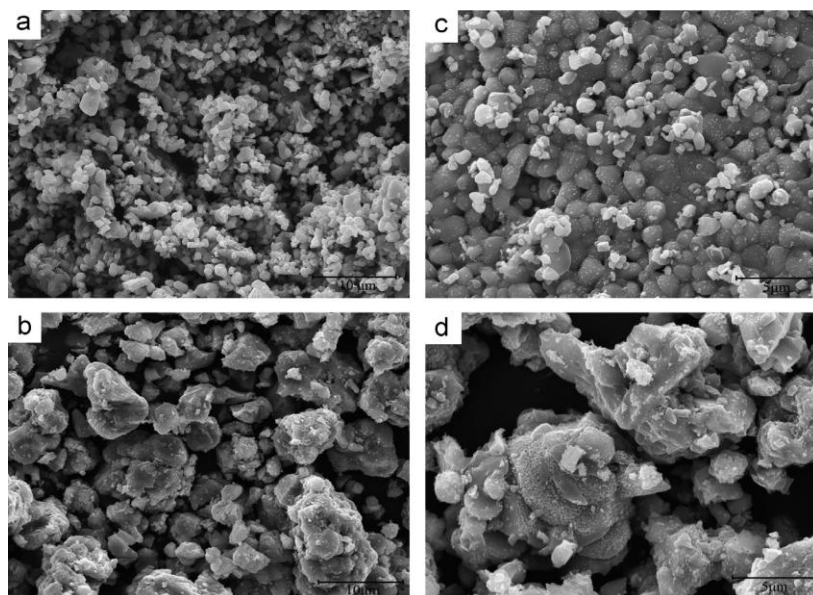


Figure 2.2. SEM micrographs of FeTiO<sub>3</sub> samples

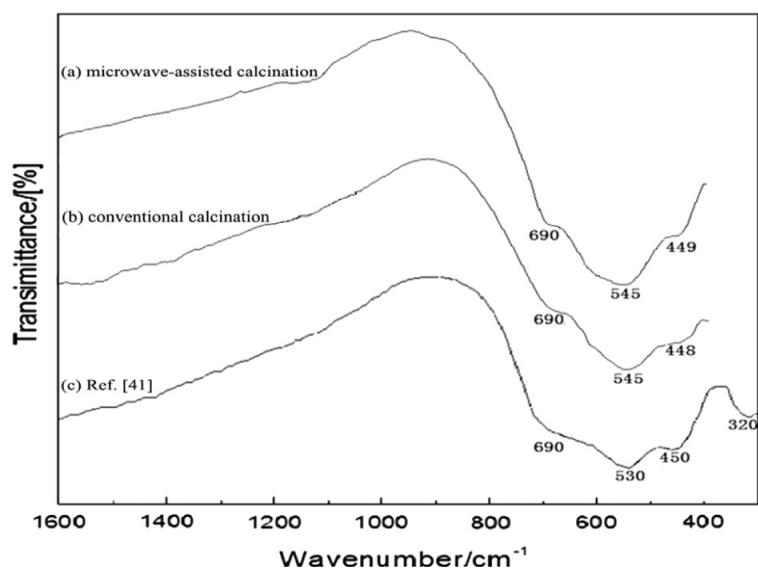


Figure 2.3. FT-IR spectrums of FeTiO<sub>3</sub> samples [62].

### 2.3. Microwave assisted synthesis of Co<sub>3</sub>O<sub>4</sub> nanoparticles

Cobalt oxide nanoparticles synthesized through simple MW method are employed for supercapacitor studies. The MW-assisted synthesized cobalt oxide NP appears to be a promising electrode material for supercapacitor application. Cobalt oxide powder was synthesized by MW assisted precipitation method using cobalt nitrate hexahydrate (Co(NO<sub>3</sub>)<sub>2</sub>·6H<sub>2</sub>O), The resultant solution was subjected to 240 W of microwave irradiation for 5 min using household microwave oven. It was cooled to room temperature, and then

the precipitate was separated by successive washing with water and ethanol. Were characterized by SEM, FTIR and XRD techniques

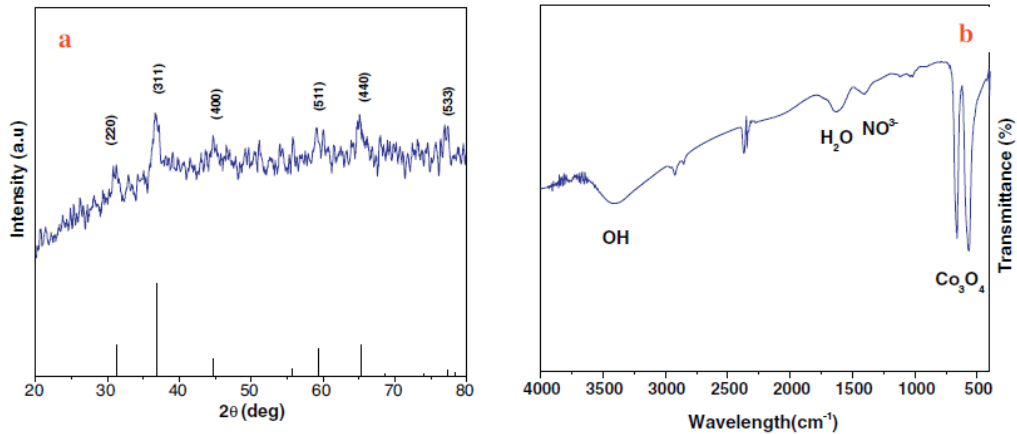


Figure 2.4. (a) XRD pattern of  $\text{Co}_3\text{O}_4$  sample, (b) FTIR spectrum of  $\text{Co}_3\text{O}_4$  [63]

#### 2.4. Nano-crystalline $\text{Sm}_{0.5}\text{Sr}_{0.5}\text{Co}(\text{Fe})\text{O}_{3-\delta}$ perovskite oxides

Nano-crystalline  $\text{Sm}_{0.5}\text{Sr}_{0.5}\text{Co}(\text{Fe})\text{O}_{3-\delta}$  (SSCF) perovskite oxides were synthesized by a MW-assisted sol–gel combustion process using glycine as the complexing agent. The properties of the resultant powder were characterized by SEM and XRD techniques. The experimental results indicated that the glycine/metal-ion ratio should be controlled at about 2 with the starting metal ion concentration and the calcinations temperature should be around  $600^\circ\text{C}$ ,  $800^\circ\text{C}$  and  $1000^\circ\text{C}$  so as to obtain the pure perovskite structure with high economical efficiency.

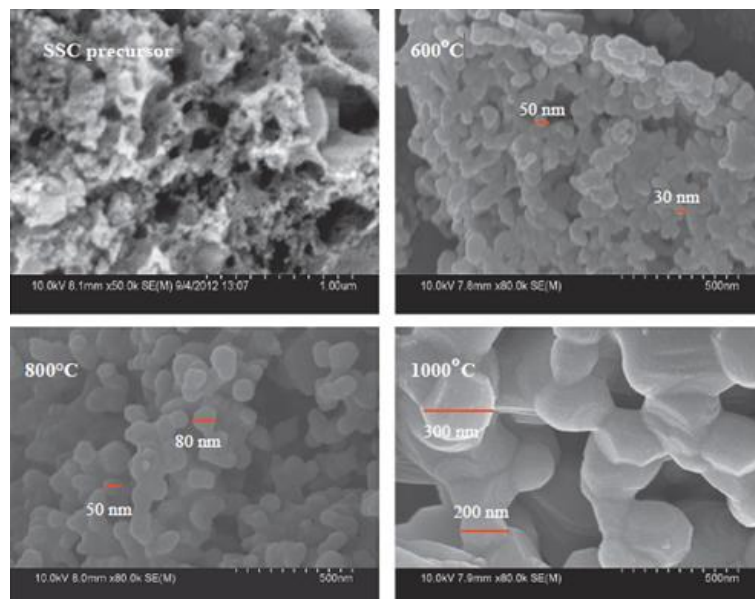


Figure 2.5. Morphology of the SSC oxide precursor and the calcined powders [64]

## 2.5. NiFe<sub>2</sub>O<sub>4</sub> Nanoparticles Produced with Microwave-Assisted Combustion Method

In this study, nickel ferrite (NiFe<sub>2</sub>O<sub>4</sub>) NPs were synthesized with MW-assisted combustion method. The structural and chemical properties of the nickel ferrite NPs the crystallite of the nickel ferrite NPs were calculated using the formula and the average particle size of the obtained NPs found as 50 nm approximately. These NPs were used to remove the arsenic from synthetically prepared wastewaters by adsorption method. The powder SEM analyses were performed with XRD pattern of the NiFe<sub>2</sub>O<sub>4</sub> NPs.

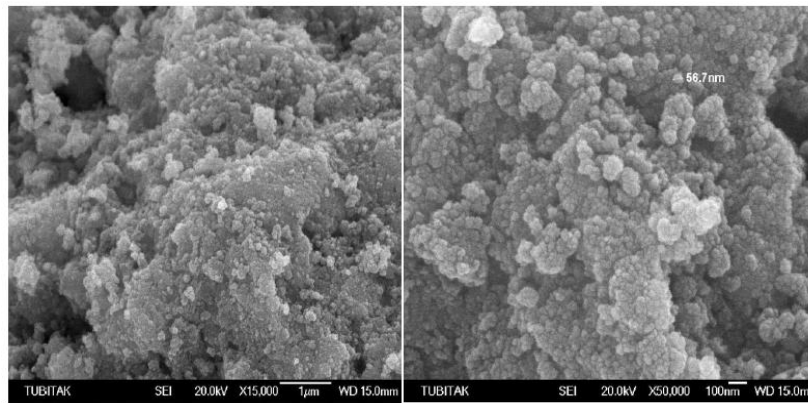


Figure 2.6. SEM images of NiFe<sub>2</sub>O<sub>4</sub> nanoparticles

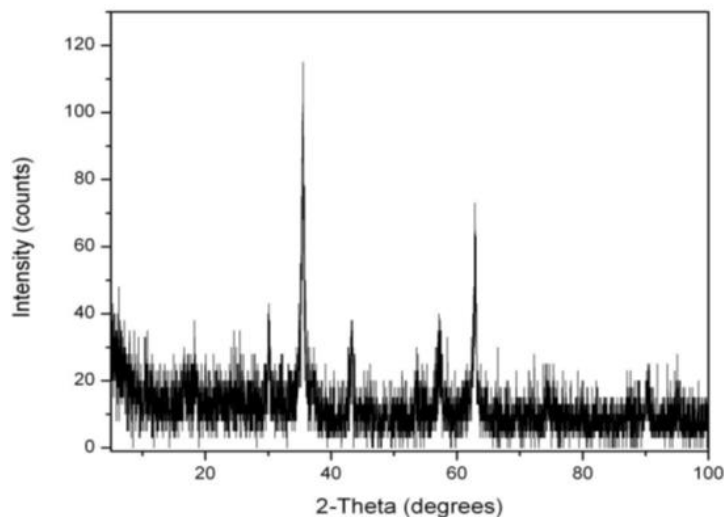


Figure 2.7. X-ray diffraction pattern of NiFe<sub>2</sub>O<sub>4</sub> nanoparticles [65]



## 2.6. Microwave-assisted rapid synthesis of alumina nanoparticles

Alumina nanoparticles Al NPs were synthesized from aluminium nitrate using extracts of tea, coffee and triphala, with the microwave-assistance using Water was taken as solvent medium. The formations of AlNP were initially monitored by the colour changes occurring in the reaction mixture during the incubation period. As synthesized nanoparticles were characterized by SEM and FTIR .The AlNP were found to be spherical in shape in case of tea and coffee extracts with a size of 50–200 nm extract. Aluminium nitrate and coffee extract taken in 1:4 ratios (w/w)

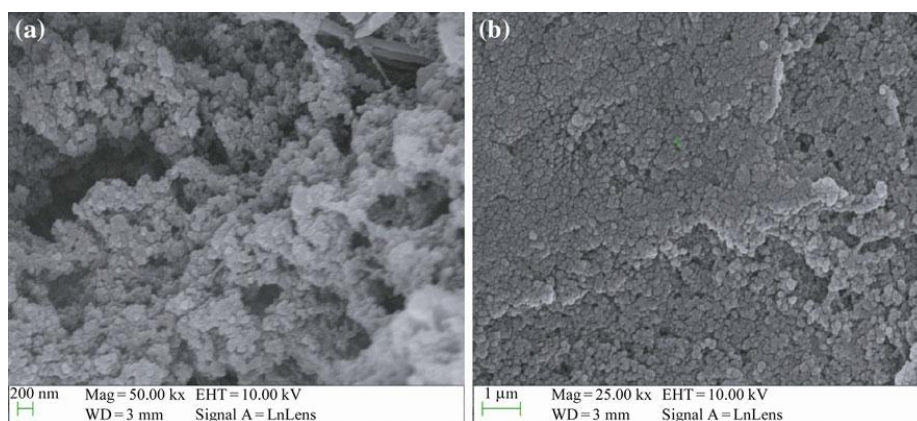


Figure 2.8. SEM images of Al NP using tea leaves extract

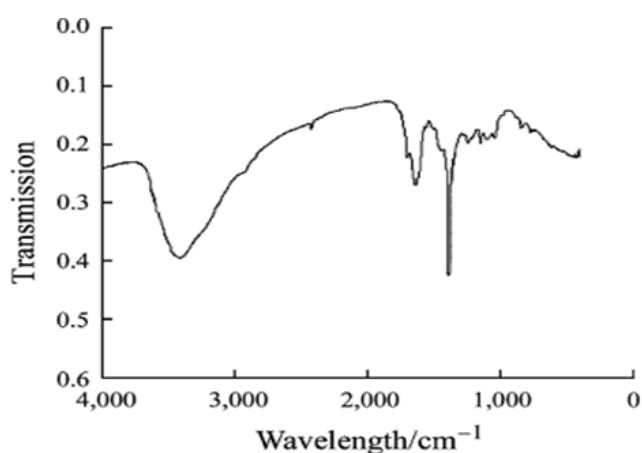


Figure 2.9. FT-IR of Al NP using tea leaves extract [66].

## 2.7. Cerium zinc molybdate nano pigment by innovative ultrasound assisted approach

Ultrasound assisted synthesis of yellow rare earth cerium zinc molybdate anticorrosion nanopigments is presented. The synthesis of nanosized cerium zinc molybdate was carried out using cerium nitrate, sodium zinc molybdate as a precursor

materials by conventional and ultrasound assisted chemical precipitation method without addition of emulsification agent analysis. The reaction mechanism for formation of cerium zinc molybdate nanoparticles is reported in reactions, Due to ultrasonic irradiation and strong alkaline medium  $\text{Na}^+$  ions gets released from sodium zinc molybdate nanoparticles during synthesis of cerium zinc molybdate. The obtained product was dried in an oven at  $100\text{ }^\circ\text{C}$ . Further, prepared sodium zinc molybdate was used for synthesis of cerium zinc molybdate, and crystallite size was found to be 27 nm from XRD, used FT-IR.

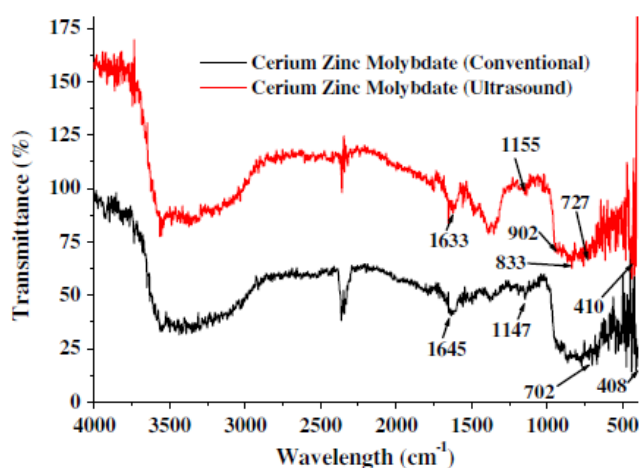


Figure 2.10. FT-IR pattern of the synthesized  $\text{Ce}_2\text{Zn}_3(\text{MoO}_4)_6$  nanoparticles [32].

## 2.8. Synthesis of $\text{Zn}_{0.7}\text{Ni}_{0.3}\text{Fe}_2\text{O}_4$ nanoparticles via microwave-assisted method

We report on the synthesis of  $\text{Zn}_{0.7}\text{Ni}_{0.3}\text{Fe}_2\text{O}_4$  NPs via MW-assisted combustion route by using urea as fuel. There is a growing interest in magnetic NPs, due to the wide range of practical applications in several important technological fields such as ferrofluids, magnetic drug delivery, and high density information storage. A variety of wet chemical methods have been reported to produce nano- sized ferrite materials. However, complex processes, expensive precursors and low production rates are common problems to many of these techniques. In order to investigate the crystal structure analyses by XRD and FT-IR analyses. The crystallite size estimated from XRD (16.4 nm).

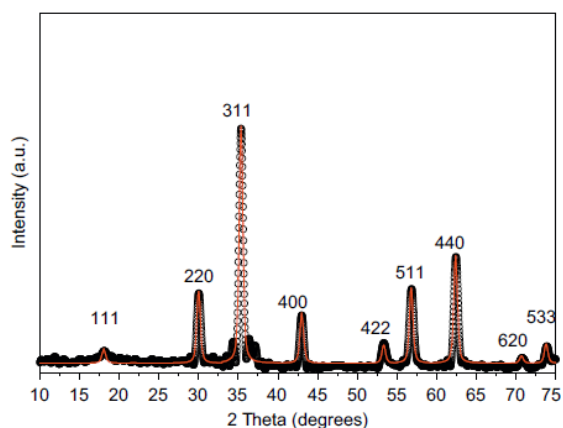


Figure 2.11. XRD and line profile fitting of ferrite powder by microwave method.

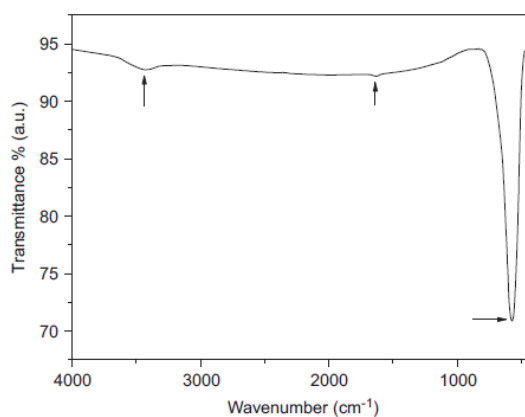


Figure 2.12. FT-IR spectrum of  $Zn_{0.7}Ni_{0.3}Fe_2O_4$  [67]

## 2.9. Microwave-assisted synthesis of CdS intercalated

CdS intercalated  $K_4Nb_6O_{17}$  (designated as  $K_4Nb_6O_{17}/CdS$ ) composite photo catalysts were synthesized using a microwave-assisted synthesis. The photocatalytic properties of these catalysts for hydrogen production were also investigated in the presence of  $Na_2S$  and  $Na_2SO_3$  sacrificial reagents. The  $K_4Nb_6O_{17}/CdS$  catalysts synthesized using microwave irradiations were found to possess higher crystallinity than their counterparts, synthesized using conventional methods. The preparation of CdS intercalated  $K_4Nb_6O_{17}$  via conventional methods can take several days to several weeks due to mass transfer limitations. Additionally, the preparation process is difficult to control, and the crystal structure of  $K_4Nb_6O_{17}$  could be consequently destroyed. The structure of the samples was characterized by XRD and SEM measurements.

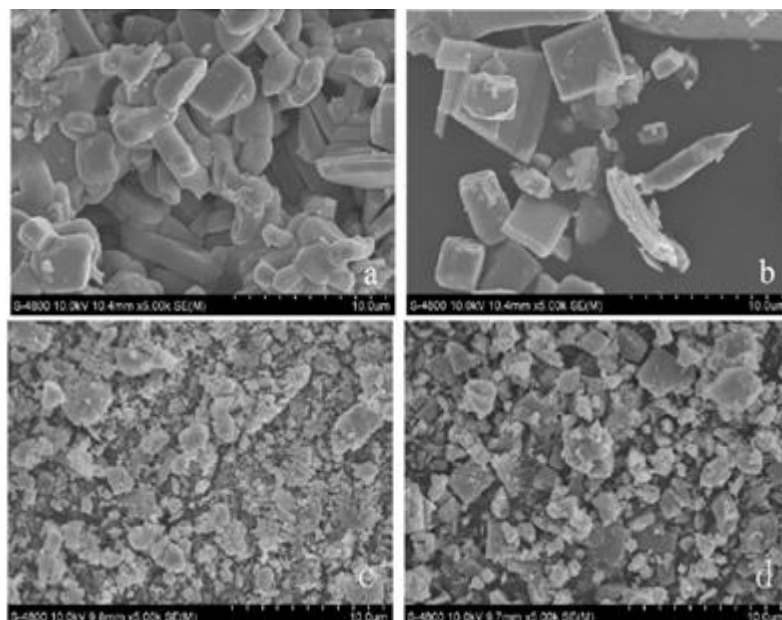


Figure 2.13. SEM of (a)  $K_4Nb_6O_{17}$  (b)  $mm-K_4Nb_6O_{17}/CdS$  (c)  $CdS$  (d)  $M-K_4Nb_6O_{17}$  [68]

## 2.10. $Ni_{0.6}Zn_{0.4}Fe_2O_4$ nano-particles prepared by conventional hydrothermal method

In this paper nano-scale  $Ni_{0.6}Zn_{0.4}Fe_2O_4$  ferrite powders were successfully prepared by the conventional hydro thermal method, and followed by annealing via microwave sintering in a homemade microwave oven for 7.5–15 min. This is different from the microwave-hydrothermal process or other microwave assisted synthesis process reported in the literatures. The effect of microwave annealing on the crystal structure, the morphology and the magnetic properties of  $Ni_{0.6}Zn_{0.4}Fe_2O_4$  NPs has been investigated. Comparison of MW and conventional annealing of  $Ni_{0.6}Zn_{0.4}Fe_2O_4$  NPs is discussed. Properties of the samples were characterized by SEM, FT-IR and XRD.

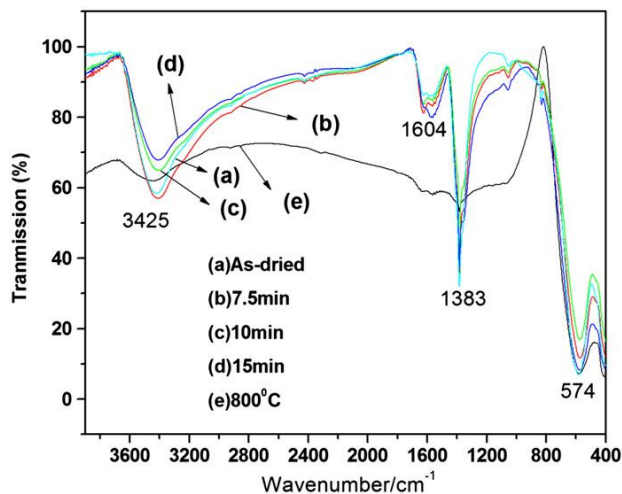


Figure 2.14. FT-IR spectra of  $Ni_{0.6}Zn_{0.4}Fe_2O_4$  ferrites

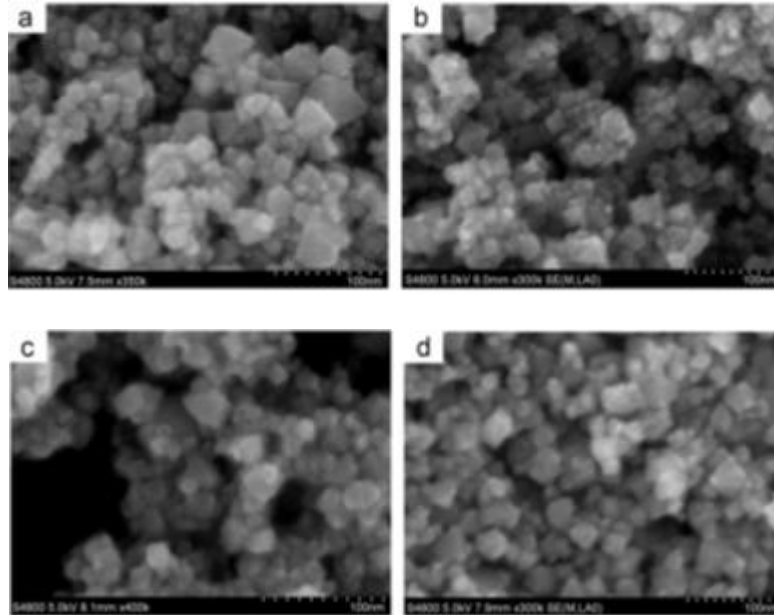


Figure 2.15. SEM graphs of  $\text{Ni}_{0.6}\text{Zn}_{0.4}\text{Fe}_2\text{O}_4$  ferrites [69].

### 2.11. Microwave-assisted synthesis of $\text{Ti}_{1-x}\text{V}_x\text{O}_2$ ( $x = 0.0 - 0.10$ ) nanopowders

$\text{Ti}_{1-x}\text{V}_x\text{O}_2$  ( $x=0.0-0.10$ ) nanopowders were successfully synthesized by a MW-assisted sol-gel technique and their crystal structure and electronic structure were investigated, the phase transformation appeared at 600 °C. This MW method has been employed to synthesize  $\text{TiO}_2$ . In the present study, the influences of the preparation methods and the concentrations of vanadium doping on the structural and optical properties of  $\text{Ti}_{1-x}\text{V}_x\text{O}_2$  nanopowders were examined in detail. The products were characterized using SEM.

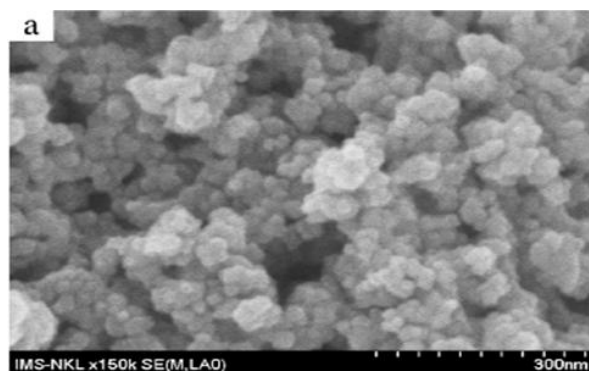


Figure 2.16. SEM images of  $\text{TiO}_2$  [70]

### 2.12. Zinc oxide nanostructures synthesized by rapid microwave irradiation methods

In this study, two different chemical solution methods were used to synthesize Zinc oxide nanostructures via a simple and fast microwave assisted method. The average

crystallite size of the flower-like and spherical nanostructures were determined to be about 55 nm and 28 nm, respectively. XRD and SEM analysis were used for characterization of the synthesized ZnO powders. Finally, our results depict that the efficiency of photocatalytic performance in the Zinc oxide nanostructures with spherical morphology is greater than that found in the flower-like Zinc oxide nanostructures as well as bulk ZnO.

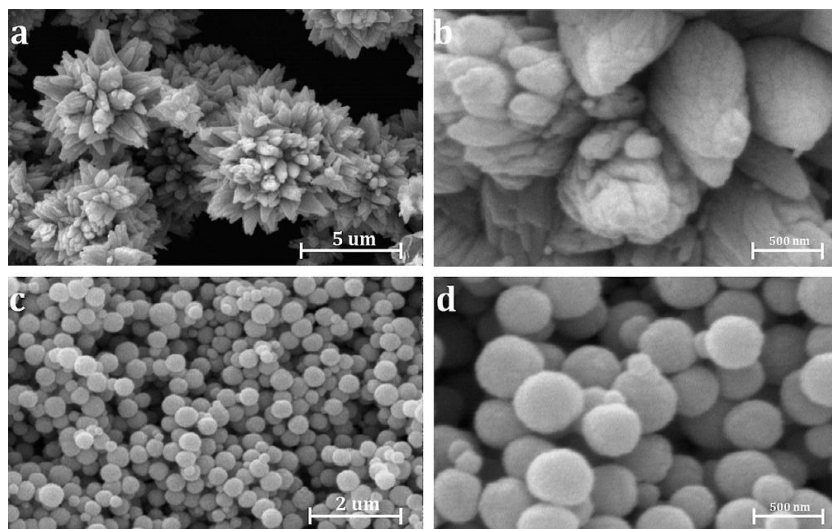


Figure 2.17. SEM images of synthesized ZnO nanostructures

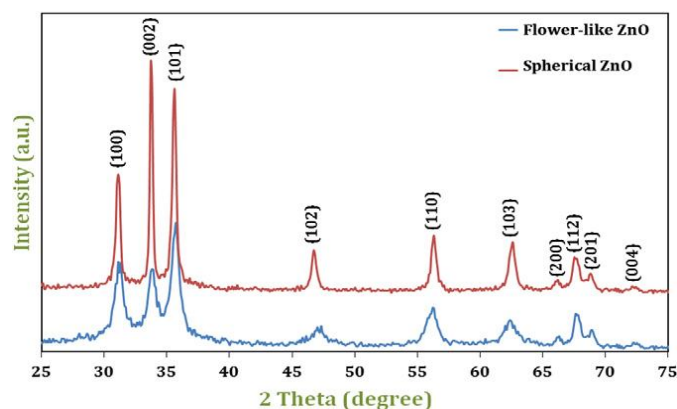


Figure 2.18. XRD patterns of the synthesized ZnO nanostructures [12].

### 2.13. Flower-like $\text{Bi}_2\text{WO}_6$ and $\text{Bi}_2\text{O}_3\text{-Bi}_2\text{WO}_6$ composite by Microwave-assisted

Flower-like  $\text{Bi}_2\text{WO}_6$  and  $\text{Bi}_2\text{O}_3\text{-Bi}_2\text{WO}_6$  composite microstructures have been synthesized via a facile and rapid microwave-assisted hydrothermal method through controlling the experimental parameters. In this article, we describe a facile and rapid microwave-assisted hydrothermal approach to synthesize flower-like  $\text{Bi}_2\text{WO}_6$  and  $\text{Bi}_2\text{O}_3\text{-}$

$\text{Bi}_2\text{WO}_6$  composite by adjusting the reaction conditions without the use of any surfactant or template. Furthermore, the experimental results confirm that these  $\text{Bi}_2\text{O}_3\text{-Bi}_2\text{WO}_6$  composites exhibit much higher photocatalytic activities for degradation of RhB compared to pure  $\text{Bi}_2\text{WO}_6$  and  $\text{Bi}_2\text{O}_3$ . The phases and morphologies of the products are characterized powder SEM and XRD

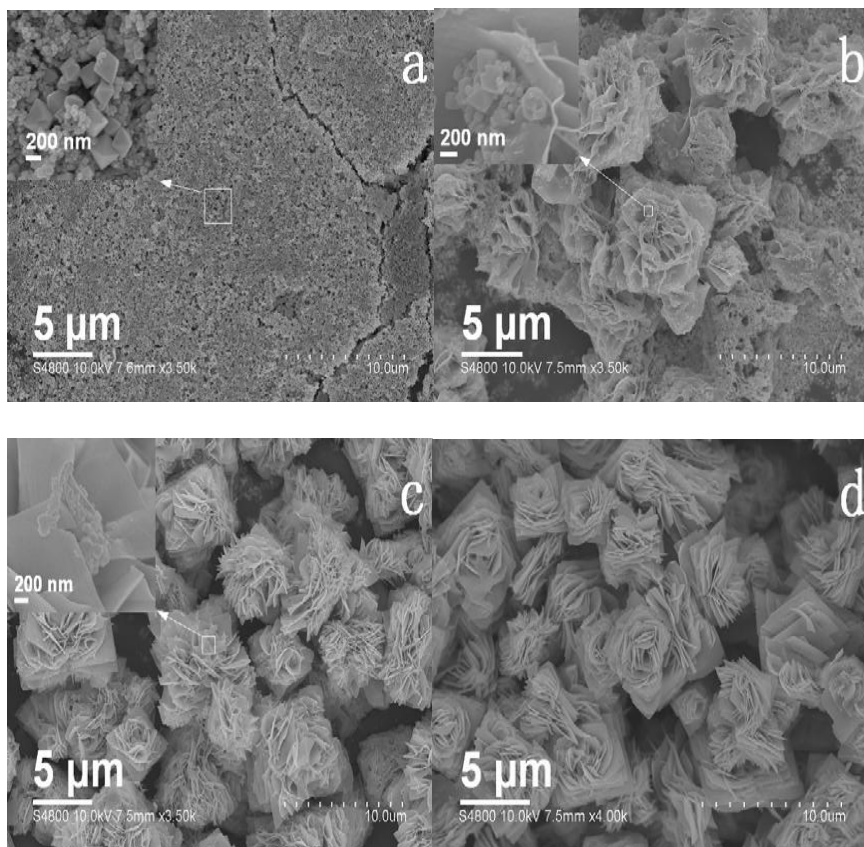


Figure 2.19. SEM of products (a) 140 °C, (b) 150 °C, (c) 160 °C and (d) 170 °C [71]

#### 2.14. Nanoparticles obtained by microwave-assisted oxidation technique

Nickel hydroxide ( $\beta\text{-Ni(OH)}_2$ ) and nickel oxy hydroxide ( $\beta\text{-NiOOH}$ ) nanoparticles assigned as P and PO, respectively, were successfully synthesized through MW-assisted oxidation technique using sodium hydroxide as the precipitating agent and sodium hypochlorite as the oxidizing agent. Due to their small sizes, nanoparticles exhibit novel material properties that are significantly different from their bulk counterparts. The performance of  $\text{Ni(OH)}_2$  depends on its size, morphology and structural characteristics. The as-prepared materials were well characterized by FT-IR, XRD and SEM analytical

techniques. Particle size of the products depends on NaOH concentration and calcination temperature.

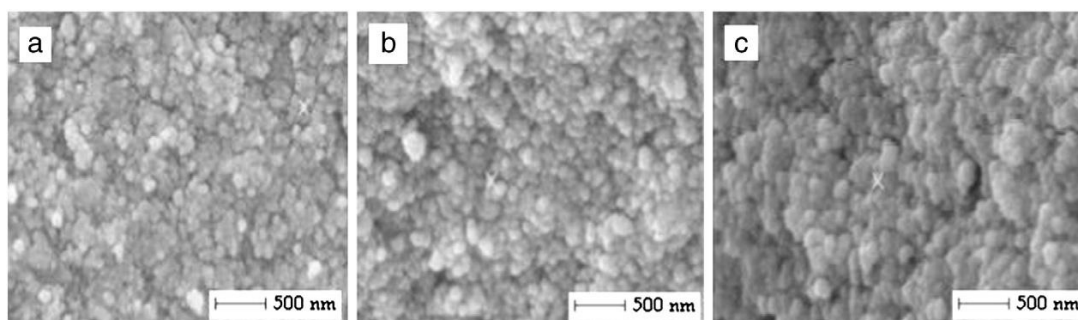


Figure 2.20. SEM images of NiO nanoparticles

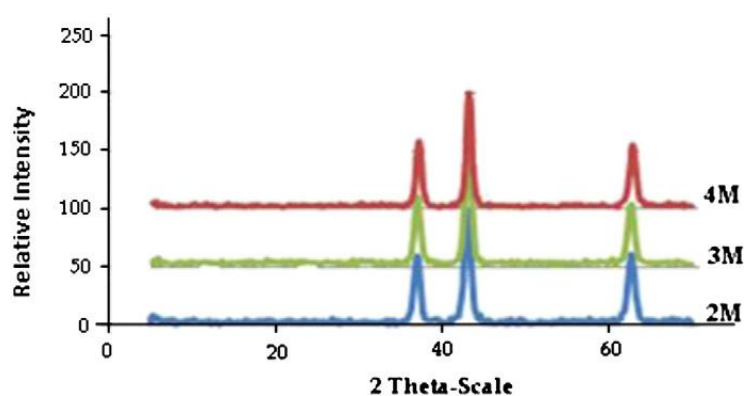


Figure 2.21. XRD patterns of NiO nanoparticles

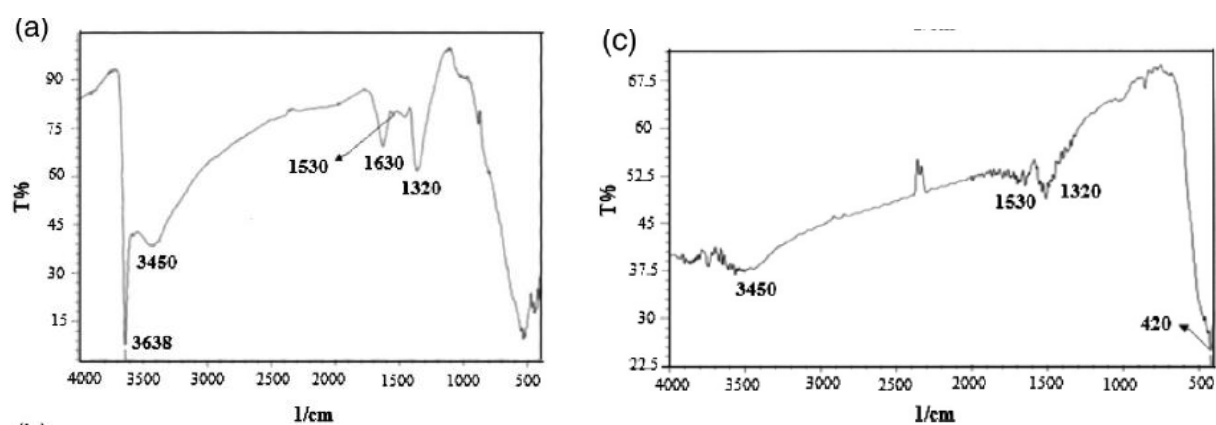


Figure 2.22. (a) FT-IR spectrum of  $\beta$ -Ni(OH)<sub>2</sub> precursor and (c) final product (NiO) [72].



## 2.15. Synthesis of cadmium-doped copper oxide nanoparticles

Pure and cadmium-doped copper oxide nanoparticles have been successfully prepared by a microwave assisted solvothermal method using copper acetate as the starting material. The particle sizes have been obtained as, 10-14 nm for pure CuO and 42-87 nm for cadmium-doped CuO nanoparticles. The synthesized both pure and cadmium doped copper oxide nanoparticles have been characterized by using XRD, SEM and EDX analysis techniques.

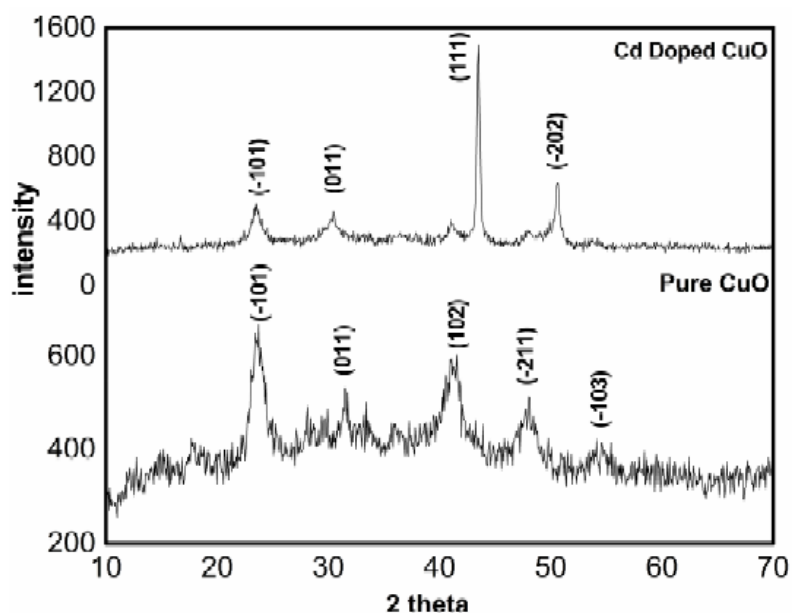


Figure 2.23. XRD spectrum of both pure and cadmium-doped CuO nanoparticles

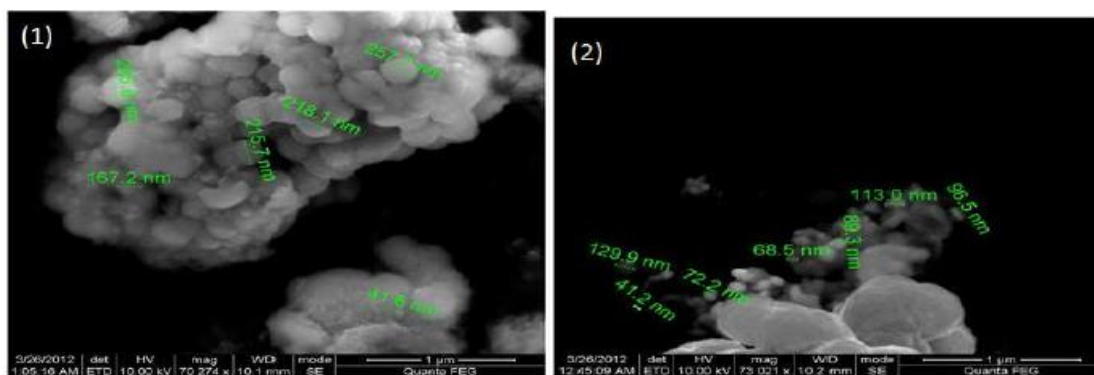


Figure 2.24. SEM of pure CuO nanoparticles (1), cadmium-doped CuO NPs(2) [15].

### 3. MATERIAL AND METHOD

#### 3.1. Chemical substance

All chemicals were analytical grade and oxidation was used throughout, shows the chemicals used in the present work.

<u>Materials name</u>	<u>Chemical formula</u>	<u>Molecular Weight</u>
1) Ferric nitrate nona hydrate	$\text{Fe}(\text{NO}_3)_3 \cdot 9\text{H}_2\text{O}$	404 g/mol
2) Aluminum acetylacetonate	$\text{Al}(\text{C}_5\text{H}_7\text{O}_2)_3$	324.31 g/mol
3) Indium chloride	$\text{InCl}_3$	221.18 g/mol
4) Cobalt(II) chloride hexahydrate	$\text{CoCl}_2 \cdot 6\text{H}_2\text{O}$	237.93 g/mol
5) Nickel chloride hexahydrate	$\text{NiCl}_2 \cdot 6\text{H}_2\text{O}$	237.69 g/mol
6) Copper chloride dihydrate	$\text{CuCl}_2 \cdot 2\text{H}_2\text{O}$	170.48 g/mol
7) Aluminum chloride	$\text{AlCl}_3$	133.34 g/mol
8) Cobalt (II) acetate tetra_hydrate	$\text{Co}(\text{C}_2\text{H}_3\text{O}_2)_2 \cdot 4\text{H}_2\text{O}$	249.09 g/mol
9) Platinum(II) chloride	$\text{PtCl}_2$	265.99 g/mol
10) Palladium chloride	$\text{PdCl}_2$	177.33 g/mol
11) Thiourea	$\text{SC}(\text{NH}_2)_2$	76.12 g/mol
12) Ethylene glycol (1,2-Ethanediol )	$\text{C}_2\text{H}_6\text{O}_2$	62.07 g/mol
13) Acetone (2-Propanone)	$\text{C}_3\text{H}_6\text{O}$	58.08 g/mol
14) Methanol	$\text{CH}_4\text{O}$	32.04 g/mol
15) Distilled water (D.W)	$\text{H}_2\text{O}$	18.02 g/mol
16) Absolute ethanol	$\text{C}_2\text{H}_6\text{O}$	46.07 g/mol

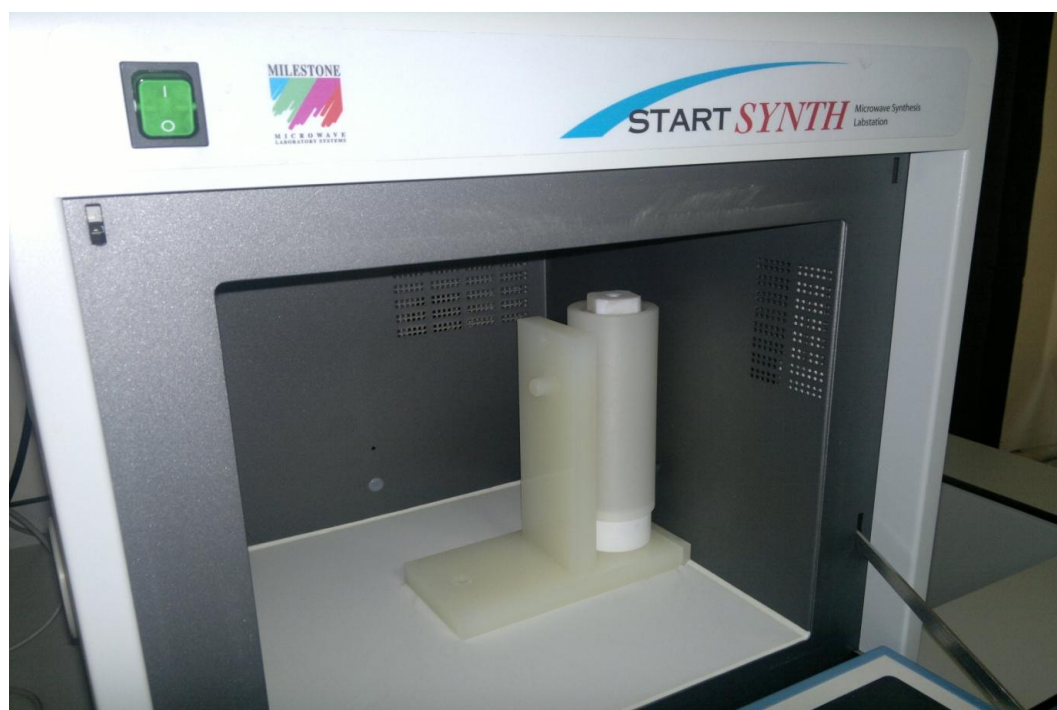


Figure 3.1. Microwave used in synthesized.



Figure 3.2. This FT-IR used for analysis.



Figure 3.3. This XRD used for analysis.



Figure 3.4. This SEM and EDX used for analysis.

### 3.2. Overview our work

Nanoparticles may be synthesized using various starting materials by different physical and chemical methods, with the produced particles differing in elemental composition, shape, size, and chemical or physical properties. The results show that nearly monodisperse nanoparticles have been successfully prepared without using surfactants.

We used same method and technical microwave heating for solution in 600 W, 200 °C at 1h, but changed chemical substances.

Type of microwave-assisted for synthesized NPs (MILESTONE Marker, STARTSYNTH Microwave Synthesis Labstation Model) we used.

The products were characterized using four technical's:

- 1- X-ray diffraction XRD X-pert pro PANALITICAL,  $\text{CuK}\alpha$  radiation,  $\lambda = 0.154 \text{ nm}$  at 40 KV and 30 mA.
- 2- Scanning electron microscopy SEM and Energy Dispersive X-Ray spectroscopy EDX same machine but different result characterizations ( ZEISS Marker and EVO/LS10 Model)
- 3- Fourier transforms infrared spectroscopy FTIR (Perkin Elmer Marker, Spectrum 400 Model, FT-IR Spectrometer Scan  $(4000-400) \text{ cm}^{-1}$ ).

In this study, the use of water as a solvent offers a more green or environmentally benign process, removing the requirement of organic solvents or hazardous substances. From the viewpoint of inorganic chemistry, the approach is a good candidate since the reaction can proceed at a mild temperature in water in a sealed environment. Thiourea and ethylene glycol robust design was used for the optimization of variables which are potentially affective in the synthesis procedure.

Direct reaction of anion and cation correspond to an insoluble inorganic salt. The control of precipitated particle morphology during precipitation reaction is complex processes and needs complete interpretation the multi-interactions between the reagents and operation parameters. However, experimental investigation on the effect of same parameters on the particle size via statistical optimization of the variables may be a useful and facile technique. Thus, in this investigation, effect of same parameters such as concentration in aqueous solutions, flow rate for addition of reagent to solution, and temperature of reactor on the particle size of produced was studied.

The EG agent used for chemical precipitation can interact with ions through ethylene oxygen groups (-CH<sub>2</sub>CH<sub>2</sub>O-) in the molecules and mediate the size and morphology nanoparticles. At the same time, EG can enwrap the precipitations and reduce the aggregation among the NPs. In addition, EG have large exclusion volume in aqueous solutions, and thus can provide additional strict hindrance among the NPs, which can also inhibit particle aggregation. Chemical precipitation with MW-assisted method is simple easily to produce high yield and hence rapid reaction occurs. EG also acts as a reducing agent to reduce the metal ion to metal oxide. The easing of the nucleation limited process greatly assists in small particle formation. The EG additive and reaction by product were excluded through calcinations conveniently (*calcinations*: To heat (a substance) to a high temperature but below the melting or fusing point, causing loss of moisture, reduction or oxidation, and the decomposition of nitrates and other compounds).

Organic compounds (e.g. glycine, urea, thiourea, citric acid, alanine and carbohydrazide) as a fuel have been mixed directly with metal nitrates and chlorides enhance the efficiency of high yield synthesis. Actually, thiourea is used as a fuel and precipitating agent in synthesis reactions. When thiourea is used as fuel along with chloride and nitrate salt of a cation and heated at 200 °C the exothermic reaction between anion (oxidant reactant) and thiourea (fuel) leads to formation of corresponding nanocrystalline

oxides. The main advantage is that necessary heat for synthesis is obtained directly from the reaction in which the metal salts act both as oxidants and as cation sources, while the organic compound functions as the fuel. Among the known fuels, thiourea and urea seems to be the most convenient fuel to be employed, given that it is cheap and readily available commercially as well as its employment is safer in comparison with carcinogenic hydrazine-based hydrazide fuels.

Thiourea complexes decompose at a temperature of about 200°C the reaction to proceed slowly and control easily. Analytical grade compounds used in experiments were purchased from Merck, Fluka and Sigma-Aldrich. An appropriate ratio of metal salts thiourea to serve as fuel and EG were dissolved in MW tube with deionized water and then was placed in a kitchen-type microwave oven at a chosen power.

### 3.3. Experimental

#### 3.3.1. Synthesis of $\text{Ru}_{0.4}\text{Fe}_{0.6}\text{Al}_2\text{O}_3$ nanoparticles

Spherical  $\text{Ru}_{0.4}\text{Fe}_{0.6}\text{Al}_2\text{O}_3$  architectures were prepared by a microwave-assisted process. All of the raw materials were of analytical grade reagents and were used without further purification. In a typical experimental procedure,  $\text{Ru}_{0.4}\text{Fe}_{0.6}\text{Al}_2\text{O}_3$  was prepared from a mixture including (0.4 mmol, 0.105g) of  $\text{RuCl}_3 \cdot 3\text{H}_2\text{O}$ , (0.7 mmol, 0.283g) of  $\text{Fe}(\text{NO}_3)_3 \cdot 9\text{H}_2\text{O}$ , (2 mmol, 0.649 g) of Aluminum acetylacetonate ( $\text{Al}(\text{C}_5\text{H}_7\text{O}_2)_3$ ), each substance dissolved in small amount of deionized water with vigorous stirring in microwave teflon container tube (50 ml) and then thiourea (1 mmol, 0.076 g) was added to metal solution mixture and dissolved in addition of 10 ml deionized water to form a black-blue solution. At the end tube was filled with 10 ml of ethylene glycol (EG) and closed with teflon closer. The obtained mixture was located at the center of a microwave system and irradiated in constant power (600 W). The exposure time was 60 min at 200 °C. After the reaction was terminated, the product was allowed to cool to room temperature, the resulting dark black powders were rinsed and washed with deionized water and absolute ethanol several time until free from impurities. The precipitate was dried at 75 °C in a vacuum oven for 10 h to get the sample of  $\text{Ru}_{0.4}\text{Fe}_{0.6}\text{Al}_2\text{O}_3$ . Pure nanoparticles could be obtained The SEM, EDX, XRD and FT-IR of  $\text{Ru}_{0.4}\text{Fe}_{0.6}\text{Al}_2\text{O}_3$  nanoparticles, is shown in Figure 4.1a, 4.1b, 4.2, 4.3, 4.4, respectively.

Its structure were analyzed by X-ray Diffraction (XRD) using the Cu-K $\alpha$  radiation with 0.154 nm wavelength at 2 $\theta$  angle range from 10 to 70. The morphologies of the samples were observed by Scanning Electron Microscopy (SEM), using a Scanning electron microscopy (SEM) and Energy Dispersive X-Ray spectroscopy (EDX) employing an accelerating voltage of 15 Kv, same machine but different result characterizations (ZEISS Marker and EVO/LS10 Model). The Fourier Transform Infrared spectra (FT-IR) of the samples were recorded using a Perkin Elmer Marker, Spectrum 400 Model, FT-IR spectrometer.

### 3.3.2. Synthesis of Ru<sub>0.63</sub>Co<sub>0.37</sub>Al<sub>2</sub>O<sub>3</sub> nanoparticles

Spherical Ru<sub>0.63</sub>Co<sub>0.37</sub>Al<sub>2</sub>O<sub>3</sub> architectures were prepared by a microwave-assisted process. All of the raw materials were of analytical grade reagents and were used without further purification. In a typical experimental procedure, Ru<sub>0.63</sub>Co<sub>0.37</sub>Al<sub>2</sub>O<sub>3</sub> was prepared from a mixture including (0.4 mmol 0.105g) of RuCl<sub>3</sub>.3H<sub>2</sub>O, (0.6 mmol, 0.1495g) of Cobalt (II) chloride hexahydrate, CoCl<sub>2</sub>.6H<sub>2</sub>O, ( 2 mmol, 0.267g ) of Aluminum chloride (AlCl<sub>3</sub>), each substance dissolved in small amount of deionized water with vigorous stirring in microwave teflon container tube (50 ml) and then (1 mmol, 0.076 g) thiourea was added to metal solution mixture and dissolved in addition of 10 ml deionized water to form a black-blue solution. At the end tube was filled with 10 ml of EG and closed with teflon closer. The obtained mixture was located at the center of a microwave system and irradiated in constant power (600 W). The exposure time was 60 min at 200 °C. After the reaction was terminated, the product was allowed to cool to room temperature, the resulting dark black powders were rinsed and washed with deionized water and absolute ethanol several time until free from impurities. The precipitate was dried at 75 °C in a vacuum oven for 10 h to get the sample of Ru<sub>0.63</sub>Co<sub>0.37</sub>Al<sub>2</sub>O<sub>3</sub>. Pure nanoparticles could be obtained The SEM, EDX, XRD and FT-IR of Ru<sub>0.63</sub>Co<sub>0.37</sub>Al<sub>2</sub>O<sub>3</sub> nanoparticles, is shown in Figure 4.5a, 4.5b, 4.6, 4.7 and 4.8, respectively.

### 3.3.3. Synthesis of Ru<sub>0.93</sub>Ni<sub>0.07</sub>Al<sub>2</sub>O<sub>3</sub> nanoparticle

Spherical Ru<sub>0.93</sub>Ni<sub>0.07</sub>Al<sub>2</sub>O<sub>3</sub> architectures were prepared by a microwave-assisted process. All of the raw materials were of analytical grade reagents and were used without further purification. In a typical experimental procedure, Ru<sub>0.93</sub>Ni<sub>0.07</sub>Al<sub>2</sub>O<sub>3</sub> was prepared



from a mixture including (0.4 mmol, 0.105 g) of  $\text{RuCl}_3 \cdot 3\text{H}_2\text{O}$ , (0.6 mmol 0.143 g) of Nickel chloride hexahydrate  $\text{NiCl}_2 \cdot 6\text{H}_2\text{O}$ , (2 mmol, 0.267 g) of Aluminum chloride  $\text{AlCl}_3$ , each substance dissolved in small amount of deionized water with vigorous stirring in microwave Teflon container tube (50 ml) and then thiourea (1 m mol, 0.076 g) was added to metal solution mixture and dissolved in addition of 10 ml deionized water to form a black-blue solution. At the end tube was filled with 10 ml of EG and closed with teflon closer. The obtained mixture was located at the center of a microwave system and irradiated in constant power (600 W). The exposure time was 60 min at 200 °C. After the reaction was terminated, the product was allowed to cool to room temperature, the resulting dark black powders were rinsed and washed with deionized water and absolute ethanol several time until free from impurities. The precipitate was dried at 75 °C in a vacuum oven for 10 h to get the sample of  $\text{Ru}_{0.93}\text{Ni}_{0.07}\text{Al}_2\text{O}_3$ . Pure nanoparticles could be obtained The SEM, EDX, XRD and FT-IR of  $\text{Ru}_{0.93}\text{Ni}_{0.07}\text{Al}_2\text{O}_3$  nanoparticles, is shown in Figure 4.9a, 4.9b, 4.10, 4.11 and 4.12, respectively.

#### **3.3.4. Synthesis of $\text{Ru}_{0.54}\text{Cu}_{0.46}\text{Al}_2\text{O}_3$ nanoparticles**

Spherical  $\text{Ru}_{0.54}\text{Cu}_{0.46}\text{Al}_2\text{O}_3$  architectures were prepared by a microwave-assisted process. All of the raw materials were of analytical grade reagents and were used without further purification. In a typical experimental procedure,  $\text{Ru}_{0.54}\text{Cu}_{0.46}\text{Al}_2\text{O}_3$  was prepared from a mixture including (0.4 mmol, 0.105 g) of  $\text{RuCl}_3 \cdot 3\text{H}_2\text{O}$ , (0.6 mmol, 0.102 g) of Copper chloride dihydrate  $\text{CuCl}_2 \cdot 2\text{H}_2\text{O}$ , (2 mmol, 0.267 g) of Aluminum chloride ( $\text{AlCl}_3$ ), each substance dissolved in small amount of deionized water with vigorous stirring in microwave teflon container tube (50 ml) and then thiourea (1 mmol, 0.076 g) was added to metal solution mixture and dissolved in addition of 10 ml deionized water to form a black-blue solution. At the end tube was filled with 10 ml of EG and closed with teflon closer. The obtained mixture was located at the center of a microwave system and irradiated in constant power (600 W). The exposure time was 60 min at 200 °C. After the reaction was terminated, the product was allowed to cool to room temperature, the resulting dark black powders were rinsed and washed with deionized water and absolute ethanol several time until free from impurities. The precipitate was dried at 75 °C in a vacuum oven for 10 h to get the sample of  $\text{Ru}_{0.54}\text{Cu}_{0.46}\text{Al}_2\text{O}_3$ . Pure nanoparticles could be obtained The SEM, EDX,

XRD and FT-IR of  $\text{Ru}_{0.54}\text{Cu}_{0.46}\text{Al}_2\text{O}_3$  nanoparticles, is shown in Figure 4.13a, 4.13b, 4.14, 4.15 and 4.16, respectively.

### 3.3.5. Synthesis of $\text{Ru}_{0.62}\text{In}_{0.38}\text{Al}_2\text{O}_3$ nanoparticles

Spherical  $\text{Ru}_{0.62}\text{In}_{0.38}\text{Al}_2\text{O}_3$  architectures were prepared by a microwave-assisted process. All of the raw materials were of analytical grade reagents and were used without further purification. In a typical experimental procedure,  $\text{Ru}_{0.62}\text{In}_{0.38}\text{Al}_2\text{O}_3$  was prepared from a mixture including (0.4 mmol 0.105 g) of Ruthenium (III) chloride trihydrate  $\text{RuCl}_3 \cdot 3\text{H}_2\text{O}$ , (0.6 mmol, 0.133g) of Indium chloride  $\text{InCl}_3$ , (2 mmol 0.649 g) of Aluminum acetylacetonate ( $\text{Al}(\text{C}_5\text{H}_7\text{O}_2)_3$ ), each substance dissolved in small amount of deionized water with vigorous stirring in microwave teflon container tube (50 ml) and then thiourea (1 mmol, 0.076 g) was added to metal solution mixture and dissolved in addition of 10 ml deionized water to form a black-blue solution. At the end tube was filled with 10 ml of EG and closed with teflon closer. The obtained mixture was located at the center of a microwave system and irradiated in constant power (600 W). The exposure time was 60 min at 200 °C. After the reaction was terminated, the product was allowed to cool to room temperature, the resulting dark black powders were rinsed and washed with deionized water and absolute ethanol several time until free from impurities. The precipitate was dried at 75 °C in a vacuum oven for 10 h to get the sample of  $\text{Ru}_{0.62}\text{In}_{0.38}\text{Al}_2\text{O}_3$ . Pure nanoparticles could be obtained The SEM, EDX, XRD and FT-IR of  $\text{Ru}_{0.62}\text{In}_{0.38}\text{Al}_2\text{O}_3$  nanoparticles, is shown in Figure 4.17, 4.18, 4.19 and 4.20, respectively.

### 3.3.6. Synthesis of $\text{Ru}_{0.77}\text{Co}_{0.23}\text{In}_2\text{O}_3$ nanoparticles

Spherical  $\text{Ru}_{0.77}\text{Co}_{0.23}\text{In}_2\text{O}_3$  architectures were prepared by a microwave-assisted process. All of the raw materials were of analytical grade reagents and were used without further purification. In a typical experimental procedure,  $\text{Ru}_{0.77}\text{Co}_{0.23}\text{In}_2\text{O}_3$  was prepared from a mixture including (0.4 mmol 0.105g) of Ruthenium (III) chloride trihydrate  $\text{RuCl}_3 \cdot 3\text{H}_2\text{O}$ , (2 mmol 0.443 g) of Indium chloride,  $\text{InCl}_3$ , (0.6 mmol 0.1495g) of  $\text{Co}(\text{C}_2\text{H}_3\text{O}_2)_2 \cdot 4\text{H}_2\text{O}$ , each substance dissolved in small amount of deionized water with vigorous stirring in microwave teflon container tube (50 ml) and then thiourea (1 mmol, 0.076 g) was added to metal solution mixture and dissolved in addition of 10 ml deionized water to form a black-blue solution. At the end tube was filled with 10 ml of EG and

closed with teflon closer. The obtained mixture was located at the center of a microwave system and irradiated in constant power (600 W). The exposure time was 60 min at 200 °C. After the reaction was terminated, the product was allowed to cool to room temperature, the resulting dark black powders were rinsed and washed with deionized water and absolute ethanol several time until free from impurities. The precipitate was dried at 75 °C in a vacuum oven for 10 h to get the sample of  $\text{Ru}_{0.77}\text{Co}_{0.23}\text{In}_2\text{O}_3$ . Pure nanoparticles could be obtained The SEM, EDX, XRD and FT-IR of  $\text{Ru}_{0.77}\text{Co}_{0.23}\text{In}_2\text{O}_3$  nanoparticles, is shown in Figure 4.21a, 4.21b, 4.22, 4.23 and 4.24, respectively.

### 3.3.7. Synthesis of $\text{Ru}_{0.65}\text{Ni}_{0.35}\text{In}_2\text{O}_3$ nanoparticles

Spherical  $\text{Ru}_{0.65}\text{Ni}_{0.35}\text{In}_2\text{O}_3$  architectures were prepared by a microwave-assisted process. All of the raw materials were of analytical grade reagents and were used without further purification. In a typical experimental procedure,  $\text{Ru}_{0.65}\text{Ni}_{0.35}\text{In}_2\text{O}_3$  was prepared from a mixture including (0.4 mmol, 0.105 g) of Ruthenium (III) chloride trihydrate  $\text{RuCl}_3 \cdot 3\text{H}_2\text{O}$ , (2 mmol 0.443 g) of Indium chloride  $\text{InCl}_3$ , (0.6 mmol, 0.143 g) of Nickel chloride hexahydrate  $\text{NiCl}_2 \cdot 6\text{H}_2\text{O}$ , each substance dissolved in small amount of deionized water with vigorous stirring in microwave teflon container tube (50 ml) and then thiourea (1 mmol, 0.076 g) was added to metal solution mixture and dissolved in addition of 10 ml deionized water to form a black-blue solution. At the end tube was filled with 10 ml of EG and closed with teflon closer. The obtained mixture was located at the center of a microwave system and irradiated in constant power (600 W). The exposure time was 60 min at 200 °C. After the reaction was terminated, the product was allowed to cool to room temperature, the resulting dark black powders were rinsed and washed with deionized water and absolute ethanol several time until free from impurities. The precipitate was dried at 75 °C in a vacuum oven for 10 h to get the sample of  $\text{Ru}_{0.65}\text{Ni}_{0.35}\text{In}_2\text{O}_3$ . Pure nanoparticles could be obtained The SEM, EDX, XRD and FT-IR of  $\text{Ru}_{0.65}\text{Ni}_{0.35}\text{In}_2\text{O}_3$  nanoparticles, is shown in Figure 4.25, 4.26, 4.27 and 4.28, respectively.

### 3.3.8. Synthesis of $\text{Ru}_{0.92}\text{Pd}_{0.08}\text{In}_2\text{O}_3$ nanoparticles

Spherical  $\text{Ru}_{0.92}\text{Pd}_{0.08}\text{In}_2\text{O}_3$  architectures were prepared by a microwave-assisted process. All of the raw materials were of analytical grade reagents and were used without further purification. In a typical experimental procedure,  $\text{Ru}_{0.92}\text{Pd}_{0.08}\text{In}_2\text{O}_3$  was prepared from a mixture including (0.4 mmol 0.105 g) of Ruthenium (III) chloride trihydrate  $\text{RuCl}_3 \cdot 3\text{H}_2\text{O}$ , (2 mmol 0.0443 g) of Indium chloride,  $\text{InCl}_3$ , (0.6 mmol, 0.106 g) of Palladium chloride,  $\text{PdCl}_2$ , each substance dissolved in small amount of deionized water with vigorous stirring in microwave teflon container tube (50 ml) and then thiourea (1 mmol, 0.076 g) was added to metal solution mixture and dissolved in addition of 10 ml deionized water to form a black-blue solution. At the end tube was filled with 10 ml of EG and closed with teflon closer. The obtained mixture was located at the center of a microwave system and irradiated in constant power (600 W). The exposure time was 60 min at 200 °C. After the reaction was terminated, the product was allowed to cool to room temperature, the resulting dark black powders were rinsed and washed with deionized water and absolute ethanol several time until free from impurities. The precipitate was dried at 75 °C in a vacuum oven for 10 h to get the sample of  $\text{Ru}_{0.92}\text{Pd}_{0.08}\text{In}_2\text{O}_3$ . Pure nanoparticles could be obtained The SEM, EDX, XRD and FT-IR of  $\text{Ru}_{0.92}\text{Pd}_{0.08}\text{In}_2\text{O}_3$  nanoparticles, is shown in Figure 4.29a, 4.29b, 4.30, 4.31 and 4.32, respectively.

### 3.3.9. Synthesis of $\text{Ru}_{0.54}\text{Pt}_{0.46}\text{In}_2\text{O}_3$ nanoparticles

Spherical  $\text{Ru}_{0.54}\text{Pt}_{0.46}\text{In}_2\text{O}_3$  architectures were prepared by a microwave-assisted process. All of the raw materials were of analytical grade reagents and were used without further purification. In a typical experimental procedure,  $\text{Ru}_{0.54}\text{Pt}_{0.46}\text{In}_2\text{O}_3$  was prepared from a mixture including (0.4 mmol, 0.105g) of Ruthenium (III) chloride trihydrate  $\text{RuCl}_3 \cdot 3\text{H}_2\text{O}$ , (2 mmol 0.443 g) of Indium chloride,  $\text{InCl}_3$ , (0.6 mmol 0.160 g) of Platinum (II) chloride,  $\text{PtCl}_2$ , each substance dissolved in small amount of deionized water with vigorous stirring in microwave teflon container tube (50 ml) and then thiourea (1 mmol, 0.076 g) was added to metal solution mixture and dissolved in addition of 10 ml deionized water to form a black-blue solution. At the end tube was filled with 10 ml of EG and closed with teflon closer. The obtained mixture was located at the center of a microwave system and irradiated in constant power (600 W). The exposure time was 60 min at 200 °C. After the reaction was terminated, the product was allowed to cool to room temperature, the resulting dark black powders were rinsed and washed with deionized water and

absolute ethanol several time until free from impurities. The precipitate was dried at 75 °C in a vacuum oven for 10 h to get the sample of  $\text{Ru}_{0.54}\text{Pt}_{0.46}\text{In}_2\text{O}_3$ . Pure nanoparticles could be obtained The SEM, EDX, XRD and FT-IR of  $\text{Ru}_{0.54}\text{Pt}_{0.46}\text{In}_2\text{O}_3$  nanoparticles, is shown in Figure 4.33a, 4.33b, 4.34, 4.35 and 4.36, respectively.

### 3.3.10. Synthesis of $\text{Ru}_{0.56}\text{Cu}_{0.44}\text{In}_2\text{O}_3$ nanoparticles

Spherical  $\text{Ru}_{0.56}\text{Cu}_{0.44}\text{In}_2\text{O}_3$  architectures were prepared by a microwave-assisted process. All of the raw materials were of analytical grade reagents and were used without further purification. In a typical experimental procedure,  $\text{Ru}_{0.56}\text{Cu}_{0.44}\text{In}_2\text{O}_3$  was prepared from a mixture including (0.4 mmol, 0.105 g) of Ruthenium (III) chloride trihydrate  $\text{RuCl}_3 \cdot 3\text{H}_2\text{O}$ , (2 mmol 0.443 g) of Indium chloride  $\text{InCl}_3$ , (0.6 mmol, 0.102 g) of Copper chloride dihydrate  $\text{CuCl}_2 \cdot 2\text{H}_2\text{O}$ , each substance dissolved in small amount of deionized water with vigorous stirring in microwave teflon container tube (50 ml) and then thiourea (1 mmol, 0.076 g) was added to metal solution mixture and dissolved in addition of 10 ml deionized water to form a black-blue solution. At the end tube was filled with 10 ml of EG and closed with teflon closer. The obtained mixture was located at the center of a microwave system and irradiated in constant power (600 W). The exposure time was 60 min at 200 °C. After the reaction was terminated, the product was allowed to cool to room temperature, the resulting dark black powders were rinsed and washed with deionized water and absolute ethanol several time until free from impurities. The precipitate was dried at 75 °C in a vacuum oven for 10 h to get the sample of  $\text{Ru}_{0.56}\text{Cu}_{0.44}\text{In}_2\text{O}_3$ . Pure nanoparticles could be obtained The SEM, EDX, XRD and FT-IR of  $\text{Ru}_{0.56}\text{Cu}_{0.44}\text{In}_2\text{O}_3$  nanoparticles, is shown in Figure 4.37a, 4.37b, 4.38, 4.39 and 4.40, respectively.

## 4. RESULTS AND DISCUSSION

### 4.1. NPs of $\text{Ru}_{0.4}\text{Fe}_{0.6}\text{Al}_2\text{O}_3$

#### 4.1.1. SEM analysis of $\text{Ru}_{0.4}\text{Fe}_{0.6}\text{Al}_2\text{O}_3$

The surface morphology of  $\text{Ru}_{0.4}\text{Fe}_{0.6}\text{Al}_2\text{O}_3$  was investigated by the scanning electron microscopy images SEM as shown in Figure 4.1a and 4.1b. From the images, figures show the formation of nanoparticles for  $\text{Ru}_{0.4}\text{Fe}_{0.6}\text{Al}_2\text{O}_3$ . It can be observed from Figures 4.1a and 4.1b that the structure is actually composed of numerous nanosphere that are intercrossed with each other to form amorphous like structure. This is probably due to the polarization of the molecules under the rapidly changing electro-magnetic field of the microwave reactor, which may result in transient, localized high temperatures for the reaction system, leading to fast synthesis with desired morphology. Figure 4.1b shows that the average diameter of nanoparticles less than 100 nm. Real particle size can not be measured because of amorphes structure. It is a well-known fact that the temperature and reaction time are the two important factors in determining the morphology of the nanomaterials. In the conventional method, the reaction time is kept as 3 h, at 400 °C, which resulted in the formation of nanoparticles. But in microwave method, because of rapid heating, which is achieved within the few minutes, due to the suppressed diffusion process, the nano-amorphous would have been formed. The morphology is irregular and the product is amorphous phase [73].

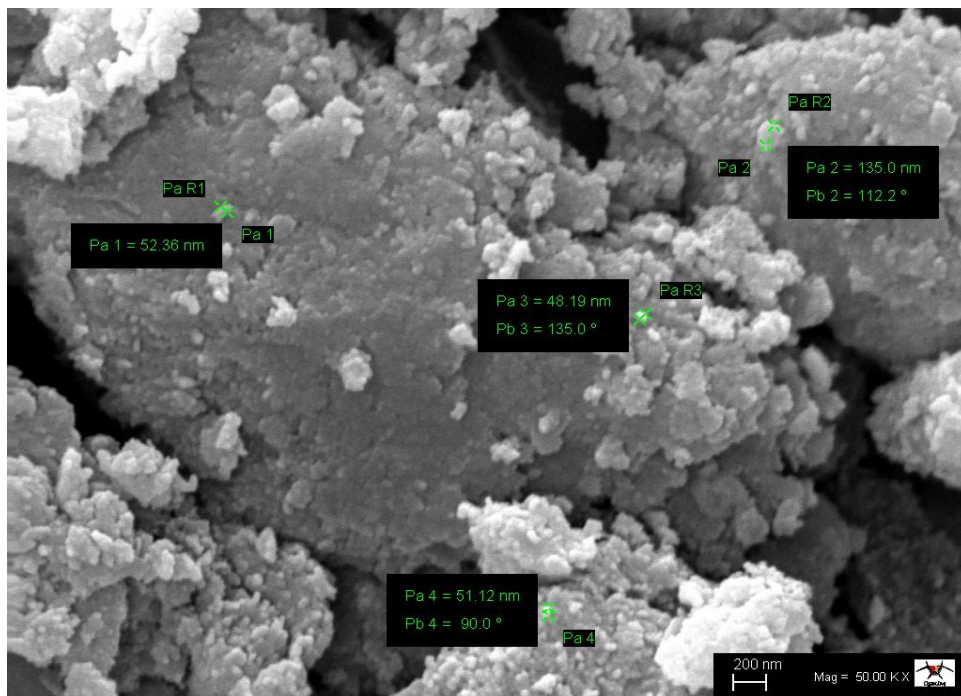


Figure 4.1a. SEM image of Ru<sub>0.4</sub>Fe<sub>0.6</sub>Al<sub>2</sub>O<sub>3</sub> nanoparticles prepared.

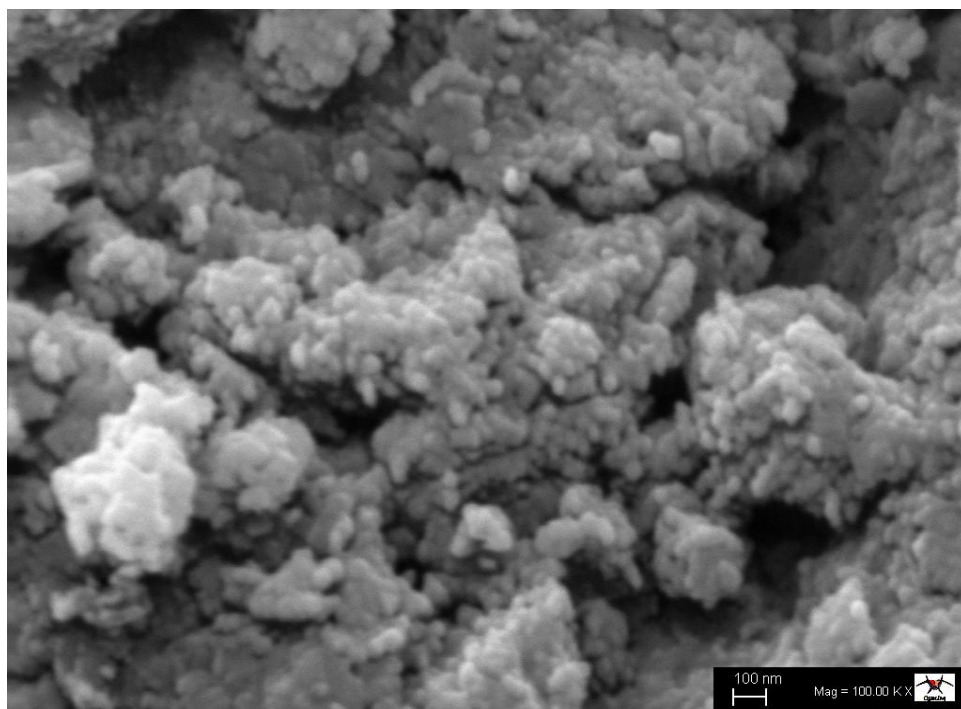


Figure 4.1b. SEM image of Ru<sub>0.4</sub>Fe<sub>0.6</sub>Al<sub>2</sub>O<sub>3</sub> nanoparticles prepared.

#### 4.1.2. EDX analysis of $\text{Ru}_{0.4}\text{Fe}_{0.6}\text{Al}_2\text{O}_3$

The formation of pure  $\text{Ru}_{0.4}\text{Fe}_{0.6}\text{Al}_2\text{O}_3$  was confirmed by means of energy dispersive X-ray analysis (EDX) as shown in Figure 4.2. The EDX result showed the presence of  $\text{Ru}_{0.4}\text{Fe}_{0.6}\text{Al}_2\text{O}_3$  by the appearance of Ru, Fe, Al and O peaks in the spectrum. The absence of carbon, nitrogen and other impurities are also evidenced from the EDX spectrum. This analysis confirmed that the sample  $\text{Ru}_{0.4}\text{Fe}_{0.6}\text{Al}_2\text{O}_3$  prepared by microwave-assisted method. Hence, the result is definitive evidence to suggest that the sample does not contain any other element and are indeed free from other impurities. The peaks at 2.1–2.2 keV in the EDX spectra are due to the gold, which is coated on the samples before recording SEM [74].

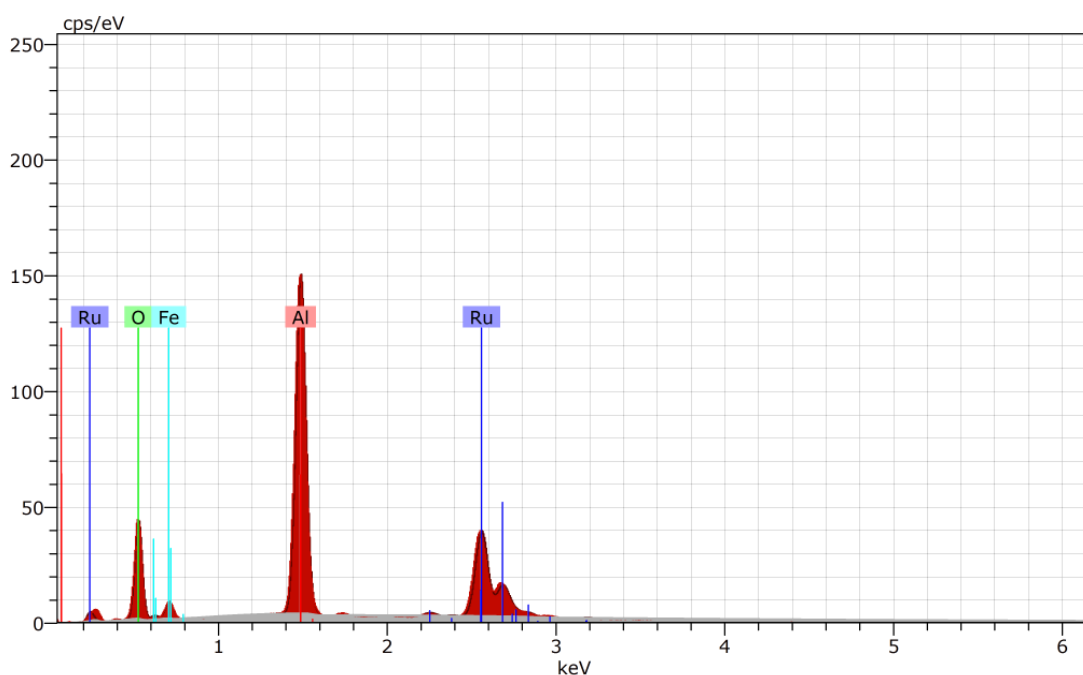


Figure 4.2. EDX spectrum of  $\text{Ru}_{0.4}\text{Fe}_{0.6}\text{Al}_2\text{O}_3$  nanoparticles

#### 4.1.3. XRD analysis of $\text{Ru}_{0.4}\text{Fe}_{0.6}\text{Al}_2\text{O}_3$

Powder characterization, shaping and conventional sintering the crystalline phase was identified by XRD using the  $\text{Cu-K}\alpha$  radiation with 0.154 nm wavelength at  $2\theta$  angle range from 10 to 70. In order to investigate the crystal structure of the obtained powder material XRD analysis was performed and the resultant pattern of the as-prepared sample is presented in Fig. 1. In agreement with XRD patterns, a crystalline product appeared after



60 min of reaction at 200 °C. As shown in Figure 4.3, X-ray diffraction (XRD) can be used to study the phase purity of the obtained  $\text{Ru}_{0.4}\text{Fe}_{0.6}\text{Al}_2\text{O}_3$  nanoparticles.

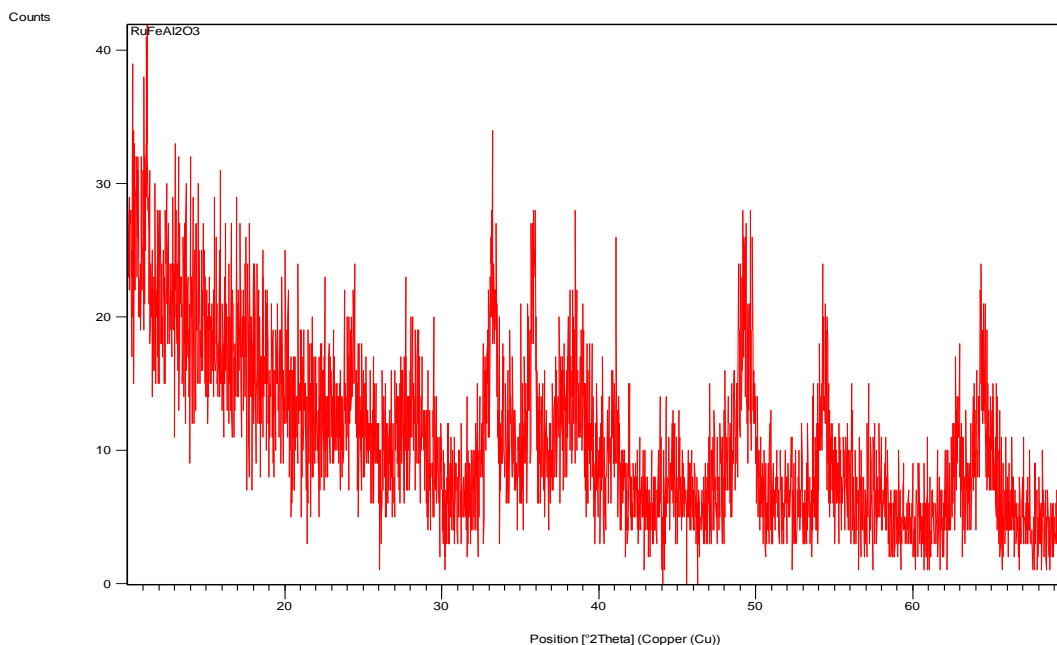


Figure 4.3. X-ray diffraction patterns of the  $\text{Ru}_{0.4}\text{Fe}_{0.6}\text{Al}_2\text{O}_3$  nanoparticles

#### 4.1.4. FT-IR analysis of $\text{Ru}_{0.4}\text{Fe}_{0.6}\text{Al}_2\text{O}_3$

The FT-IR spectroscopy is the most powerful and useful technique adopted by all the chemists to analyze, confirm and elucidate the structure of compounds and to identify the functional groups present in them. To confirm the formation of  $\text{Ru}_{0.4}\text{Fe}_{0.6}\text{Al}_2\text{O}_3$  nanoparticles, the FT-IR spectra of the  $\text{Ru}_{0.4}\text{Fe}_{0.6}\text{Al}_2\text{O}_3$  powders synthesized by microwave-assisted method at the ignition temperature of 200 °C, were obtained. Figure 4.4 shows FT-IR spectra of nanoparticles in the range 400–4000  $\text{cm}^{-1}$ . The peaks around 3311 and 1617  $\text{cm}^{-1}$  can be attributed to the stretching vibrations of hydrogen-bonded surface water molecules and the free hydroxyl (-OH) groups of water molecules from ambient atmosphere, respectively [75]. The absorption bands at 2076 and 1167  $\text{cm}^{-1}$  are related to the stretching vibration of thiocarbonyl (C=S) and ethylene glycol (C–O) groups of the residual organic fuel and reducing agent. The absorption bands in the range 410–879  $\text{cm}^{-1}$  appears due to the formation of metal oxides. These intense and weak absorption band are visible at 400–1062  $\text{cm}^{-1}$  range are associated with the bending and stretching modes of the metal–oxygen and the metal-oxygen-metal bonds corresponding to  $\text{Ru}_{0.4}\text{Fe}_{0.6}\text{Al}_2\text{O}_3$

nanoparticle. Moreover the spectra of the  $\text{Ru}_{0.4}\text{Fe}_{0.6}\text{Al}_2\text{O}_3$  showed the peak at  $1411\text{ cm}^{-1}$ , which is assigned to the Al-O stretching vibrations [76].

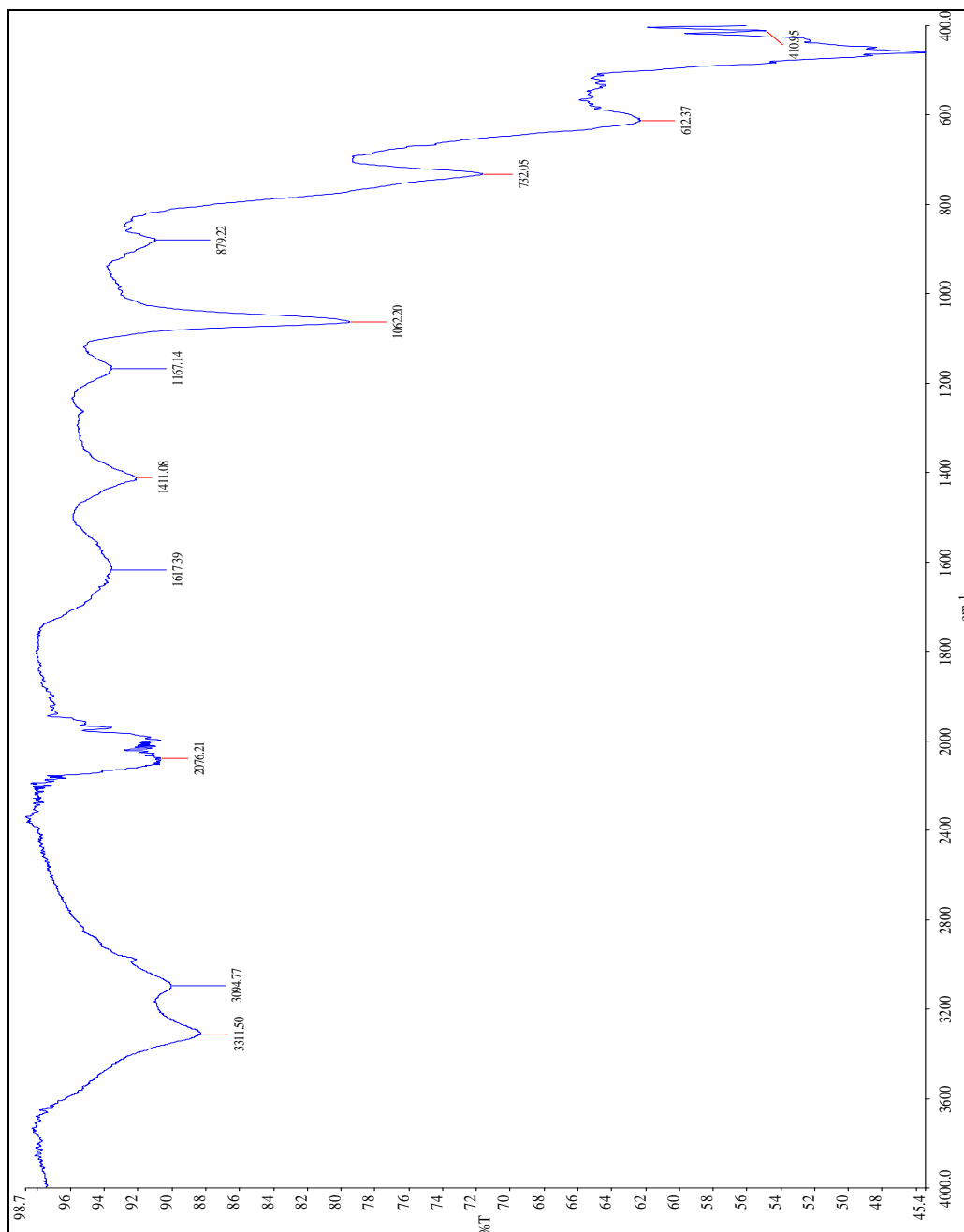


Figure 4.4. The FT-IR spectra of  $\text{Ru}_{0.4}\text{Fe}_{0.6}\text{Al}_2\text{O}_3$  nanoparticles

## 4.2. NPs of $\text{Ru}_{0.63}\text{Co}_{0.37}\text{Al}_2\text{O}_3$

### 4.2.1. SEM analysis of $\text{Ru}_{0.63}\text{Co}_{0.37}\text{Al}_2\text{O}_3$

The surface morphology of  $\text{Ru}_{0.63}\text{Co}_{0.37}\text{Al}_2\text{O}_3$  was investigated by the SEM as shown in Figures 4.5a and 4.5b. From the images, Figures shows the formation of nanoparticles for  $\text{Ru}_{0.63}\text{Co}_{0.37}\text{Al}_2\text{O}_3$ . It can be observed from Figures 4.5a and 4.5b. That the structure is actually composed of numerous nanosphere that are intercrossed with each other to form amorphous like structure. This is probably due to the polarization of the molecules under the rapidly changing electro-magnetic field of the microwave reactor, which may result in transient, localized high temperatures for the reaction system, leading to fast synthesis with desired morphology. Figure 4.5b shows that the average diameter of nanoparticles less than 100 nm. Real particle size can not be measured because of amorphous structure. It is a well-known fact that the temperature and reaction time are the two important factors in determining the morphology of the nanomaterials. In the conventional method, the reaction time is kept as 3 h, at 400 °C, which resulted in the formation of nanoparticles. But in microwave method, because of rapid heating, which is achieved within the few minutes, due to the suppressed diffusion process, the nano-amorphous would have been formed.

The morphologies of the final products are characterized by SEM Figure 4.5b is a typical low-magnification SEM image of  $\text{Ru}_{0.63}\text{Co}_{0.37}\text{Al}_2\text{O}_3$ , which is composed of many uniform flower-like microstructures with a diameter of ca. 5 nm. The high-magnification SEM image figure 4.5b reveals that the flower-like microstructure is built from many thin sheets with a thickness about 10 nm. These nanoflakes are intercrossed each other and aggregated together to form flower-like microstructures. At 200 °C, the novel  $\text{Ru}_{0.63}\text{Co}_{0.37}\text{Al}_2\text{O}_3$  flower-like microstructures and nanoparticles were harvested as Figure 4.5b.

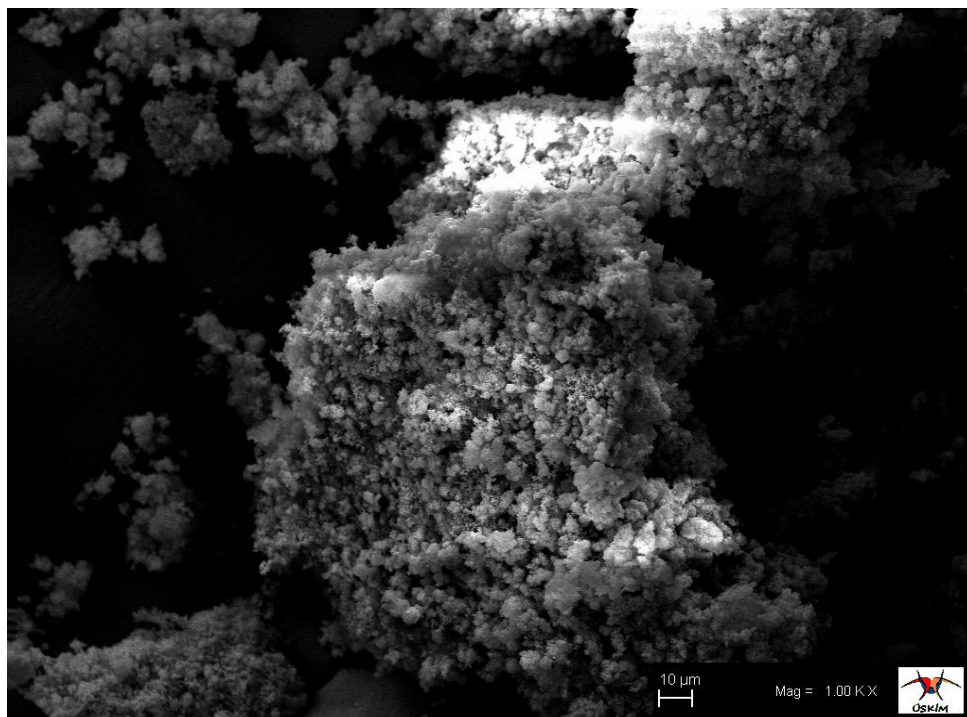


Figure 4.5 a. SEM images of Ru<sub>0.63</sub>Co<sub>0.37</sub>Al<sub>2</sub>O<sub>3</sub> nanoparticles prepared

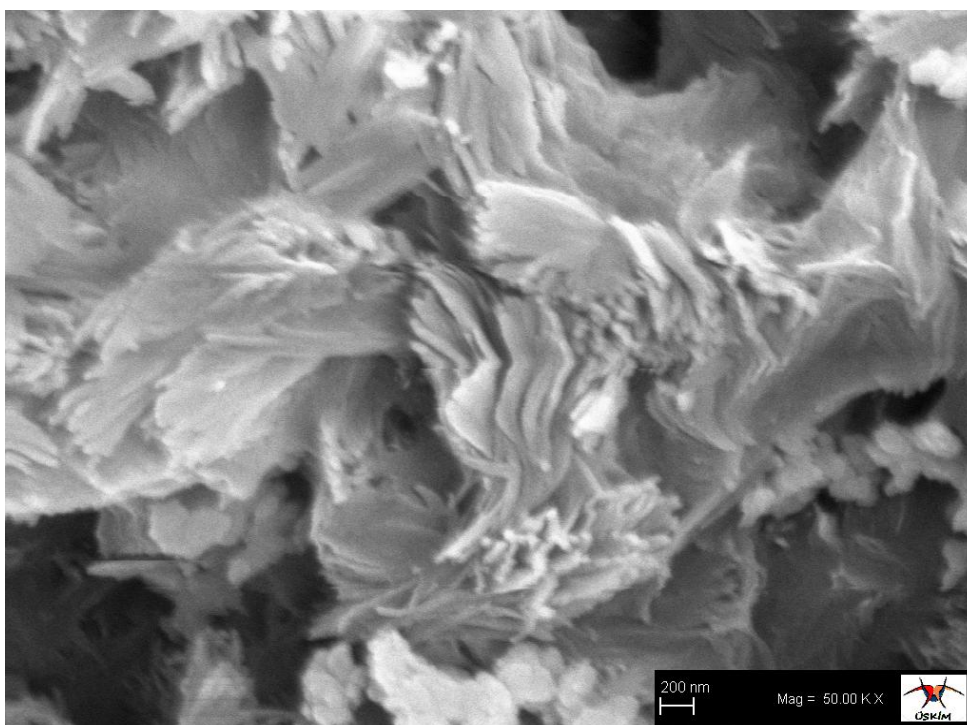


Figure 4.5 b. SEM images of Ru<sub>0.63</sub>Co<sub>0.37</sub>Al<sub>2</sub>O<sub>3</sub> nanoparticles prepared

#### 4.2.2. EDX analysis of $\text{Ru}_{0.63}\text{Co}_{0.37}\text{Al}_2\text{O}_3$

The formation of pure  $\text{Ru}_{0.63}\text{Co}_{0.37}\text{Al}_2\text{O}_3$  was confirmed by means of EDX as shown in Figure 4.6. The EDX result showed the presence of  $\text{Ru}_{0.63}\text{Co}_{0.37}\text{Al}_2\text{O}_3$  by the appearance of Ru, Co, Al and O peaks in the spectrum. The absence of carbon, nitrogen and other impurities are also evidenced from the EDX spectrum. This analysis confirmed that the sample  $\text{Ru}_{0.63}\text{Co}_{0.37}\text{Al}_2\text{O}_3$  prepared by microwave-assisted method. Hence, the result is definitive evidence to suggest that the sample does not contain any other element and are indeed free from other impurities. The peaks at 2.1–2.2 keV in the EDX spectra are due to the gold, which is coated on the samples before recording SEM.

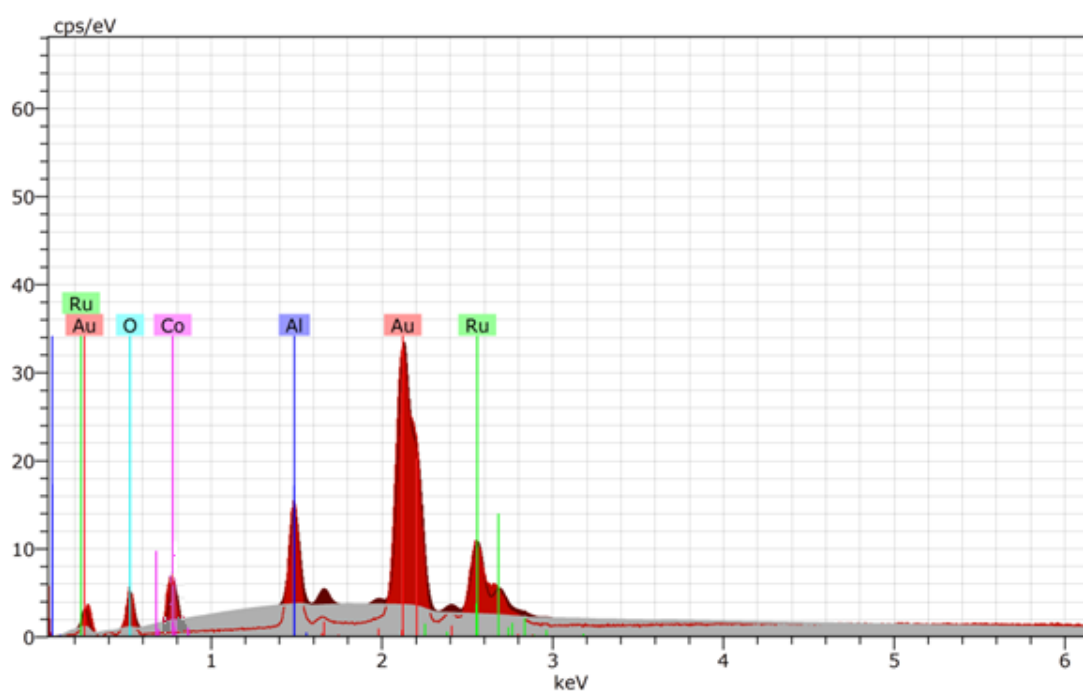


Figure 4.6. EDX spectrum of  $\text{Ru}_{0.63}\text{Co}_{0.37}\text{Al}_2\text{O}_3$  nanoparticles

#### 4.2.3. XRD analysis of $\text{Ru}_{0.63}\text{Co}_{0.37}\text{Al}_2\text{O}_3$

Powder characterization, shaping and conventional sintering the crystalline phase was identified by XRD using the  $\text{Cu-K}\alpha$  radiation with 0.154 nm wavelength at  $2\theta$  angle range from 10 to 70. In order to investigate the crystal structure of the obtained powder material XRD analysis was performed and the resultant pattern of the as-prepared sample is presented in Figure 4.7. In agreement with XRD patterns, a crystalline product appeared

after 60 min of reaction at 200 °C. As shown in Figure 4.7, XRD can be used to study the phase purity of the obtained  $\text{Ru}_{0.63}\text{Co}_{0.37}\text{Al}_2\text{O}_3$  nanoparticles.

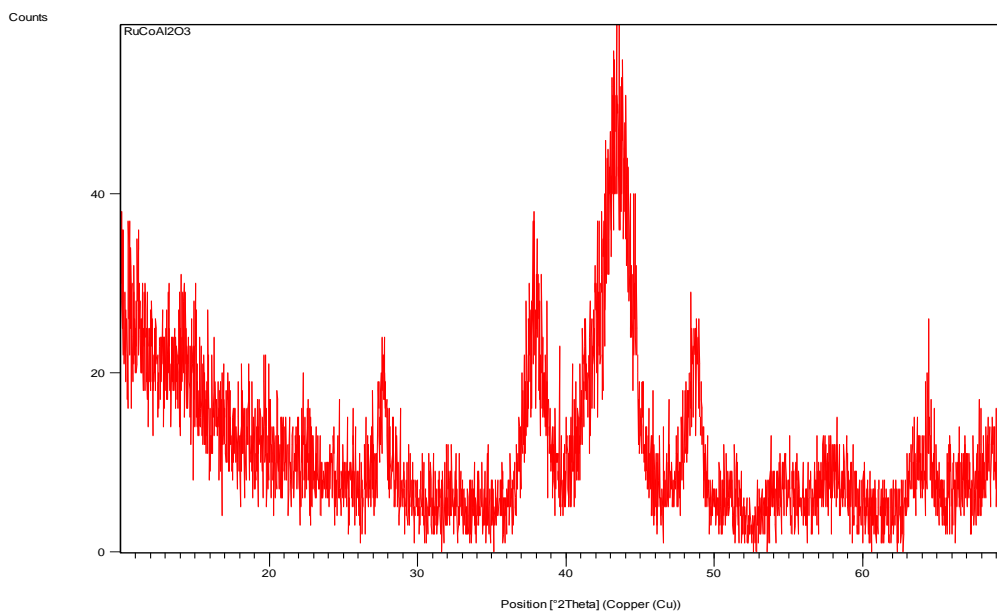


Figure 4.7. X-ray diffraction patterns of the  $\text{Ru}_{0.63}\text{Co}_{0.37}\text{Al}_2\text{O}_3$  nano particles

#### 4.2.4. FT-IR analysis of $\text{Ru}_{0.63}\text{Co}_{0.37}\text{Al}_2\text{O}_3$

The FT-IR spectroscopy is the most powerful and useful technique adopted by all the chemists to analyze, confirm and elucidate the structure of compounds and to identify the functional groups present in them. To confirm the formation of  $\text{Ru}_{0.63}\text{Co}_{0.37}\text{Al}_2\text{O}_3$  nanoparticles, the FT-IR spectra of the  $\text{Ru}_{0.63}\text{Co}_{0.37}\text{Al}_2\text{O}_3$  powders synthesized by microwave-assisted method at the ignition temperature of 200 °C, were obtained. Figure 4.8 show FT-IR spectra of nanoparticles in the range 400–4000  $\text{cm}^{-1}$ . The peaks around 3272 and 1616  $\text{cm}^{-1}$  can be attributed to the stretching vibrations of hydrogen-bonded surface water molecules and the free hydroxyl (-OH) groups of water molecules from ambient atmosphere, respectively. The absorption bands in the range 404–881  $\text{cm}^{-1}$  appears due to the formation of metal oxides. These intense and weak absorption band are visible at 400–1064  $\text{cm}^{-1}$  range are associated with the bending and stretching modes of the metal–oxygen and the metal-oxygen-metal bonds corresponding to  $\text{Ru}_{0.63}\text{Co}_{0.37}\text{Al}_2\text{O}_3$  nanoparticle. Moreover the spectra of the  $\text{Ru}_{0.63}\text{Co}_{0.37}\text{Al}_2\text{O}_3$  showed the very weak peak at 1445  $\text{cm}^{-1}$ , which is assigned to the Al-O stretching vibrations.

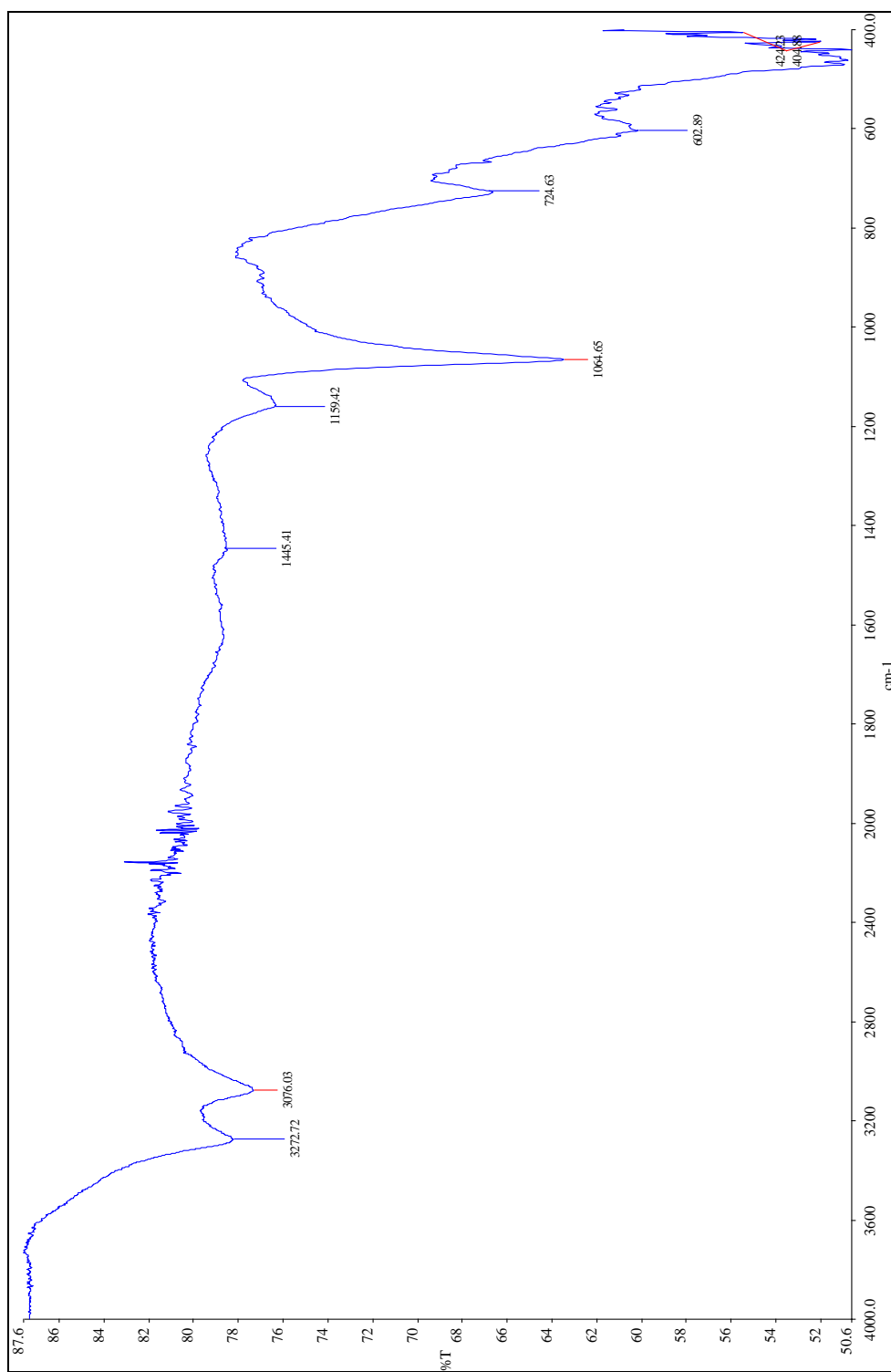


Figure 4.8. The FT-IR spectra of Ru<sub>0.63</sub>Co<sub>0.37</sub>Al<sub>2</sub>O<sub>3</sub> nanoparticles

### 4.3. NPs of $\text{Ru}_{0.93}\text{Ni}_{0.07}\text{Al}_2\text{O}_3$

#### 4.3.1. SEM analysis of $\text{Ru}_{0.93}\text{Ni}_{0.07}\text{Al}_2\text{O}_3$

The surface morphology of  $\text{Ru}_{0.93}\text{Ni}_{0.07}\text{Al}_2\text{O}_3$  was investigated by the SEM as shown in Figure 4.9a and 4.9b. From the images, Figures shows the formation of nanoparticles for  $\text{Ru}_{0.93}\text{Ni}_{0.07}\text{Al}_2\text{O}_3$ . It can be observed from Figure 4.9a and 4.9b. That the structure is actually composed of numerous nanosphere that are intercrossed with each other to form amorphous like structure. This is probably due to the polarization of the molecules under the rapidly changing electro-magnetic field of the microwave reactor, which may result in transient, localized high temperatures for the reaction system, leading to fast synthesis with desired morphology. Figure 4.9b show that the average diameter of nanoparticles less than 100 nm. Real particle size can not be measured because of amorphes structure. It is a well-known fact that the temperature and reaction time are the two important factors in determining the morphology of the nanomaterials. In the conventional method, the reaction time is kept as 3 h, at 400 °C, which resulted in the formation of nanoparticles. But in microwave method, because of rapid heating, which is achieved within the few minutes, due to the suppressed diffusion process, the nano-amorphous would have been formed.

The morphologies of the final products are characterized by SEM. Figure 4.9b is a typical low-magnification SEM image of  $\text{Ru}_{0.93}\text{Ni}_{0.07}\text{Al}_2\text{O}_3$ , which is composed of many uniform flower-like microstructures with a range diameter of 36-66 nm. The high-magnification SEM image Figure 4.9b reveals that the flower-like microstructure is built from many thin sheets with a thickness about 10 nm. These nanoflakes are intercrossed each other and aggregated together to form flower-like microstructures. At 200 °C, the novel  $\text{Ru}_{0.93}\text{Ni}_{0.07}\text{Al}_2\text{O}_3$  flower-like microstructures and nanoparticles were harvested as Figure 4.9b [77].



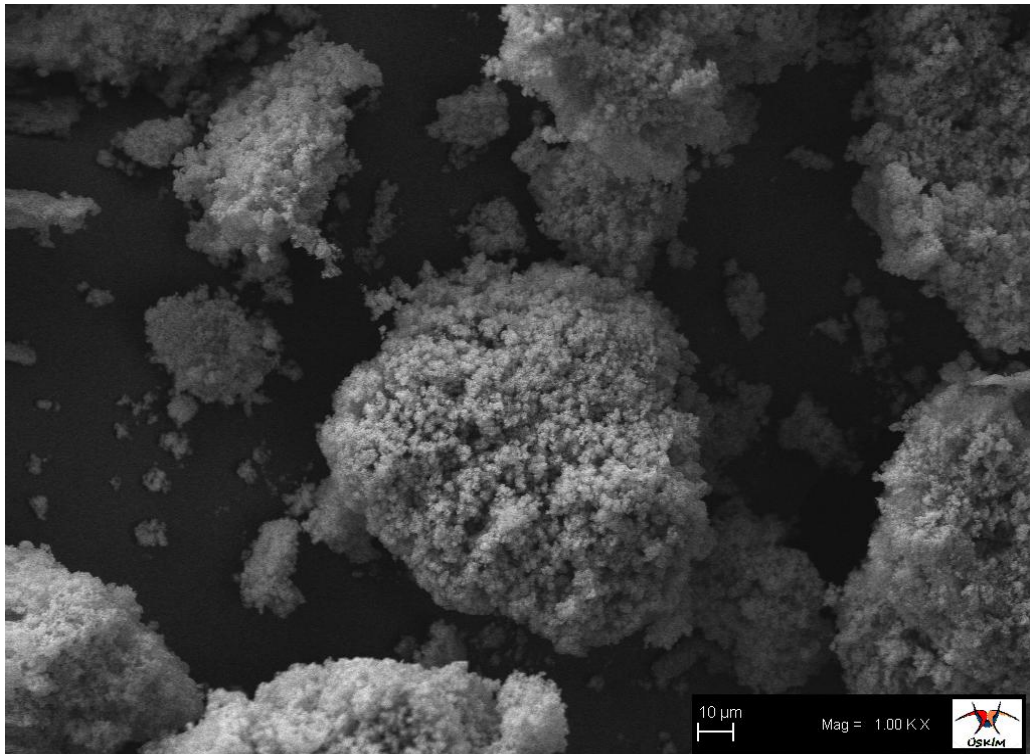


Figure 4.9a. SEM images of  $\text{Ru}_{0.93}\text{Ni}_{0.07}\text{Al}_2\text{O}_3$  nanoparticles prepared

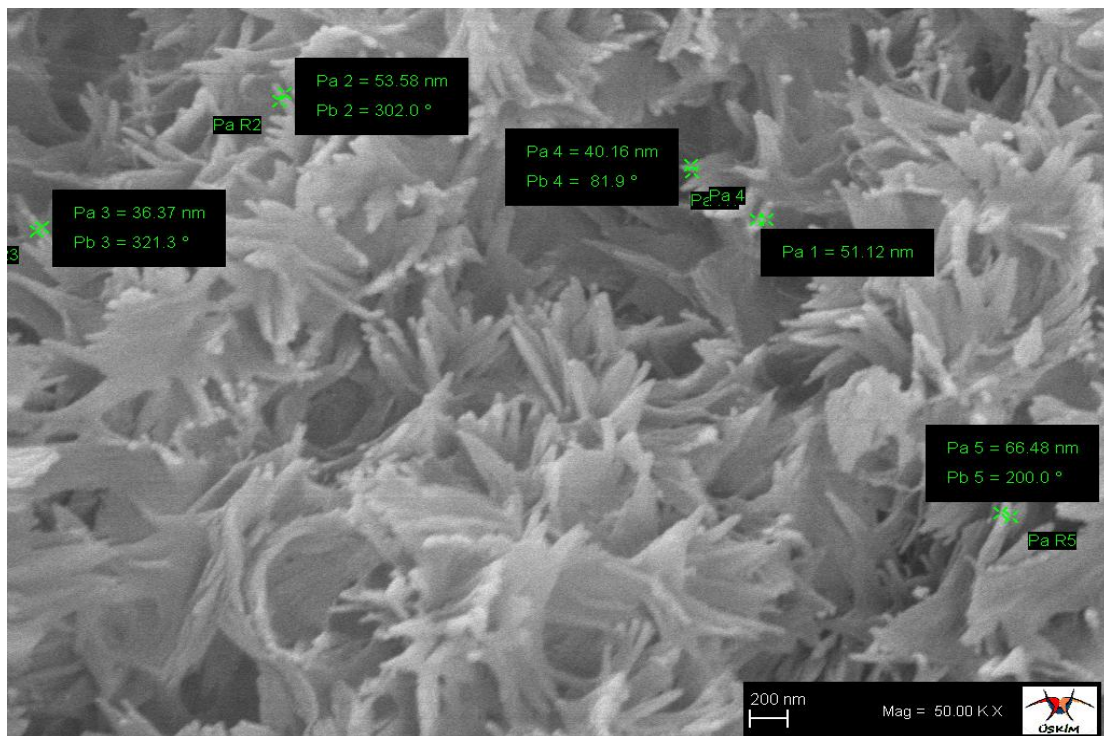


Figure 4.9b. SEM images of  $\text{Ru}_{0.93}\text{Ni}_{0.07}\text{Al}_2\text{O}_3$  nanoparticles prepared

#### 4.3.2. EDX analysis of $\text{Ru}_{0.93}\text{Ni}_{0.07}\text{Al}_2\text{O}_3$

The formation of pure  $\text{Ru}_{0.93}\text{Ni}_{0.07}\text{Al}_2\text{O}_3$  was confirmed by means of EDX as shown in Figure 4.10. The EDX result showed the presence of  $\text{Ru}_{0.93}\text{Ni}_{0.07}\text{Al}_2\text{O}_3$  by the appearance of Ru, Ni, Al and O peaks in the spectrum. The absence of carbon, nitrogen and other impurities are also evidenced from the EDX spectrum. This analysis confirmed that the sample  $\text{Ru}_{0.93}\text{Ni}_{0.07}\text{Al}_2\text{O}_3$  prepared by microwave-assisted method. Hence, the result is definitive evidence to suggest that the sample does not contain any other element and are indeed free from other impurities. The peaks at 2.1–2.2 keV in the EDX spectra are due to the gold, which is coated on the samples before recording SEM.

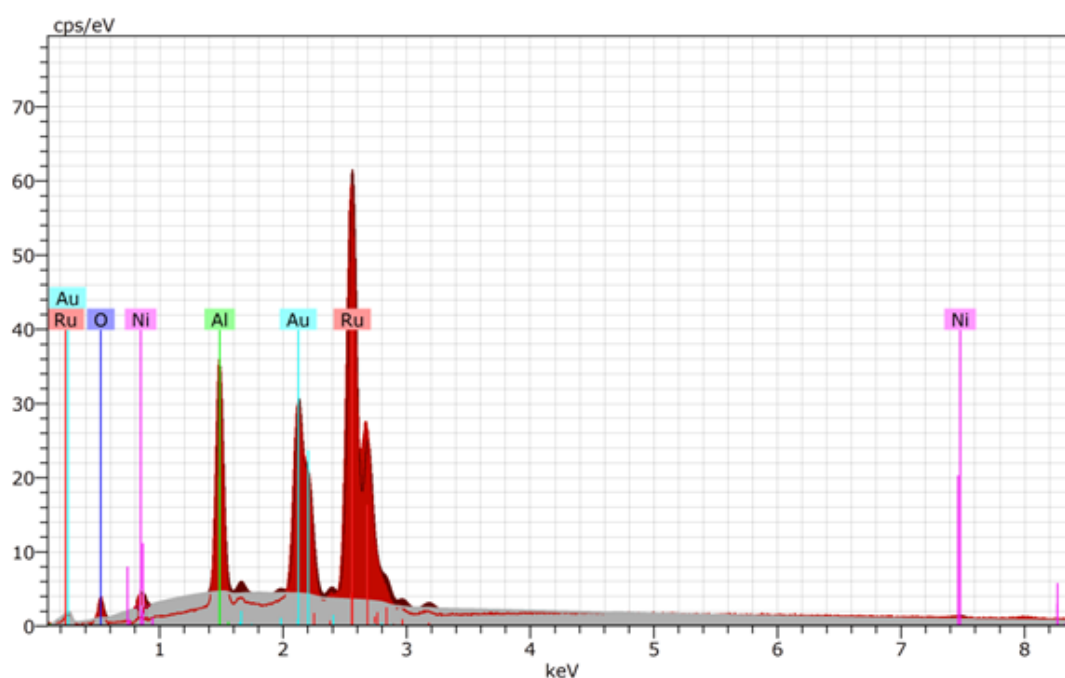


Figure 4.10. EDX spectrum of  $\text{Ru}_{0.93}\text{Ni}_{0.07}\text{Al}_2\text{O}_3$  nanoparticles

#### 4.3.3. XRD analysis of $\text{Ru}_{0.93}\text{Ni}_{0.07}\text{Al}_2\text{O}_3$

Powder characterization, shaping and conventional sintering the crystalline phase was identified by XRD using the  $\text{Cu-K}\alpha$  radiation with 0.154 nm wavelength at  $2\theta$  angle range from 10 to 70. In order to investigate the crystal structure of the obtained powder material XRD analysis was performed and the resultant pattern of the as-prepared sample is presented in Figure 4.11. In agreement with XRD patterns, a crystalline product

appeared after 60 min of reaction at 200 °C. As shown in Figure 4.11, XRD can be used to study the phase purity of the obtained  $\text{Ru}_{0.93}\text{Ni}_{0.07}\text{Al}_2\text{O}_3$  nanoparticles.

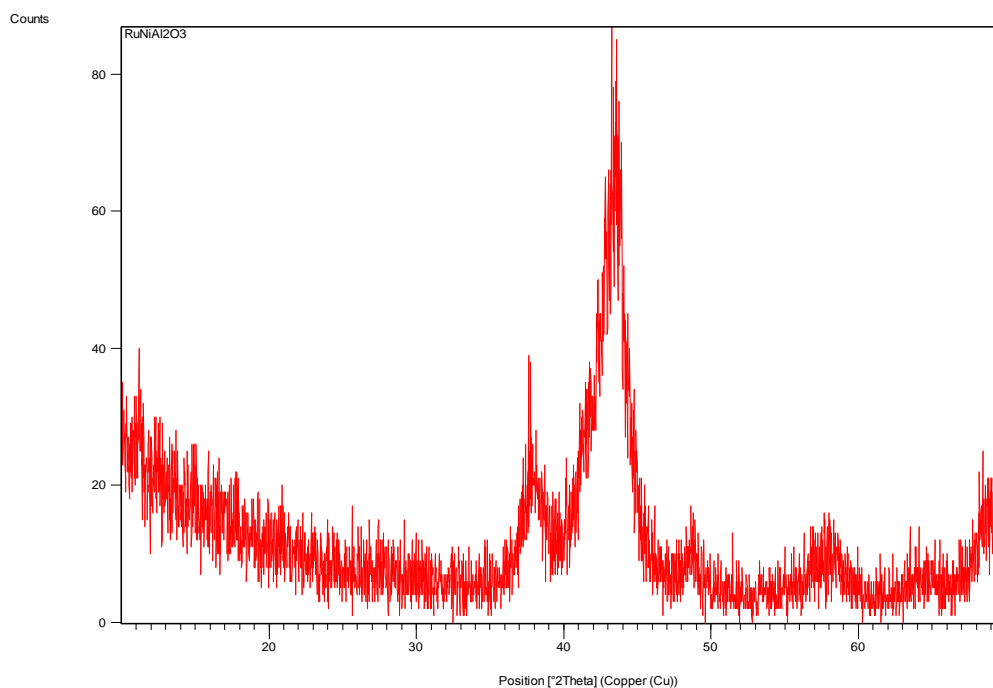


Figure 4.11. X-ray diffraction patterns of the  $\text{Ru}_{0.93}\text{Ni}_{0.07}\text{Al}_2\text{O}_3$  nanoparticles

#### 4.3.4. FT-IR analysis of $\text{Ru}_{0.93}\text{Ni}_{0.07}\text{Al}_2\text{O}_3$

The FT-IR spectroscopy is the most powerful and useful technique adopted by all the chemists to analyze, confirm and elucidate the structure of compounds and to identify the functional groups present in them. To confirm the formation of  $\text{Ru}_{0.93}\text{Ni}_{0.07}\text{Al}_2\text{O}_3$  nanoparticles, the FT-IR spectra of the  $\text{Ru}_{0.93}\text{Ni}_{0.07}\text{Al}_2\text{O}_3$  powders synthesized by microwave-assisted method at the ignition temperature of 200 °C, were obtained. Figure 4.12 shows FT-IR spectra of nanoparticles in the range 400–4000  $\text{cm}^{-1}$ . The very weak peaks around 3292 and 1605  $\text{cm}^{-1}$  can be attributed to the stretching vibrations of hydrogen-bonded surface water molecules and the free hydroxyl (-OH) groups of water molecules from ambient atmosphere, respectively. The absorption bands in the range 400–882  $\text{cm}^{-1}$  appears due to the formation of metal oxides. These intense and weak absorption band are visible at 400–1060  $\text{cm}^{-1}$  range are associated with the bending and stretching modes of the metal–oxygen and the metal-oxygen-metal bonds corresponding to

$\text{Ru}_{0.93}\text{Ni}_{0.07}\text{Al}_2\text{O}_3$  nanoparticle. Moreover the spectra of the  $\text{Ru}_{0.93}\text{Ni}_{0.07}\text{Al}_2\text{O}_3$  showed the very weak shoulder peak at  $1411\text{ cm}^{-1}$ , which is assigned to the Al-O stretching vibrations.

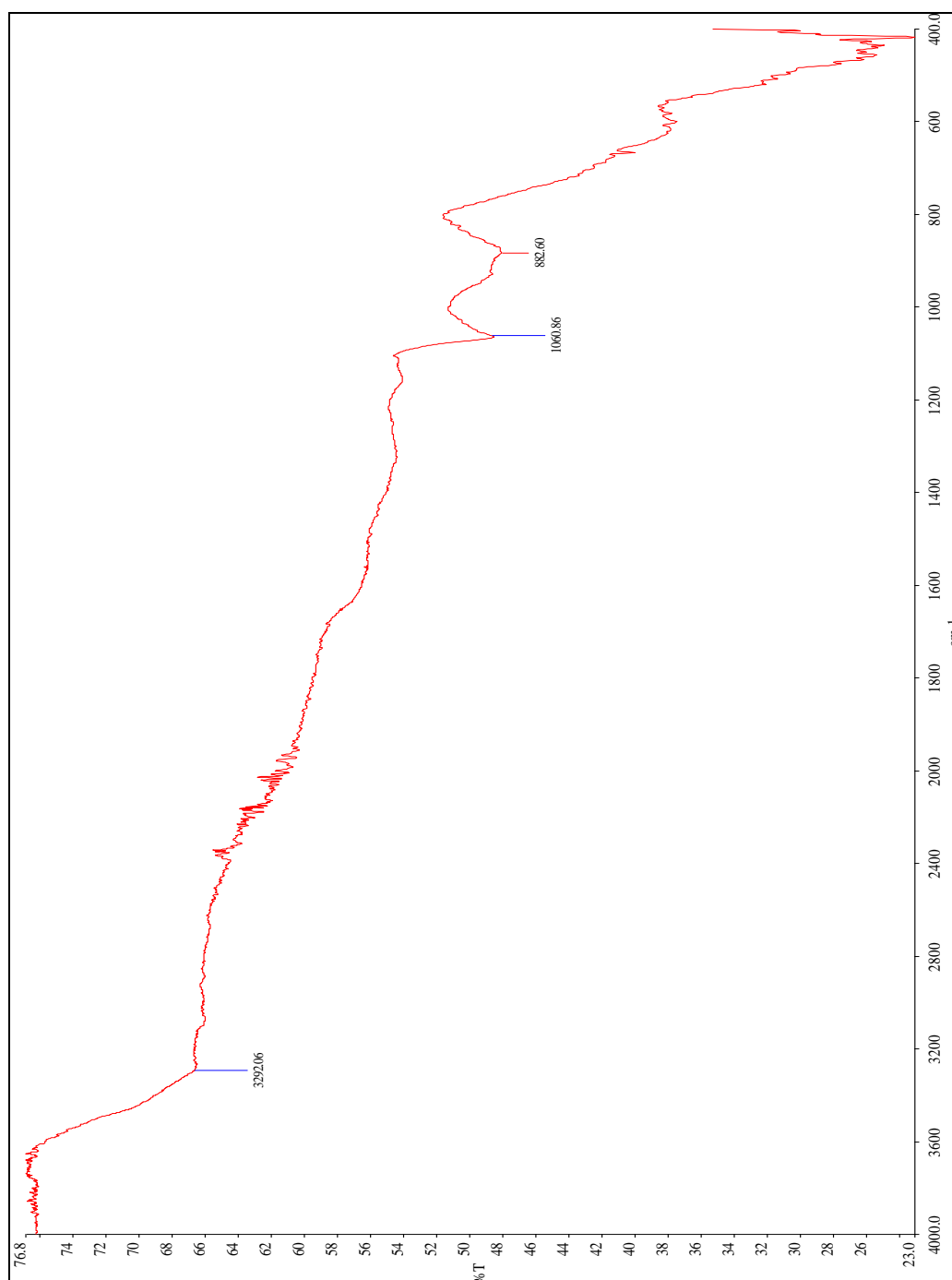


Figure 4.12. The FT-IR spectra of  $\text{Ru}_{0.93}\text{Ni}_{0.07}\text{Al}_2\text{O}_3$  nanoparticles

#### 4.4. NPs of $\text{Ru}_{0.54}\text{Cu}_{0.46}\text{Al}_2\text{O}_3$

##### 4.4.1. SEM analysis of $\text{Ru}_{0.54}\text{Cu}_{0.46}\text{Al}_2\text{O}_3$

The surface morphology of  $\text{Ru}_{0.54}\text{Cu}_{0.46}\text{Al}_2\text{O}_3$  was investigated by the SEM as shown in Figures 4.13a and 4.13b. From the images, Figure 4.13a shows the formation of nanoparticles for  $\text{Ru}_{0.54}\text{Cu}_{0.46}\text{Al}_2\text{O}_3$ . It can be observed from Figure 4.13b that the structure is actually composed of numerous nanospheres that are intercrossed with each other to form an amorphous-like structure. This is probably due to the polarization of the molecules under the rapidly changing electro-magnetic field of the microwave reactor, which may result in transient, localized high temperatures for the reaction system, leading to fast synthesis with desired morphology. Figure 4.13b shows that the average diameter of nanoparticles is less than 100 nm. Real particle size cannot be measured because of the amorphous structure. It is a well-known fact that the temperature and reaction time are the two important factors in determining the morphology of the nanomaterials. In the conventional method, the reaction time is kept as 3 h, at 400 °C, which resulted in the formation of nanoparticles. But in the microwave method, because of rapid heating, which is achieved within a few minutes, due to the suppressed diffusion process, the nano-amorphous would have been formed.

The morphologies of the final products are characterized by SEM. Figure 4.13a is a typical low-magnification SEM image of  $\text{Ru}_{0.54}\text{Cu}_{0.46}\text{Al}_2\text{O}_3$ , which is composed of many uniform flower-like microstructures with a range diameter of 28-51 nm. The high-magnification SEM image in Figure 4.13b reveals that the flower-like microstructure is built from many thin sheets with a thickness about 10 nm. These nanoflakes are intercrossed each other and aggregated together to form flower-like microstructures. At 200 °C, the novel  $\text{Ru}_{0.54}\text{Cu}_{0.46}\text{Al}_2\text{O}_3$  flower-like microstructures and nanoparticles were harvested as shown in Figure 4.13b.

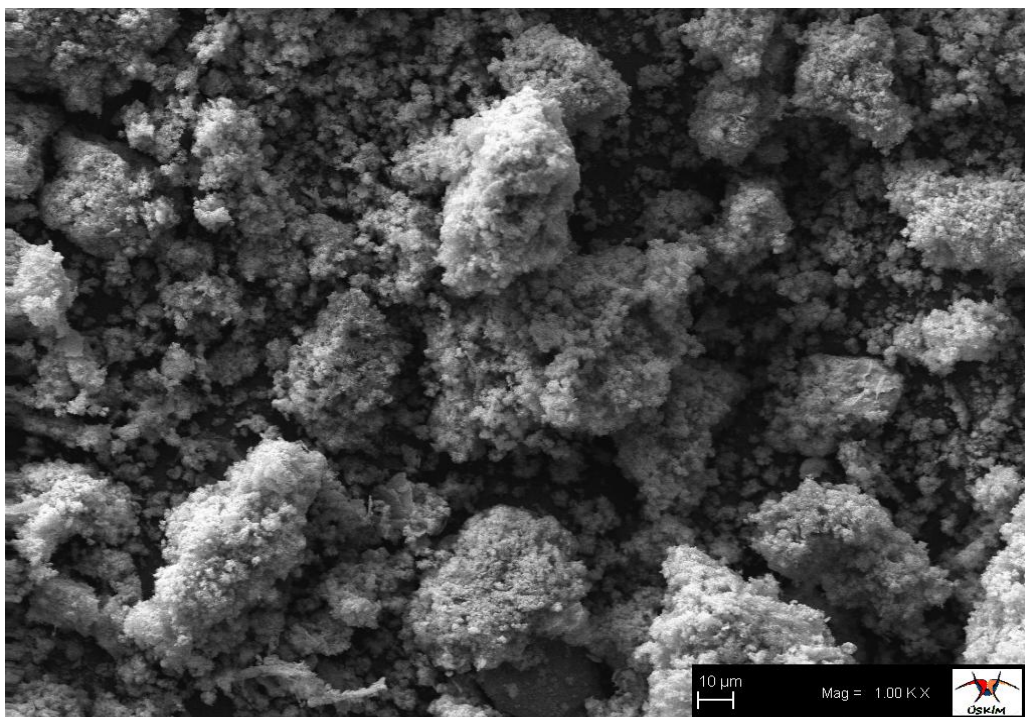


Figure 4.13a. SEM images of  $\text{Ru}_{0.54}\text{Cu}_{0.46}\text{Al}_2\text{O}_3$  nanoparticles prepared.

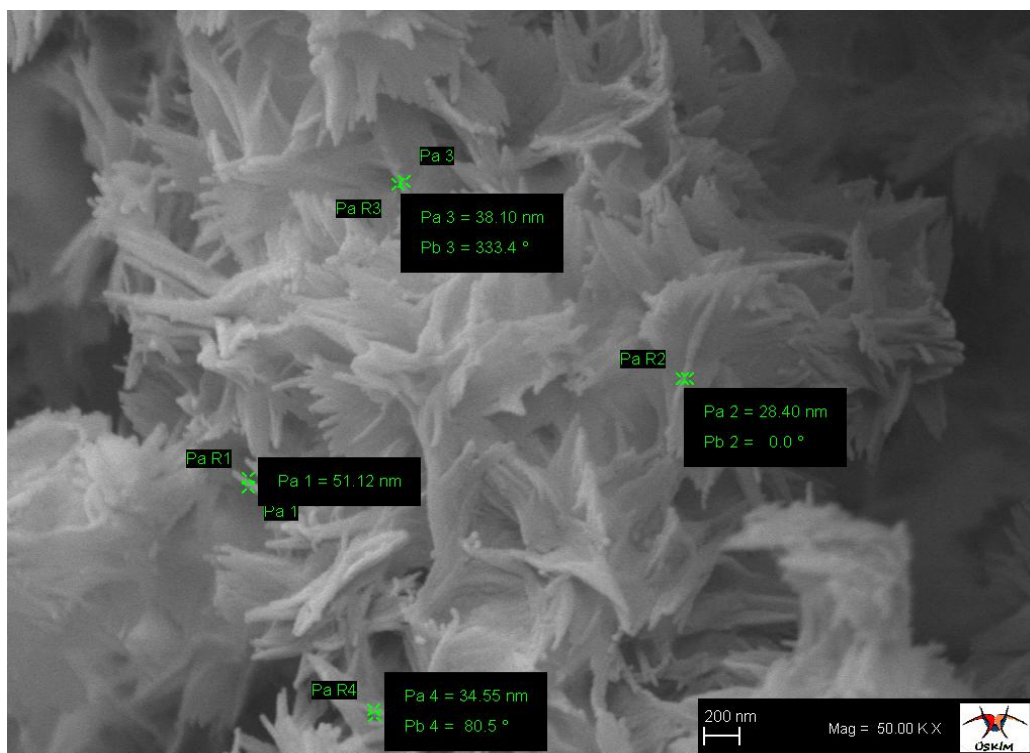


Figure 4.13b. SEM images of  $\text{Ru}_{0.54}\text{Cu}_{0.46}\text{Al}_2\text{O}_3$  nanoparticles prepared.

#### 4.4.2. EDX analysis of $\text{Ru}_{0.54}\text{Cu}_{0.46}\text{Al}_2\text{O}_3$

The formation of pure  $\text{Ru}_{0.54}\text{Cu}_{0.46}\text{Al}_2\text{O}_3$  was confirmed by means of energy dispersive X-ray analysis EDX as shown in Figure 4.14. The EDX result showed the presence of  $\text{Ru}_{0.54}\text{Cu}_{0.46}\text{Al}_2\text{O}_3$  by the appearance of Ru, Fe, Al and O peaks in the spectrum. The absence of carbon, nitrogen and other impurities are also evidenced from the EDX spectrum. This analysis confirmed that the sample  $\text{Ru}_{0.54}\text{Cu}_{0.46}\text{Al}_2\text{O}_3$  prepared by microwave-assisted method. Hence, the result is definitive evidence to suggest that the sample does not contain any other element and are indeed free from other impurities. The peaks at 2.1–2.2 keV in the EDX spectra are due to the gold, which is coated on the samples before recording SEM.

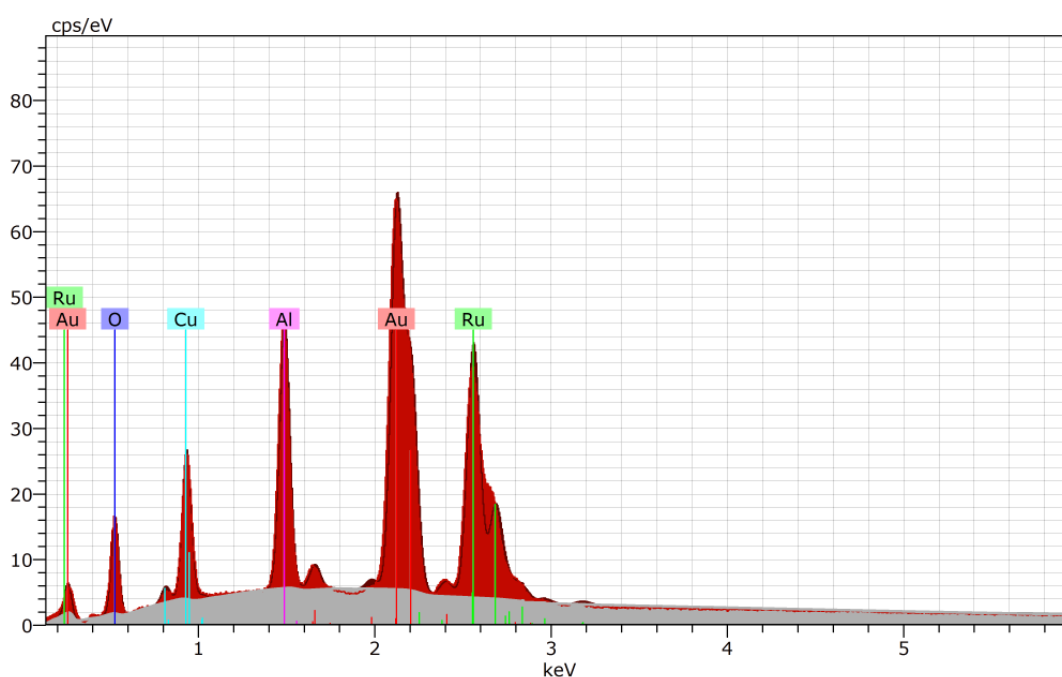


Figure 4.14. EDX spectrum of  $\text{Ru}_{0.54}\text{Cu}_{0.46}\text{Al}_2\text{O}_3$  nanoparticles

#### 4.4.3. XRD analysis of $\text{Ru}_{0.54}\text{Cu}_{0.46}\text{Al}_2\text{O}_3$

Powder characterization, shaping and conventional sintering the crystalline phase was identified by XRD using the  $\text{Cu-K}\alpha$  radiation with 0.154 nm wavelength at  $2\theta$  angle range from 10 to 70. In order to investigate the crystal structure of the obtained powder material XRD analysis was performed and the resultant pattern of the as-prepared sample is presented in Figure 4.15. In agreement with XRD patterns, a crystalline product

appeared after 60 min of reaction at 200 °C. As shown in Figure 4.15 XRD can be used to study the phase purity of the obtained  $\text{Ru}_{0.54}\text{Cu}_{0.46}\text{Al}_2\text{O}_3$  nanoparticles.

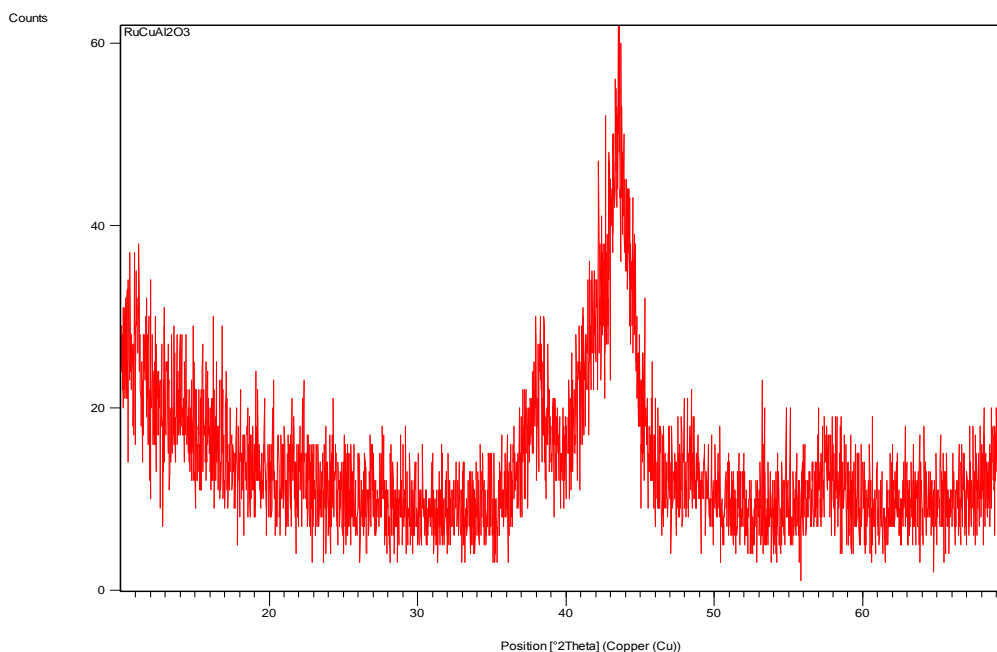


Figure 4.15. X-ray diffraction patterns of the  $\text{Ru}_{0.54}\text{Cu}_{0.46}\text{Al}_2\text{O}_3$  nanoparticles

#### 4.4.4. FT-IR analysis of $\text{Ru}_{0.54}\text{Cu}_{0.46}\text{Al}_2\text{O}_3$

The FT-IR spectroscopy is the most powerful and useful technique adopted by all the chemists to analyze, confirm and elucidate the structure of compounds and to identify the functional groups present in them. To confirm the formation of  $\text{Ru}_{0.54}\text{Cu}_{0.46}\text{Al}_2\text{O}_3$  nanoparticles, the FT-IR spectra of the  $\text{Ru}_{0.54}\text{Cu}_{0.46}\text{Al}_2\text{O}_3$  powders synthesized by microwave-assisted method at the ignition temperature of 200 °C, were obtained. Figure 4.16 shows FT-IR spectra of nanoparticles in the range 400–4000  $\text{cm}^{-1}$ . The very weak peaks around 3288 and 1617  $\text{cm}^{-1}$  can be attributed to the stretching vibrations of hydrogen-bonded surface water molecules and the free hydroxyl (-OH) groups of water molecules from ambient atmosphere, respectively. The absorption bands in the range 410–875  $\text{cm}^{-1}$  appears due to the formation of metal oxides. These intense and weak absorption band are visible at 400–1064  $\text{cm}^{-1}$  range are associated with the bending and stretching modes of the metal–oxygen and the metal-oxygen-metal bonds corresponding to  $\text{Ru}_{0.54}\text{Cu}_{0.46}\text{Al}_2\text{O}_3$  nanoparticle. Moreover the spectra of the  $\text{Ru}_{0.54}\text{Cu}_{0.46}\text{Al}_2\text{O}_3$  showed the very weak shoulder peak at 1405  $\text{cm}^{-1}$ , which is assigned to the Al-O stretching vibrations.



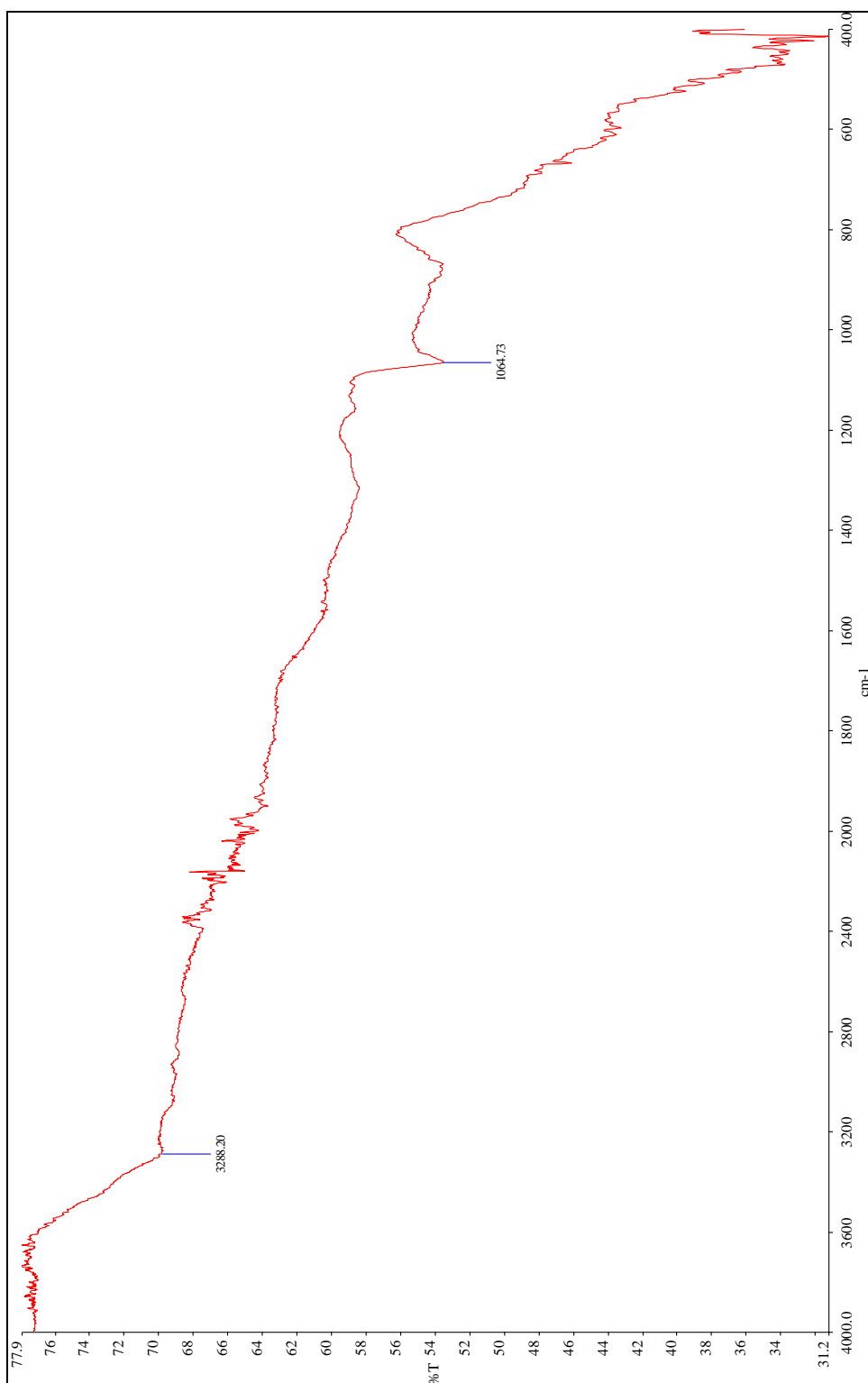


Figure 4.16. The FT-IR spectra of Ru<sub>0.54</sub>Cu<sub>0.46</sub>Al<sub>2</sub>O<sub>3</sub> nanoparticles

## 4.5. NPs of $\text{Ru}_{0.62}\text{In}_{0.38}\text{Al}_2\text{O}_3$

### 4.5.1. SEM analysis of $\text{Ru}_{0.62}\text{In}_{0.38}\text{Al}_2\text{O}_3$

The surface morphology of  $\text{Ru}_{0.62}\text{In}_{0.38}\text{Al}_2\text{O}_3$  was investigated by the SEM as shown in Figure 4.17. From the images shows the formation of nanoparticles for  $\text{Ru}_{0.62}\text{In}_{0.38}\text{Al}_2\text{O}_3$ . It can be observed from Figure 4.17. That the structure is actually composed of numerous nanosphere that are intercrossed with each other to form amorphous like structure. This is probably due to the polarization of the molecules under the rapidly changing electromagnetic field of the microwave reactor, which may result in transient, localized high temperatures for the reaction system, leading to fast synthesis with desired morphology. Figure 4.17 shows that the average diameter of nanoparticles less than 100 nm. Real particle size can not be measured because of amorphous structure. It is a well-known fact that the temperature and reaction time are the two important factors in determining the morphology of the nanomaterials. In the conventional method, the reaction time is kept as 3 h, at 400 °C, which resulted in the formation of nanoparticles. But in microwave method, because of rapid heating, which is achieved within the few minutes, due to the suppressed diffusion process, the nano-amorphous would have been formed.

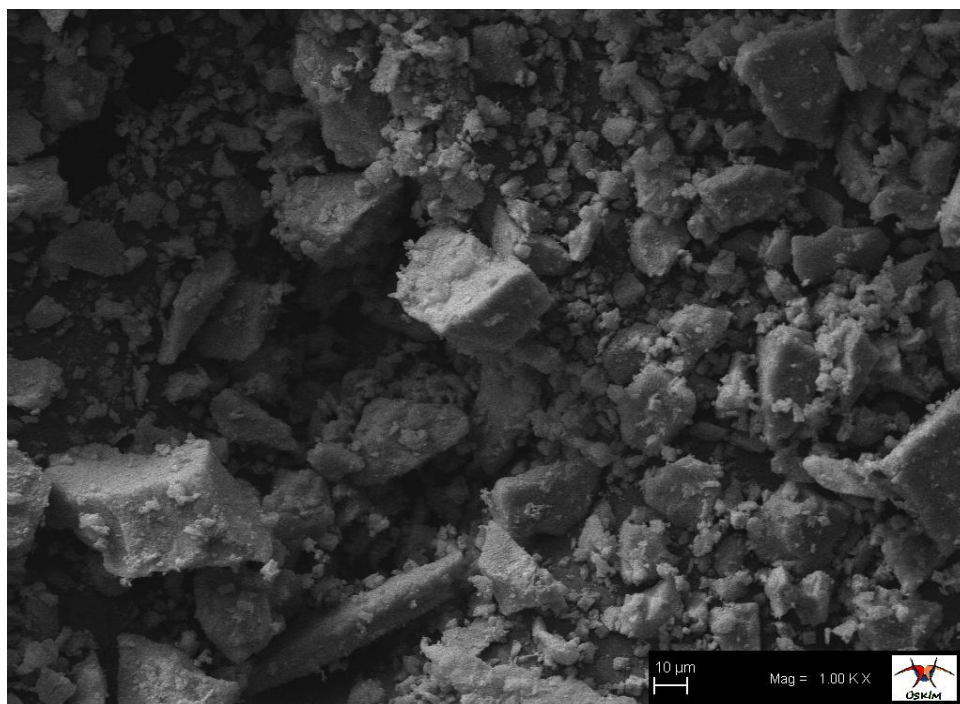


Figure 4.17. SEM images of  $\text{Ru}_{0.62}\text{In}_{0.38}\text{Al}_2\text{O}_3$  nanoparticles prepared.

#### 4.5.2. EDX analysis of $\text{Ru}_{0.62}\text{In}_{0.38}\text{Al}_2\text{O}_3$

The formation of pure  $\text{Ru}_{0.62}\text{In}_{0.38}\text{Al}_2\text{O}_3$  was confirmed by means of energy dispersive X-ray analysis EDX as shown in Figure 4.18. The EDX result showed the presence of  $\text{Ru}_{0.62}\text{In}_{0.38}\text{Al}_2\text{O}_3$  by the appearance of Ru, In, Al and O peaks in the spectrum. The absence of carbon, nitrogen and other impurities are also evidenced from the EDX spectrum. This analysis confirmed that the sample  $\text{Ru}_{0.62}\text{In}_{0.38}\text{Al}_2\text{O}_3$  prepared by microwave-assisted method. Hence, the result is definitive evidence to suggest that the sample does not contain any other element and are indeed free from other impurities. The peaks at 2.1–2.2 keV in the EDX spectra are due to the gold, which is coated on the samples before recording SEM.

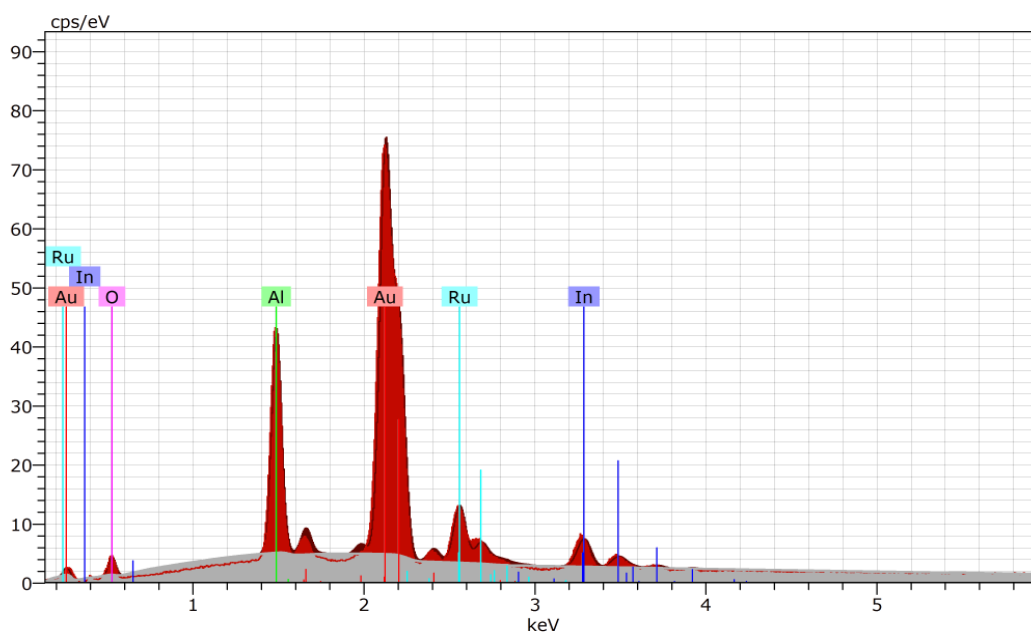


Figure 4.18. EDX spectrum of  $\text{Ru}_{0.62}\text{In}_{0.38}\text{Al}_2\text{O}_3$  nanoparticles

#### 4.5.3. XRD analysis of $\text{Ru}_{0.62}\text{In}_{0.38}\text{Al}_2\text{O}_3$

Powder characterization, shaping and conventional sintering the crystalline phase was identified by XRD using the  $\text{Cu-K}\alpha$  radiation with 0.154 nm wavelength at  $2\theta$  angle range from 10 to 70. In order to investigate the crystal structure of the obtained powder material XRD analysis was performed and the resultant pattern of the as-prepared sample is presented in Figure 4.19. In agreement with XRD patterns, a crystalline product

appeared after 60 min of reaction at 200 °C. As shown in Figure 4.19, XRD can be used to study the phase purity of the obtained  $\text{Ru}_{0.62}\text{In}_{0.38}\text{Al}_2\text{O}_3$  nanoparticles.

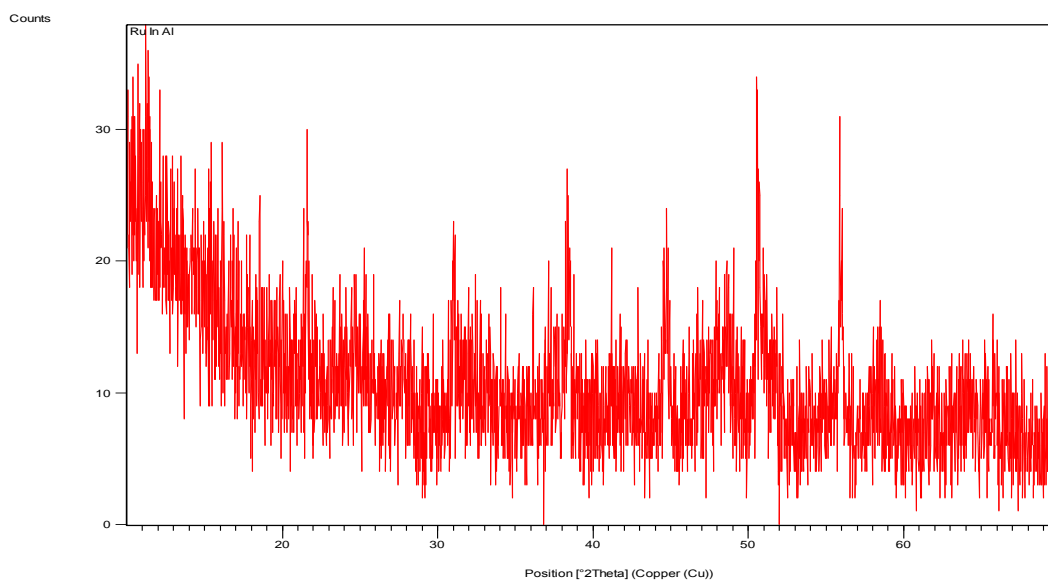


Figure 4.19. X-ray diffraction patterns of the  $\text{Ru}_{0.62}\text{In}_{0.38}\text{Al}_2\text{O}_3$  nanoparticles

#### 4.5.4. FT-IR analysis of $\text{Ru}_{0.62}\text{In}_{0.38}\text{Al}_2\text{O}_3$

The FT-IR spectroscopy is the most powerful and useful technique adopted by all the chemists to analyze, confirm and elucidate the structure of compounds and to identify the functional groups present in them. To confirm the formation of  $\text{Ru}_{0.62}\text{In}_{0.38}\text{Al}_2\text{O}_3$  nanoparticles, the FT-IR spectra of the  $\text{Ru}_{0.62}\text{In}_{0.38}\text{Al}_2\text{O}_3$  powders synthesized by microwave-assisted method at the ignition temperature of 200 °C, were obtained. Figure 4.20 shows FT-IR spectra of nanoparticles in the range 400–4000  $\text{cm}^{-1}$ . The peaks around 3295 and 1650  $\text{cm}^{-1}$  can be attributed to the stretching vibrations of hydrogen-bonded surface water molecules and the free hydroxyl (-OH) groups of water molecules from ambient atmosphere, respectively. The absorption bands in the range 410–884  $\text{cm}^{-1}$  appears due to the formation of metal oxides. These intense and weak absorption band are visible at 400–1064  $\text{cm}^{-1}$  range are associated with the bending and stretching modes of the metal–oxygen and the metal-oxygen-metal bonds corresponding to  $\text{Ru}_{0.62}\text{In}_{0.38}\text{Al}_2\text{O}_3$  nanoparticle. Moreover the spectra of the  $\text{Ru}_{0.62}\text{In}_{0.38}\text{Al}_2\text{O}_3$  showed the peak at 1411  $\text{cm}^{-1}$ , which is assigned to the Al-O stretching vibrations.

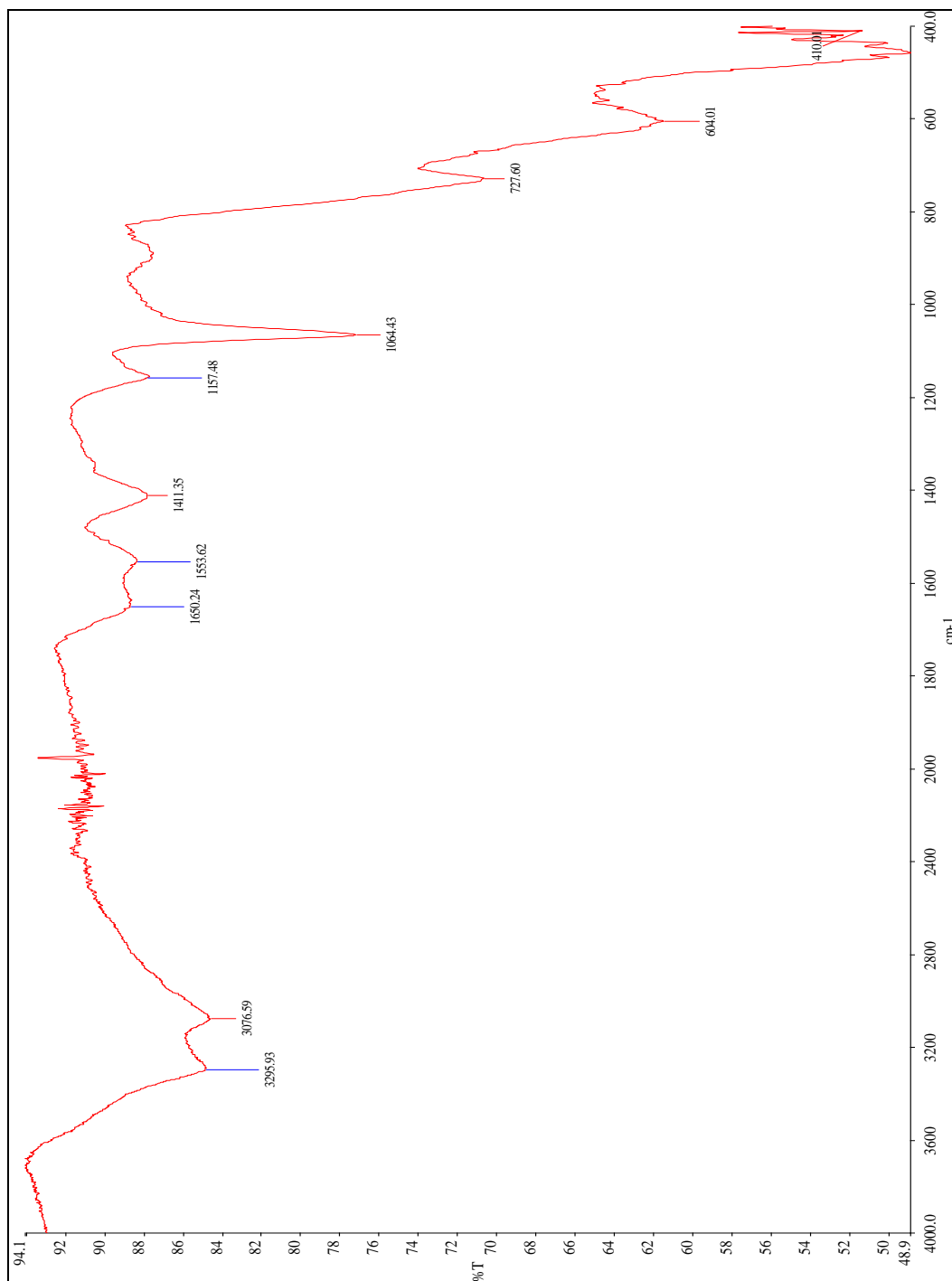


Figure 4.20. The FT-IR spectra of Ru<sub>0.62</sub>In<sub>0.38</sub>Al<sub>2</sub>O<sub>3</sub> nanoparticles

## 4.6. NPs of $\text{Ru}_{0.77}\text{Co}_{0.23}\text{In}_2\text{O}_3$

### 4.6.1. SEM analysis of $\text{Ru}_{0.77}\text{Co}_{0.23}\text{In}_2\text{O}_3$

The surface morphology of  $\text{Ru}_{0.77}\text{Co}_{0.23}\text{In}_2\text{O}_3$  was investigated by the SEM as shown in Figure 4.21a and 4.21b. The images show the formation of nanoparticles for  $\text{Ru}_{0.77}\text{Co}_{0.23}\text{In}_2\text{O}_3$ . It can be observed from Figure 4.21a that the structure is actually composed of numerous nanosphere that are intercrossed with each other to form amorphous like structure. This is probably due to the polarization of the molecules under the rapidly changing electro-magnetic field of the microwave reactor, which may result in transient, localized high temperatures for the reaction system, leading to fast synthesis with desired morphology. Figure 4.21b shows that the average diameter of nanoparticles less than 100 nm. Real particle size can not be measured because of amorphous structure. It is a well-known fact that the temperature and reaction time are the two important factors in determining the morphology of the nanomaterials. In the conventional method, the reaction time is kept as 3 h, at 400 °C, which resulted in the formation of nanoparticles. But in microwave method, because of rapid heating, which is achieved within the few minutes, due to the suppressed diffusion process, the nano-amorphous would have been formed.

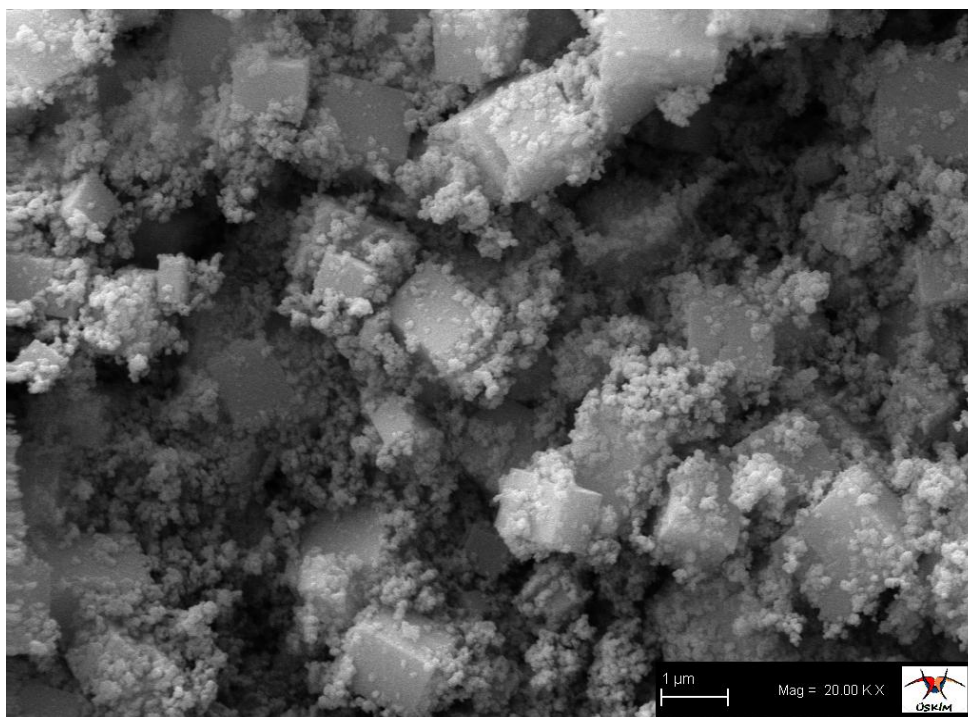


Figure 4.21a. SEM images of  $\text{Ru}_{0.77}\text{Co}_{0.23}\text{In}_2\text{O}_3$  nanoparticles prepared [78].

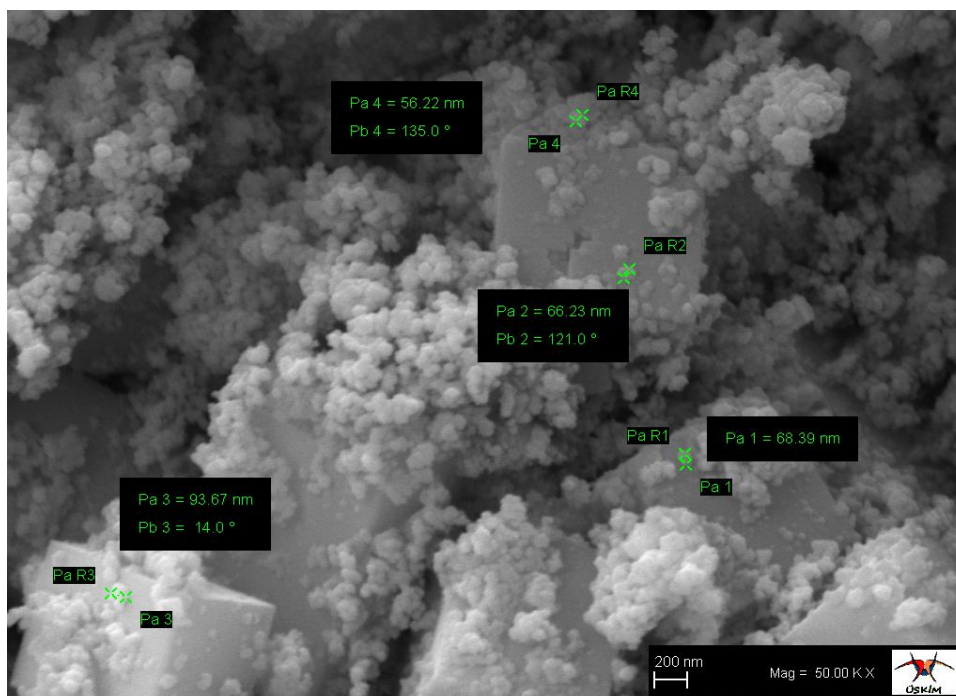


Figure 4.21b. SEM images of Ru<sub>0.77</sub>Co<sub>0.23</sub>In<sub>2</sub>O<sub>3</sub> nanoparticles prepared.

#### 4.6.2. EDX analysis of Ru<sub>0.77</sub>Co<sub>0.23</sub>In<sub>2</sub>O<sub>3</sub>

The formation of pure Ru<sub>0.77</sub>Co<sub>0.23</sub>In<sub>2</sub>O<sub>3</sub> was confirmed by means of energy dispersive X-ray analysis EDX as shown in Figure 4.22. The EDX result showed the presence of Ru<sub>0.77</sub>Co<sub>0.23</sub>In<sub>2</sub>O<sub>3</sub> by the appearance of Ru, Co, In and O peaks in the spectrum. The absence of carbon, nitrogen and other impurities are also evidenced from the EDX spectrum. This analysis confirmed that the sample Ru<sub>0.77</sub>Co<sub>0.23</sub>In<sub>2</sub>O<sub>3</sub> prepared by microwave-assisted method. Hence, the result is definitive evidence to suggest that the sample does not contain any other element and are indeed free from other impurities. The peaks at 2.1–2.2 keV in the EDX spectra are due to the gold, which is coated on the samples before recording SEM.

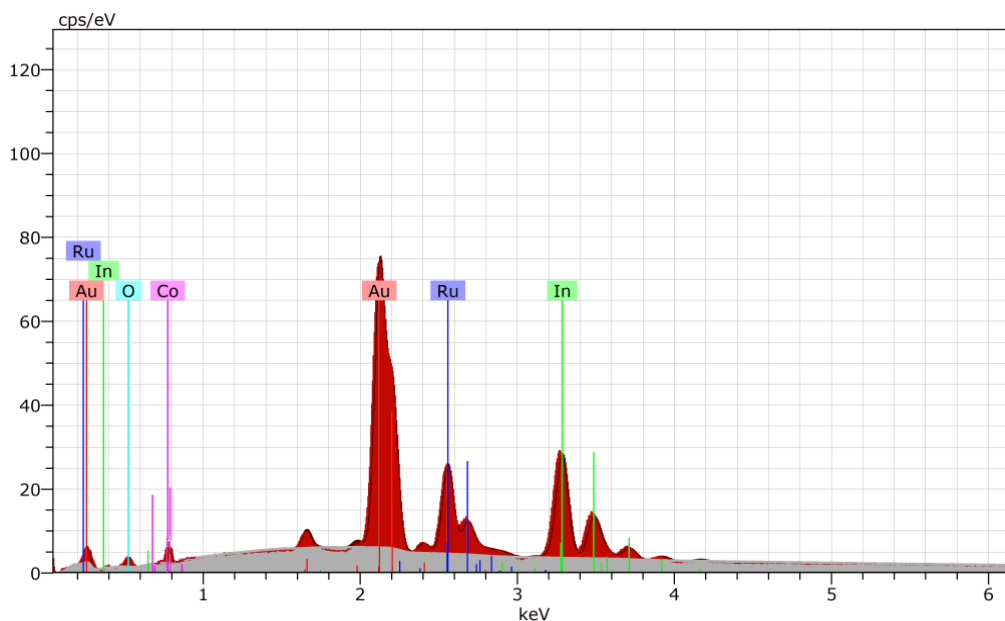


Figure 4.22. EDAX spectrum of  $\text{Ru}_{0.77}\text{Co}_{0.23}\text{In}_2\text{O}_3$  nanoparticles

#### 4.6.3. XRD analysis of $\text{Ru}_{0.77}\text{Co}_{0.23}\text{In}_2\text{O}_3$

Powder characterization, shaping and conventional sintering the crystalline phase was identified by XRD using the the Cu-K $\alpha$  radiation with 0.154 nm wavelength at  $2\theta$  angle range from 10 to 70. In order to investigate the crystal structure of the obtained powder material XRD analysis was performed and the resultant pattern of the as-prepared sample is presented in Figure 4.23. In agreement with XRD patterns, a crystalline product appeared after 60 min of reaction at 200 °C. As shown in Figure 23, XRD can be used to study the phase purity of the obtained  $\text{Ru}_{0.77}\text{Co}_{0.23}\text{In}_2\text{O}_3$  nanoparticles.



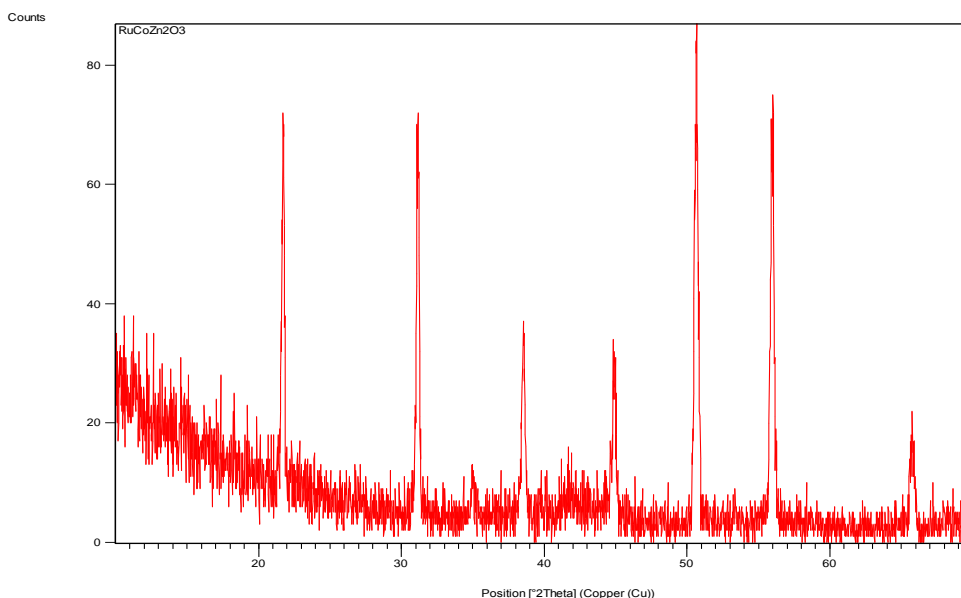


Figure 4.23. X-ray diffraction patterns of the  $\text{Ru}_{0.77}\text{Co}_{0.23}\text{In}_2\text{O}_3$  nanoparticles

#### 4.6.4. FT-IR analysis of $\text{Ru}_{0.77}\text{Co}_{0.23}\text{In}_2\text{O}_3$

The FT-IR spectroscopy is the most powerful and useful technique adopted by all the chemists to analyze, confirm and elucidate the structure of compounds and to identify the functional groups present in them. To confirm the formation of  $\text{Ru}_{0.77}\text{Co}_{0.23}\text{In}_2\text{O}_3$  nanoparticles, the FT-IR spectra of the  $\text{Ru}_{0.77}\text{Co}_{0.23}\text{In}_2\text{O}_3$  powders synthesized by microwave-assisted method at the ignition temperature of 200 °C, were obtained. Figure 4.24 shows FT-IR spectra of nanoparticles in the range 400–4000  $\text{cm}^{-1}$ . The peaks around 3206 and 1630  $\text{cm}^{-1}$  can be attributed to the stretching vibrations of hydrogen-bonded surface water molecules and the free hydroxyl (-OH) groups of water molecules from ambient atmosphere, respectively. The absorption bands in the range 418–843  $\text{cm}^{-1}$  appears due to the formation of metal oxides. These intense and weak absorption band are visible at 400–1057  $\text{cm}^{-1}$  range are associated with the bending and stretching modes of the metal–oxygen and the metal-oxygen-metal bonds corresponding to  $\text{Ru}_{0.77}\text{Co}_{0.23}\text{In}_2\text{O}_3$  nanoparticle. Moreover the spectra of the  $\text{Ru}_{0.77}\text{Co}_{0.23}\text{In}_2\text{O}_3$  showed the peak at 1394  $\text{cm}^{-1}$ , which is assigned to the In-O stretching vibrations.

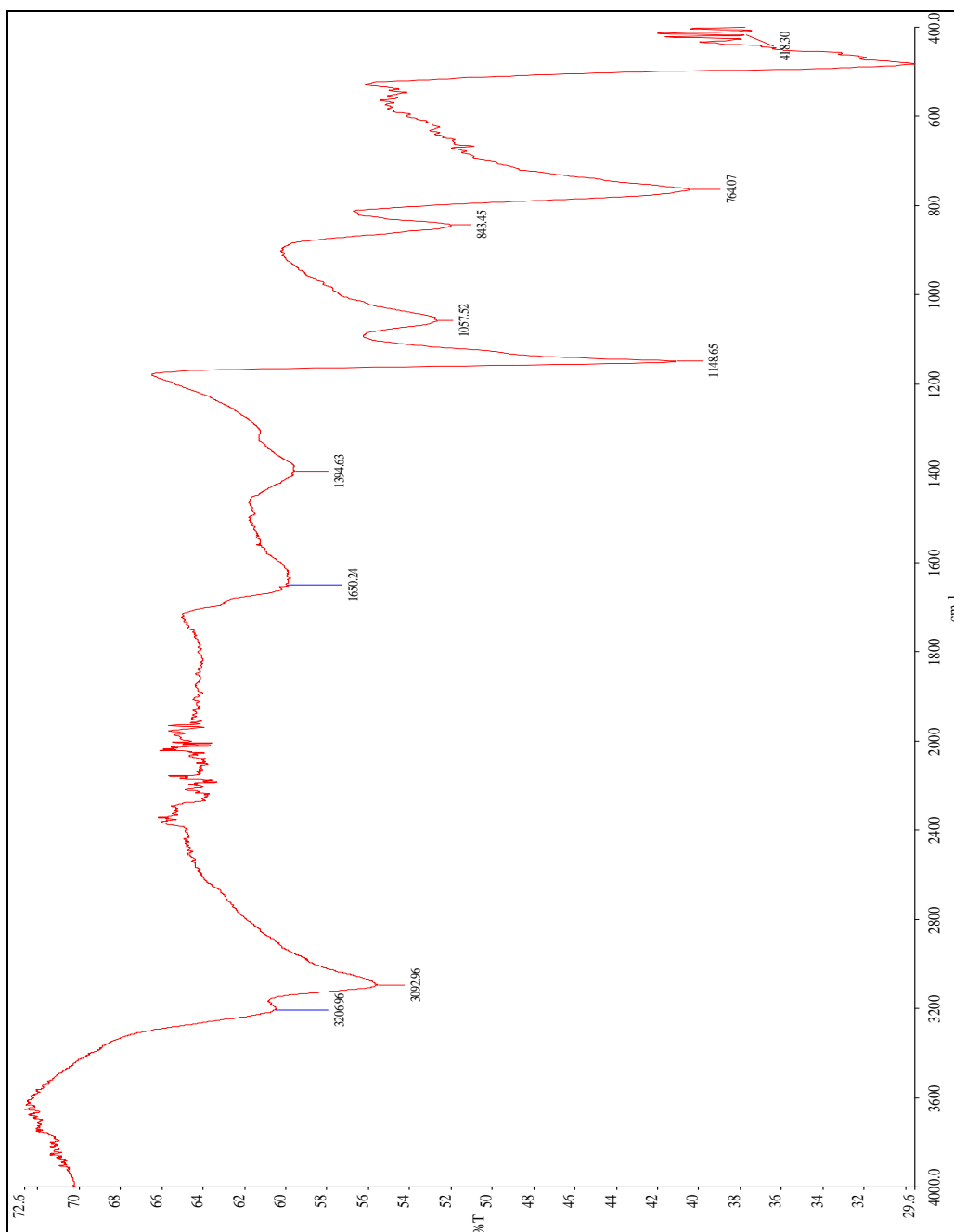


Figure 4.24. The FT-IR spectra of Ru<sub>0.77</sub>Co<sub>0.23</sub>In<sub>2</sub>O<sub>3</sub> nanoparticles

## 4.7. NPs of $\text{Ru}_{0.65}\text{Ni}_{0.35}\text{In}_2\text{O}_3$

### 4.7.1. SEM analysis of $\text{Ru}_{0.65}\text{Ni}_{0.35}\text{In}_2\text{O}_3$

The surface morphology of  $\text{Ru}_{0.65}\text{Ni}_{0.35}\text{In}_2\text{O}_3$  was investigated by the SEM as shown in Figure 4.25. The image shows the formation of nanoparticles for  $\text{Ru}_{0.65}\text{Ni}_{0.35}\text{In}_2\text{O}_3$ . It can be observed from Figure 4.25 that the structure is actually composed of numerous nanosphere that are intercrossed with each other to form amorphous like structure. This is probably due to the polarization of the molecules under the rapidly changing electromagnetic field of the microwave reactor, which may result in transient, localized high temperatures for the reaction system, leading to fast synthesis with desired morphology. The average diameter of nanoparticles less than 100 nm. Real particle size can not be measured because of amorphous structure. It is a well-known fact that the temperature and reaction time are the two important factors in determining the morphology of the nanomaterials. In the conventional method, the reaction time is kept as 3 h, at 400 °C, which resulted in the formation of nanoparticles. But in microwave method, because of rapid heating, which is achieved within the few minutes, due to the suppressed diffusion process, the nano-amorphous would have been formed.

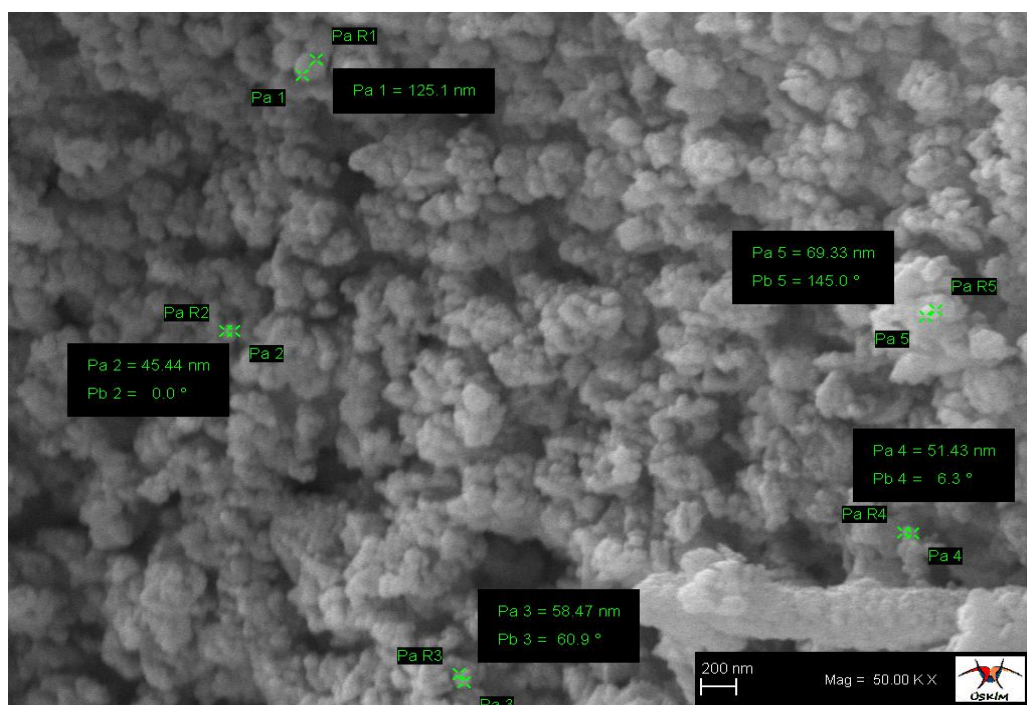


Figure 4.25. SEM images of  $\text{Ru}_{0.65}\text{Ni}_{0.35}\text{In}_2\text{O}_3$  nanoparticles prepared

#### 4.7.2. EDX analysis of $\text{Ru}_{0.65}\text{Ni}_{0.35}\text{In}_2\text{O}_3$

The formation of pure  $\text{Ru}_{0.65}\text{Ni}_{0.35}\text{In}_2\text{O}_3$  was confirmed by means of energy dispersive X-ray analysis EDX as shown in Figure 4.26. The EDX result showed the presence of  $\text{Ru}_{0.65}\text{Ni}_{0.35}\text{In}_2\text{O}_3$  by the appearance of Ru, Ni, In and O peaks in the spectrum. The absence of carbon, nitrogen and other impurities are also evidenced from the EDX spectrum. This analysis confirmed that the sample  $\text{Ru}_{0.65}\text{Ni}_{0.35}\text{In}_2\text{O}_3$  prepared by microwave-assisted method. Hence, the result is definitive evidence to suggest that the sample does not contain any other element and are indeed free from other impurities. The peaks at 2.1–2.2 keV in the EDX spectra are due to the gold, which is coated on the samples before recording SEM.

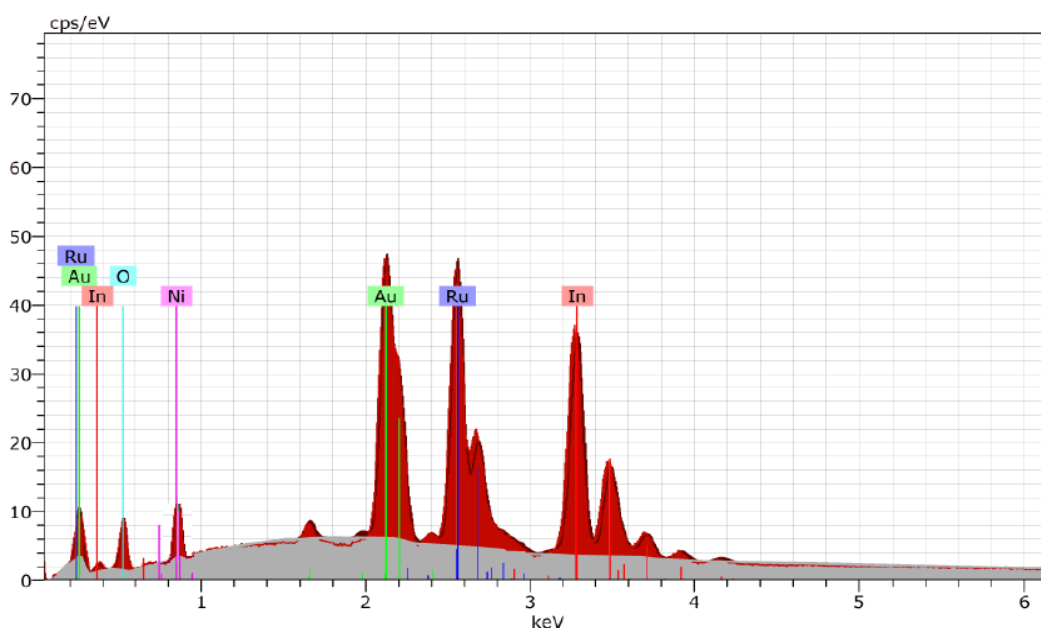


Figure 4.26. EDX spectrum of  $\text{Ru}_{0.65}\text{Ni}_{0.35}\text{In}_2\text{O}_3$  nanoparticles

#### 4.7.3. XRD analysis of $\text{Ru}_{0.65}\text{Ni}_{0.35}\text{In}_2\text{O}_3$

Powder characterization, shaping and conventional sintering the crystalline phase was identified by XRD using the  $\text{Cu-K}\alpha$  radiation with 0.154 nm wavelength at  $2\theta$  angle range from 10 to 70. In order to investigate the crystal structure of the obtained powder material XRD analysis was performed and the resultant pattern of the as-prepared sample is presented in Figure 4.26. In agreement with XRD patterns, a crystalline product appeared after 60 min of reaction at 200 °C. As shown in Figure 4.26, XRD can be used to study the phase purity of the obtained  $\text{Ru}_{0.65}\text{Ni}_{0.35}\text{In}_2\text{O}_3$  nanoparticles.

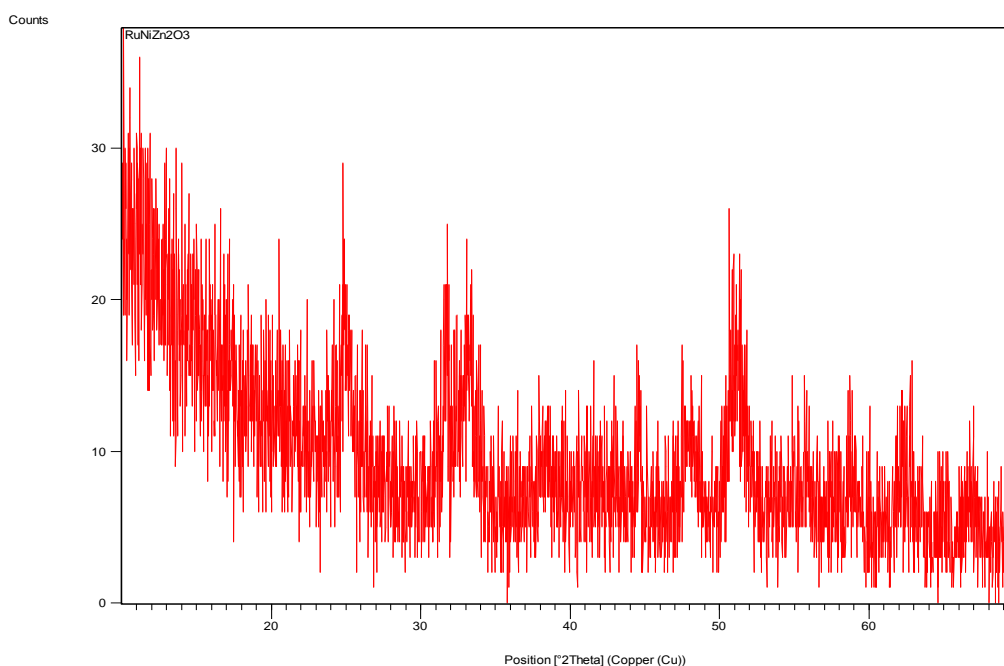


Figure 4.27. X-ray diffraction patterns of the  $\text{Ru}_{0.65}\text{Ni}_{0.35}\text{In}_2\text{O}_3$  nanoparticles

#### 4.7.4. FT-IR analysis of $\text{Ru}_{0.65}\text{Ni}_{0.35}\text{In}_2\text{O}_3$

The FT-IR spectroscopy is the most powerful and useful technique adopted by all the chemists to analyze, confirm and elucidate the structure of compounds and to identify the functional groups present in them. To confirm the formation of  $\text{Ru}_{0.65}\text{Ni}_{0.35}\text{In}_2\text{O}_3$  nanoparticles, the FT-IR spectra of the  $\text{Ru}_{0.65}\text{Ni}_{0.35}\text{In}_2\text{O}_3$  powders synthesized by microwave-assisted method at the ignition temperature of 200 °C, were obtained. Figure 4.28 shows FT-IR spectra of nanoparticles in the range 400–4000  $\text{cm}^{-1}$ . The peaks around 3179 and 1634  $\text{cm}^{-1}$  can be attributed to the stretching vibrations of hydrogen-bonded surface water molecules and the free hydroxyl (-OH) groups of water molecules from ambient atmosphere, respectively. The absorption bands in the range 405–898  $\text{cm}^{-1}$  appears due to the formation of metal oxides. These intense and weak absorption band are visible at 400–1155  $\text{cm}^{-1}$  range are associated with the bending and stretching modes of the metal–oxygen and the metal-oxygen-metal bonds corresponding to  $\text{Ru}_{0.65}\text{Ni}_{0.35}\text{In}_2\text{O}_3$  nanoparticle. Moreover the spectra of the  $\text{Ru}_{0.65}\text{Ni}_{0.35}\text{In}_2\text{O}_3$  showed the peak at 1381  $\text{cm}^{-1}$ , which is assigned to the In-O stretching vibrations.

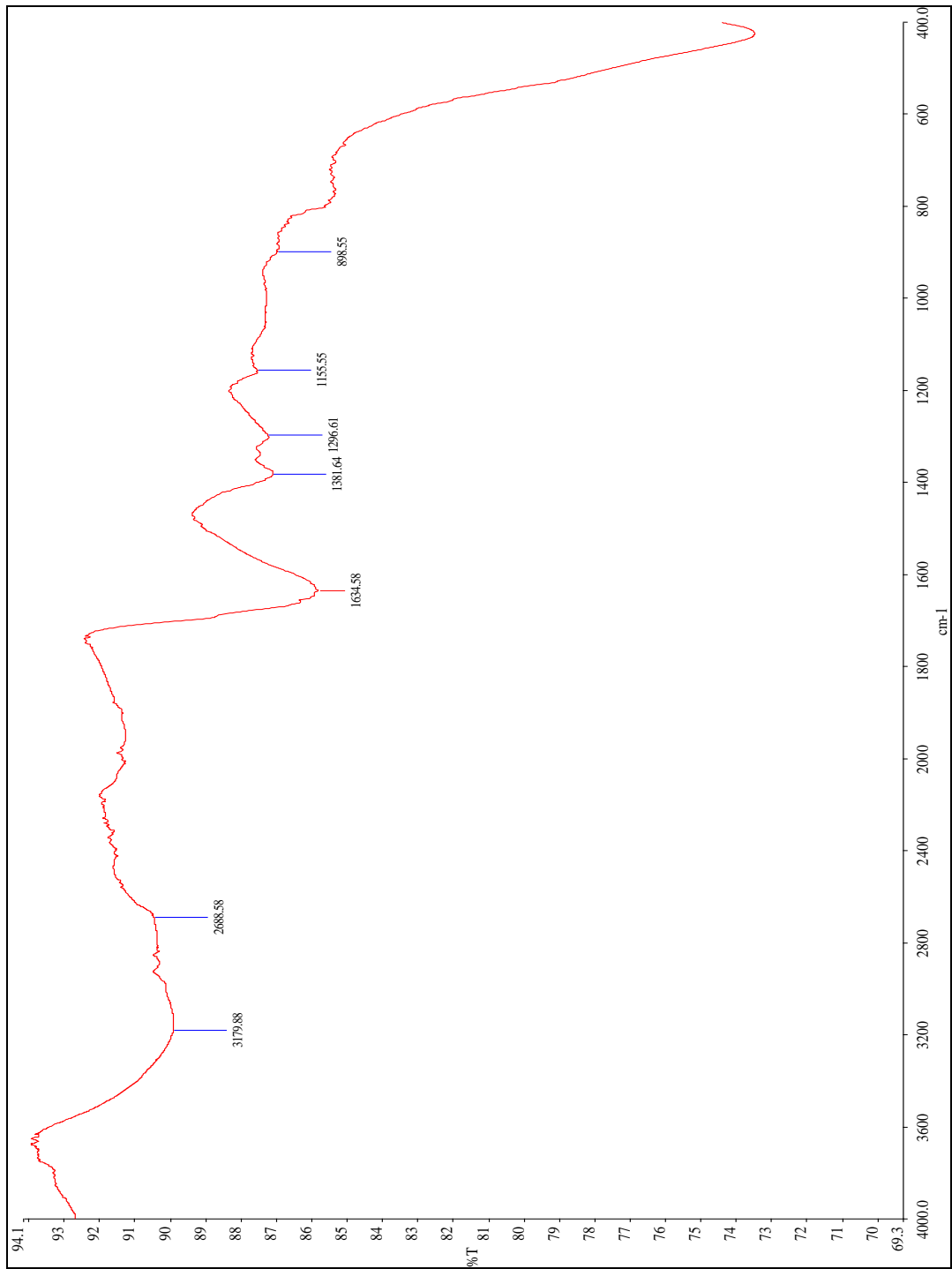


Figure 4.28. The FT-IR spectra of Ru<sub>0.65</sub>Ni<sub>0.35</sub>In<sub>2</sub>O<sub>3</sub> nanoparticles

## 4.8. NPs of $\text{Ru}_{0.92}\text{Pd}_{0.08}\text{In}_2\text{O}_3$

### 4.8.1. SEM analysis of $\text{Ru}_{0.92}\text{Pd}_{0.08}\text{In}_2\text{O}_3$

The surface morphology of  $\text{Ru}_{0.92}\text{Pd}_{0.08}\text{In}_2\text{O}_3$  was investigated by the SEM as shown in Figure 4.28a and 4.28b. From the images, Figure 4.28b shows the formation of nanoparticles for  $\text{Ru}_{0.92}\text{Pd}_{0.08}\text{In}_2\text{O}_3$ . It can be observed from Figure 4.28b that the structure is actually composed of numerous nanosphere that are intercrossed with each other to form amorphous like structure. This is probably due to the polarization of the molecules under the rapidly changing electro-magnetic field of the microwave reactor, which may result in transient, localized high temperatures for the reaction system, leading to fast synthesis with desired morphology. The average diameter of nanoparticles less than 100 nm. Real particle size can not be measured because of amorphous structure. It is a well-known fact that the temperature and reaction time are the two important factors in determining the morphology of the nanomaterials. In the conventional method, the reaction time is kept as 3 h, at 400 °C, which resulted in the formation of nanoparticles. But in microwave method, because of rapid heating, which is achieved within the few minutes, due to the suppressed diffusion process, the nano-amorphous would have been formed.

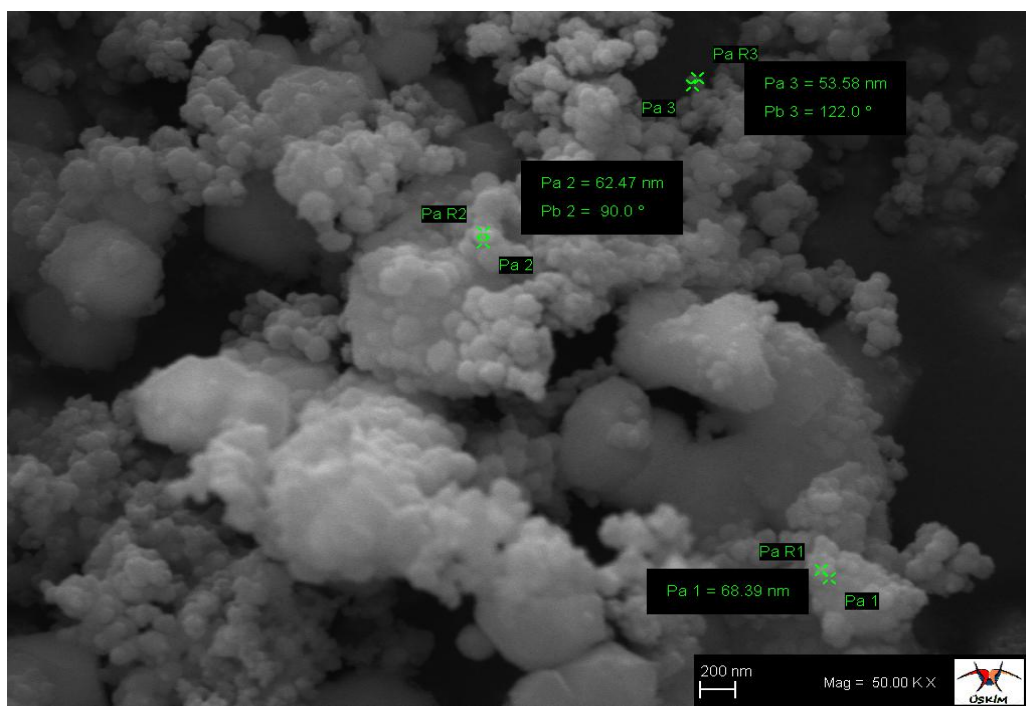


Figure 4.29a. SEM images of  $\text{Ru}_{0.92}\text{Pd}_{0.08}\text{In}_2\text{O}_3$  nanoparticles prepared

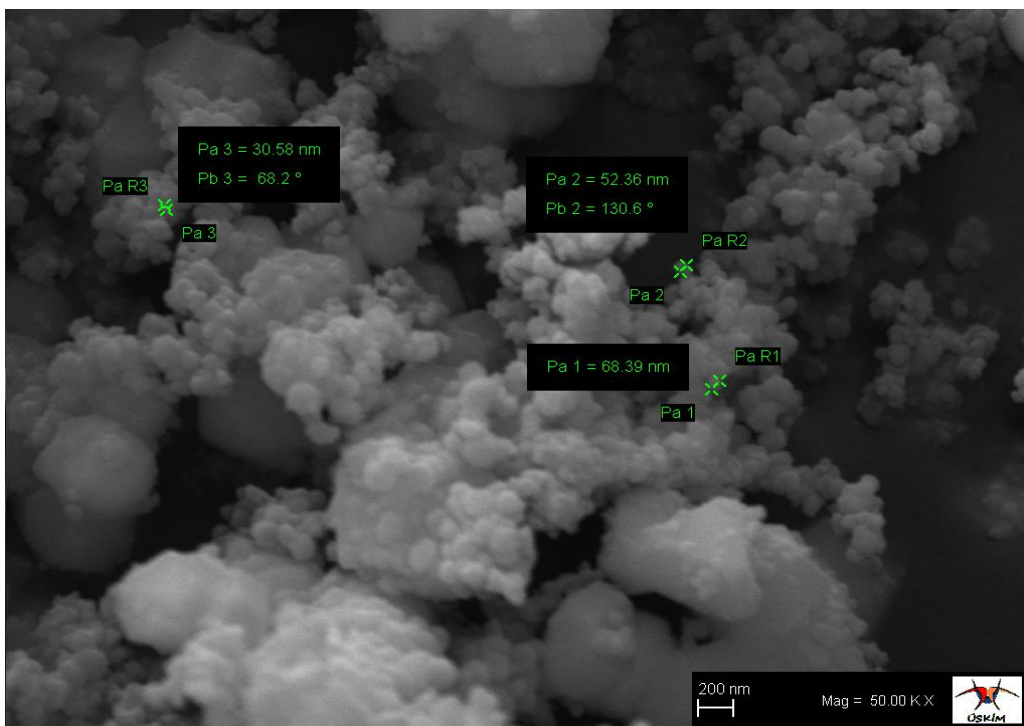


Figure 4.29b. SEM images of Ru<sub>0.92</sub>Pd<sub>0.08</sub>In<sub>2</sub>O<sub>3</sub> nanoparticles prepared

#### 4.8.2. EDX analysis of Ru<sub>0.92</sub>Pd<sub>0.08</sub>In<sub>2</sub>O<sub>3</sub>

The formation of pure Ru<sub>0.92</sub>Pd<sub>0.08</sub>In<sub>2</sub>O<sub>3</sub> was confirmed by means of Energy Dispersive X-ray analysis (EDX) as shown in Figure 4.30. The EDX result showed the presence of Ru<sub>0.92</sub>Pd<sub>0.08</sub>In<sub>2</sub>O<sub>3</sub> by the appearance of Ru, Pd, In and O peaks in the spectrum. The absence of carbon, nitrogen and other impurities are also evidenced from the EDX spectrum. This analysis confirmed that the sample Ru<sub>0.92</sub>Pd<sub>0.08</sub>In<sub>2</sub>O<sub>3</sub> prepared by microwave-assisted method. Hence, the result is definitive evidence to suggest that the sample does not contain any other element and are indeed free from other impurities. The peaks at 2.1–2.2 keV in the EDX spectra are due to the gold, which is coated on the samples before recording SEM.



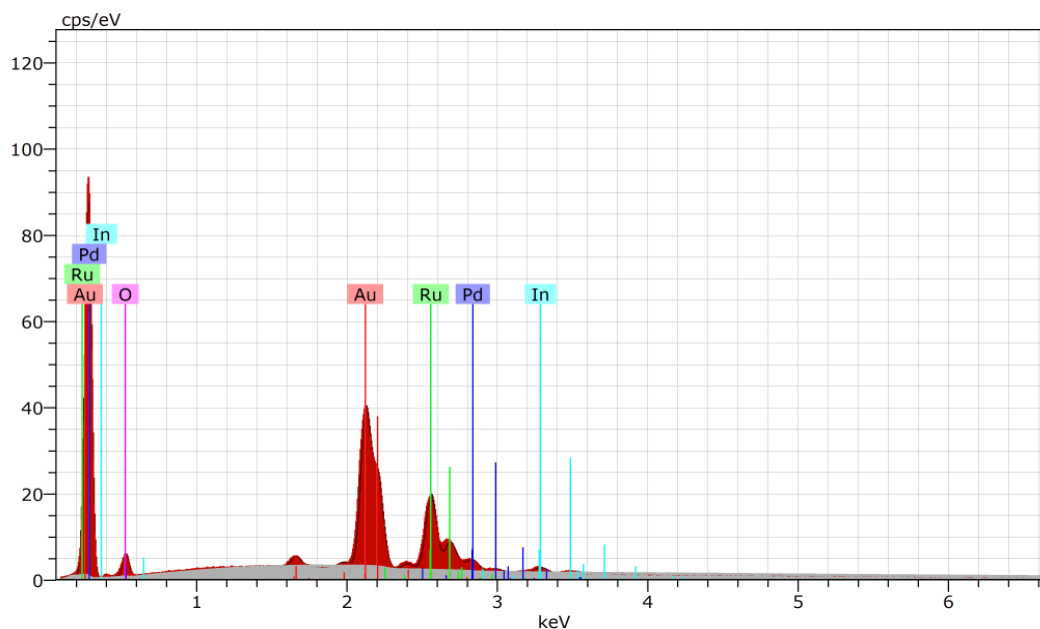


Fig.4.30. EDX spectrum of  $\text{Ru}_{0.92}\text{Pd}_{0.08}\text{In}_2\text{O}_3$  nanoparticles

#### 4.8.3. XRD analysis of $\text{Ru}_{0.92}\text{Pd}_{0.08}\text{In}_2\text{O}_3$

Powder characterization, shaping and conventional sintering the crystalline phase was identified by XRD using the  $\text{Cu-K}\alpha$  radiation with 0.154 nm wavelength at  $2\theta$  angle range from 10 to 70. In order to investigate the crystal structure of the obtained powder material XRD analysis was performed and the resultant pattern of the as-prepared sample is presented in Figure 4.28. In agreement with XRD patterns, a crystalline product appeared after 60 min of reaction at 200 °C. As shown in Figure 4.29, XRD can be used to study the phase purity of the obtained  $\text{Ru}_{0.92}\text{Pd}_{0.08}\text{In}_2\text{O}_3$  nanoparticles.

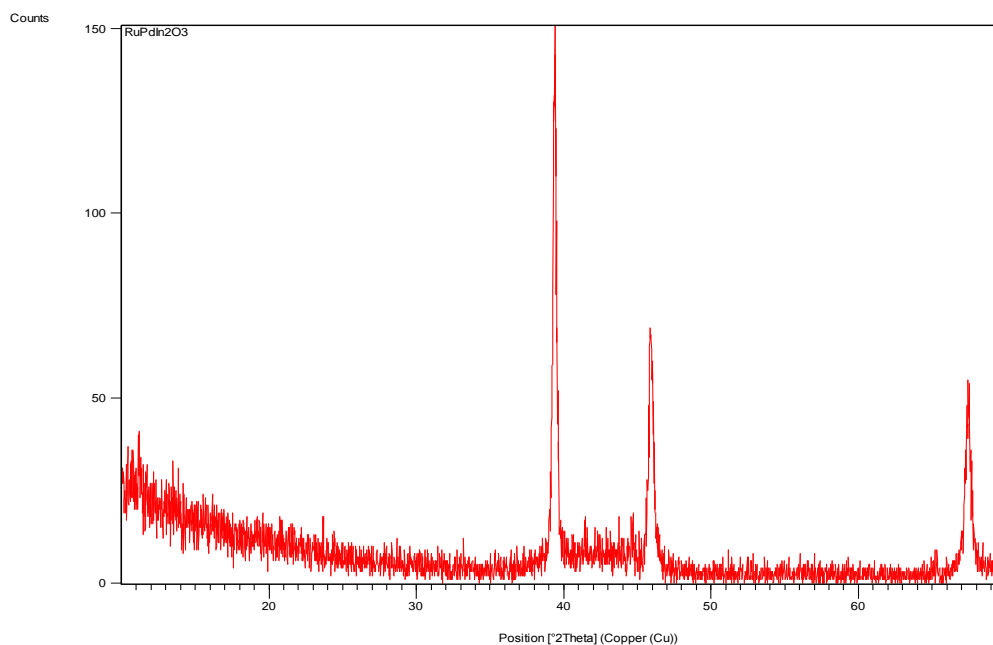


Figure 4.31. X-ray diffraction patterns of the  $\text{Ru}_{0.92}\text{Pd}_{0.08}\text{In}_2\text{O}_3$  nanoparticles

#### 4.8.4. FT-IR analysis of $\text{Ru}_{0.92}\text{Pd}_{0.08}\text{In}_2\text{O}_3$

The FT-IR spectroscopy is the most powerful and useful technique adopted by all the chemists to analyze, confirm and elucidate the structure of compounds and to identify the functional groups present in them. To confirm the formation of  $\text{Ru}_{0.92}\text{Pd}_{0.08}\text{In}_2\text{O}_3$  nanoparticles, the FT-IR spectra of the  $\text{Ru}_{0.92}\text{Pd}_{0.08}\text{In}_2\text{O}_3$  powders synthesized by microwave-assisted method at the ignition temperature of 200 °C, were obtained. Figure 4.32 shows FT-IR spectra of nanoparticles in the range 400–4000  $\text{cm}^{-1}$ . The peaks around 3311 and 1617  $\text{cm}^{-1}$  are absence can be attributed to the sample have no stretching vibrations of hydrogen-bonded surface water molecules and the free hydroxyl (-OH) groups of water molecules from ambient atmosphere, respectively, as other nanoparticles. These very weak absorption band are visible at 400–1100  $\text{cm}^{-1}$  range are associated with the bending and stretching modes of the metal–oxygen and the metal-oxygen-metal bonds corresponding to  $\text{Ru}_{0.92}\text{Pd}_{0.08}\text{In}_2\text{O}_3$  nanoparticle. Moreover the spectra of the  $\text{Ru}_{0.92}\text{Pd}_{0.08}\text{In}_2\text{O}_3$  showed the weak shoulder peak at 1390  $\text{cm}^{-1}$ , which is assigned to the In-O stretching vibrations.

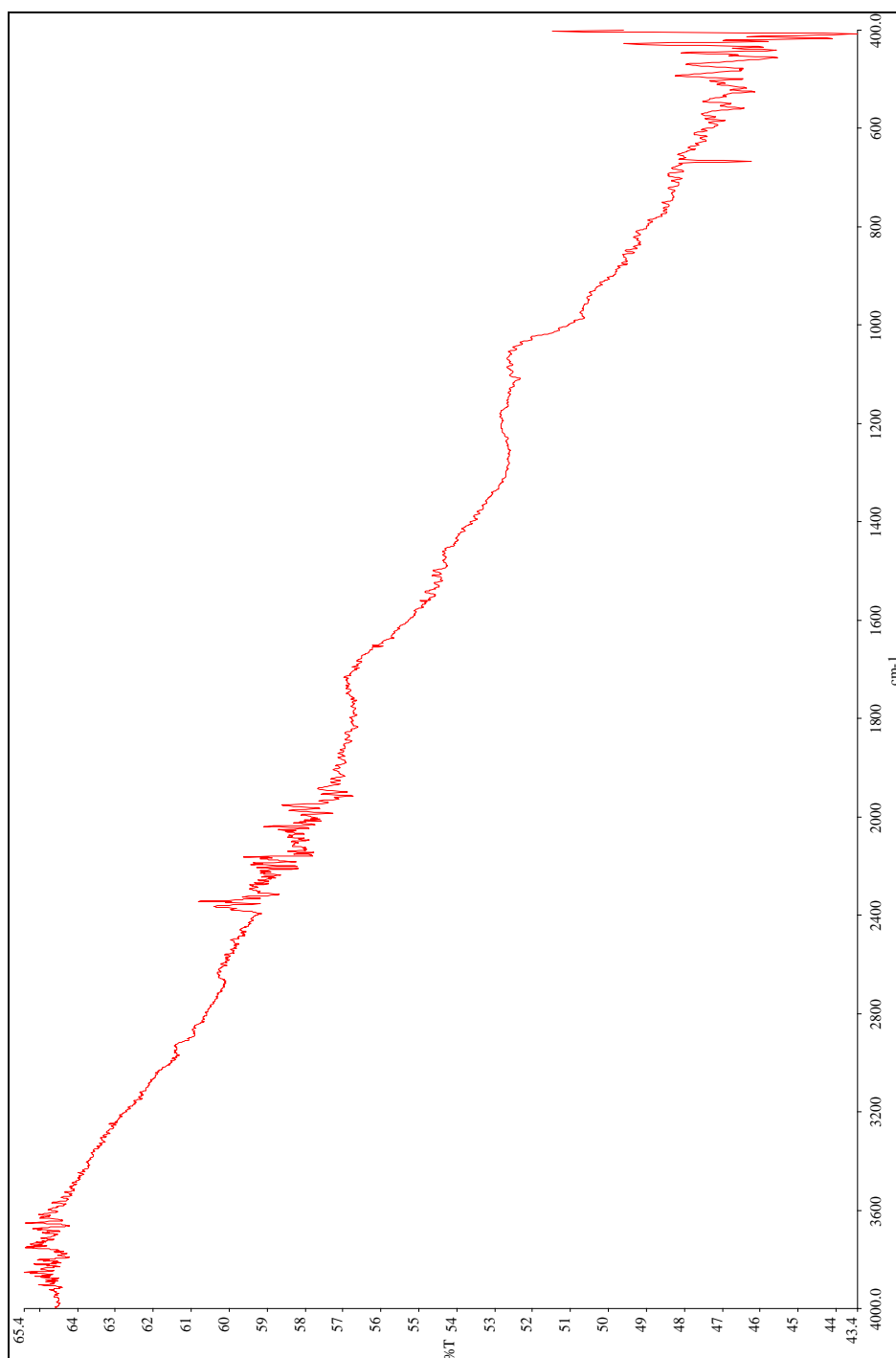


Figure 4.32. The FT-IR spectra of Ru<sub>0.92</sub>Pd<sub>0.08</sub>In<sub>2</sub>O<sub>3</sub> nanoparticles

## 4.9. NPs of $\text{Ru}_{0.54}\text{Pt}_{0.46}\text{In}_2\text{O}_3$

### 4.9.1. SEM analysis of $\text{Ru}_{0.54}\text{Pt}_{0.46}\text{In}_2\text{O}_3$

The surface morphology of  $\text{Ru}_{0.54}\text{Pt}_{0.46}\text{In}_2\text{O}_3$  was investigated by the SEM as shown in Figure 4.33a and 4.33b. Figure 4.33b shows the formation of nanoparticles for  $\text{Ru}_{0.54}\text{Pt}_{0.46}\text{In}_2\text{O}_3$ . It can be observed from Figure 4.33b that the structure is actually composed of numerous nanosphere that are intercrossed with each other to form amorphous like structure. This is probably due to the polarization of the molecules under the rapidly changing electro-magnetic field of the microwave reactor, which may result in transient, localized high temperatures for the reaction system, leading to fast synthesis with desired morphology. Figure 4.33b shows that the average diameter of nanoparticles less than 100 nm. Real particle size can not be measured because of amorphous structure. It is a well-known fact that the temperature and reaction time are the two important factors in determining the morphology of the nanomaterials. In the conventional method, the reaction time is kept as 3 h, at 400 °C, which resulted in the formation of nanoparticles. But in microwave method, because of rapid heating, which is achieved within the few minutes, due to the suppressed diffusion process, the nano-amorphous would have been formed.

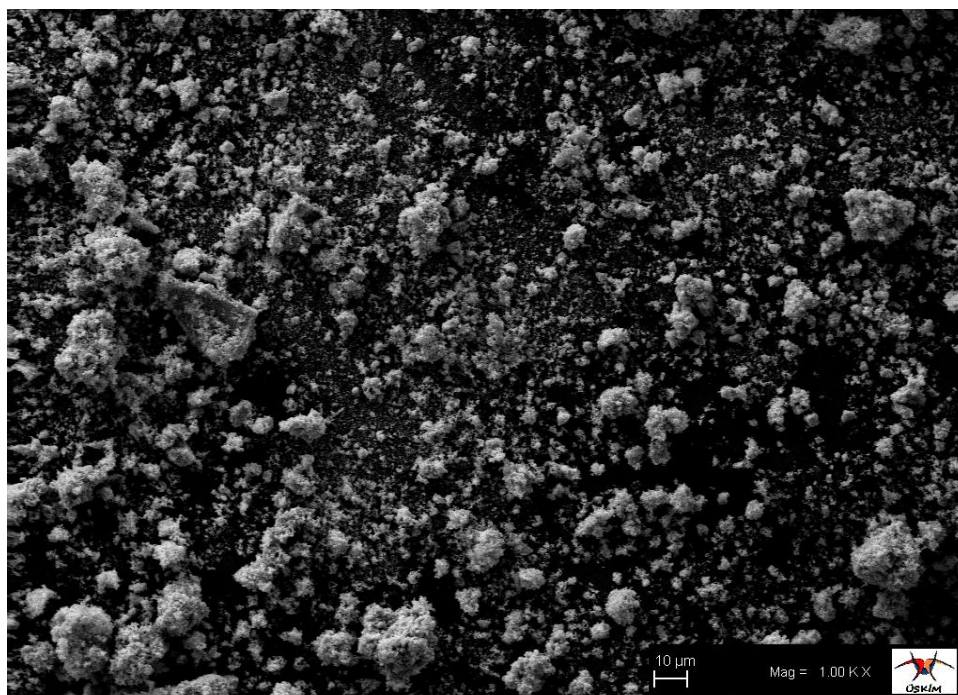


Figure 4.33a. SEM images of  $\text{Ru}_{0.54}\text{Pt}_{0.46}\text{In}_2\text{O}_3$  nanoparticles prepared.

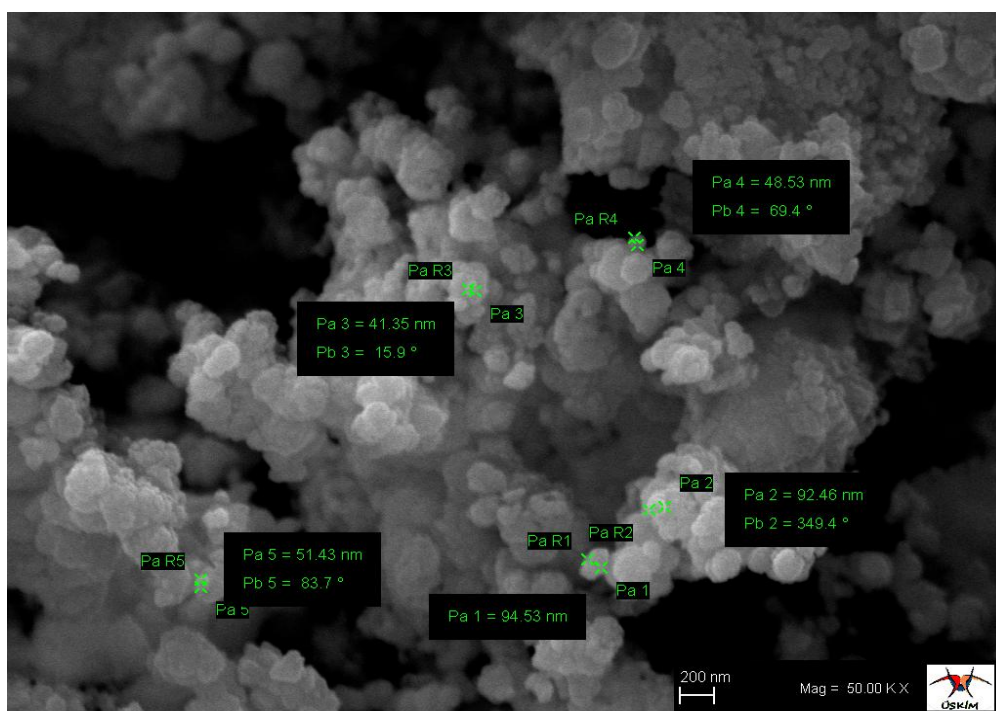


Figure 4.33b. SEM images of Ru<sub>0.54</sub>Pt<sub>0.46</sub>In<sub>2</sub>O<sub>3</sub> nanoparticles prepared.

#### 4.9.2. EDX analysis of Ru<sub>0.54</sub>Pt<sub>0.46</sub>In<sub>2</sub>O<sub>3</sub>

The formation of pure Ru<sub>0.54</sub>Pt<sub>0.46</sub>In<sub>2</sub>O<sub>3</sub> was confirmed by means of energy dispersive X-ray analysis EDX as shown in Figure 4.34. The EDX result showed the presence of Ru<sub>0.54</sub>Pt<sub>0.46</sub>In<sub>2</sub>O<sub>3</sub> by the appearance of Ru, Fe, Al and O peaks in the spectrum. The absence of carbon, nitrogen and other impurities are also evidenced from the EDX spectrum. This analysis confirmed that the sample Ru<sub>0.54</sub>Pt<sub>0.46</sub>In<sub>2</sub>O<sub>3</sub> prepared by microwave-assisted method. Hence, the result is definitive evidence to suggest that the sample does not contain any other element and are indeed free from other impurities. The peaks at 2.1–2.2 keV in the EDX spectra are due to the gold, which is coated on the samples before recording SEM.

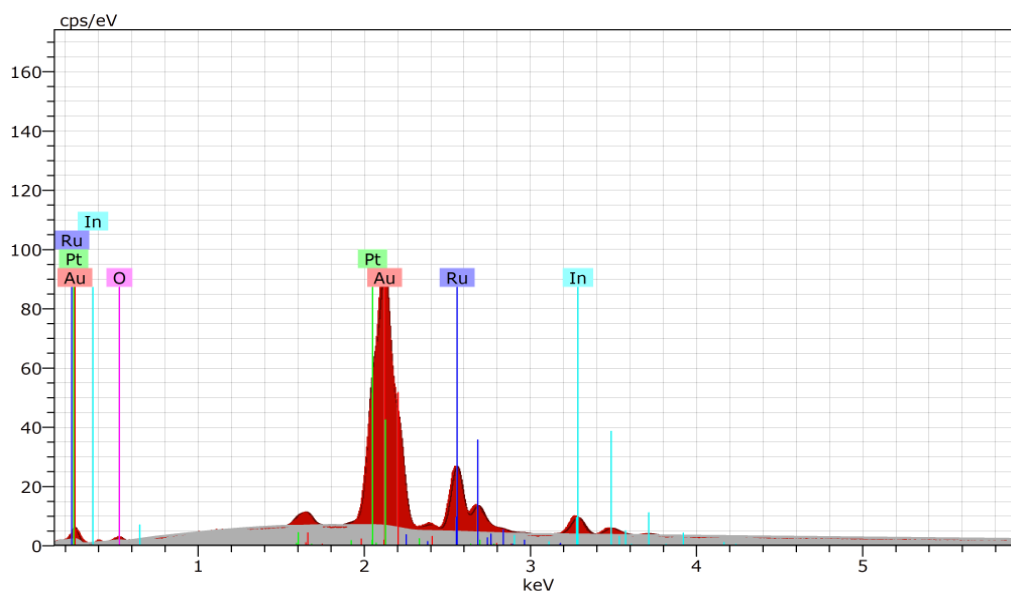


Figure 4.34. EDAX spectrum of  $\text{Ru}_{0.54}\text{Pt}_{0.46}\text{In}_2\text{O}_3$  nanoparticles

#### 4.9.3. XRD analysis of $\text{Ru}_{0.54}\text{Pt}_{0.46}\text{In}_2\text{O}_3$

Powder characterization, shaping and conventional sintering the crystalline phase was identified by XRD using the  $\text{Cu-K}\alpha$  radiation with 0.154 nm wavelength at  $2\theta$  angle range from 10 to 70. In order to investigate the crystal structure of the obtained powder material XRD analysis was performed and the resultant pattern of the as-prepared sample is presented in Fig. 1. In agreement with XRD patterns, a crystalline product appeared after 60 min of reaction at 200 °C. As shown in Figure 4.35, XRD can be used to study the phase purity of the obtained  $\text{Ru}_{0.54}\text{Pt}_{0.46}\text{In}_2\text{O}_3$  nanoparticles.

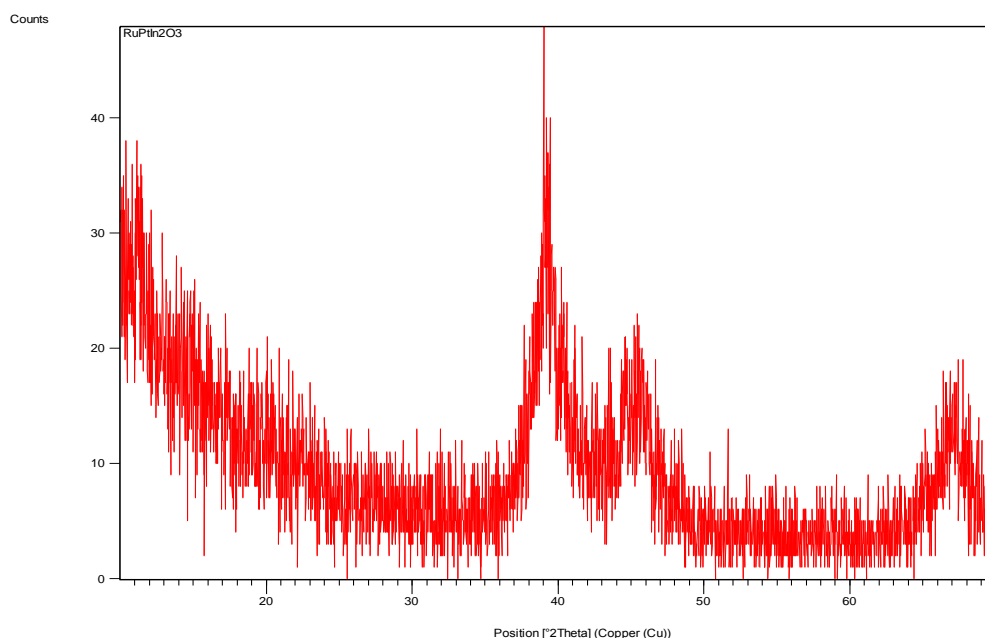


Figure 4.35. X-ray diffraction patterns of the  $\text{Ru}_{0.54}\text{Pt}_{0.46}\text{In}_2\text{O}_3$  nanoparticles

#### 4.9.4. FT-IR analysis of $\text{Ru}_{0.54}\text{Pt}_{0.46}\text{In}_2\text{O}_3$

The FT-IR spectroscopy is the most powerful and useful technique adopted by all the chemists to analyze, confirm and elucidate the structure of compounds and to identify the functional groups present in them. To confirm the formation of  $\text{Ru}_{0.54}\text{Pt}_{0.46}\text{In}_2\text{O}_3$  nanoparticles, the FT-IR spectra of the  $\text{Ru}_{0.54}\text{Pt}_{0.46}\text{In}_2\text{O}_3$  powders synthesized by microwave-assisted method at the ignition temperature of 200 °C, were obtained. Figure 4.36 shows FT-IR spectra of nanoparticles in the range 400–4000  $\text{cm}^{-1}$ . The peaks around 3287 and 1634  $\text{cm}^{-1}$  can be attributed to the stretching vibrations of hydrogen-bonded surface water molecules and the free hydroxyl (-OH) groups of water molecules from ambient atmosphere, respectively. The absorption bands in the range 406–892  $\text{cm}^{-1}$  appears due to the formation of metal oxides. These intense and weak absorption band are visible at 400–1066  $\text{cm}^{-1}$  range are associated with the bending and stretching modes of the metal–oxygen and the metal–oxygen–metal bonds corresponding to  $\text{Ru}_{0.54}\text{Pt}_{0.46}\text{In}_2\text{O}_3$  nanoparticle. Moreover the spectra of the  $\text{Ru}_{0.54}\text{Pt}_{0.46}\text{In}_2\text{O}_3$  showed the peak at 1406  $\text{cm}^{-1}$ , which is assigned to the In-O stretching vibrations.

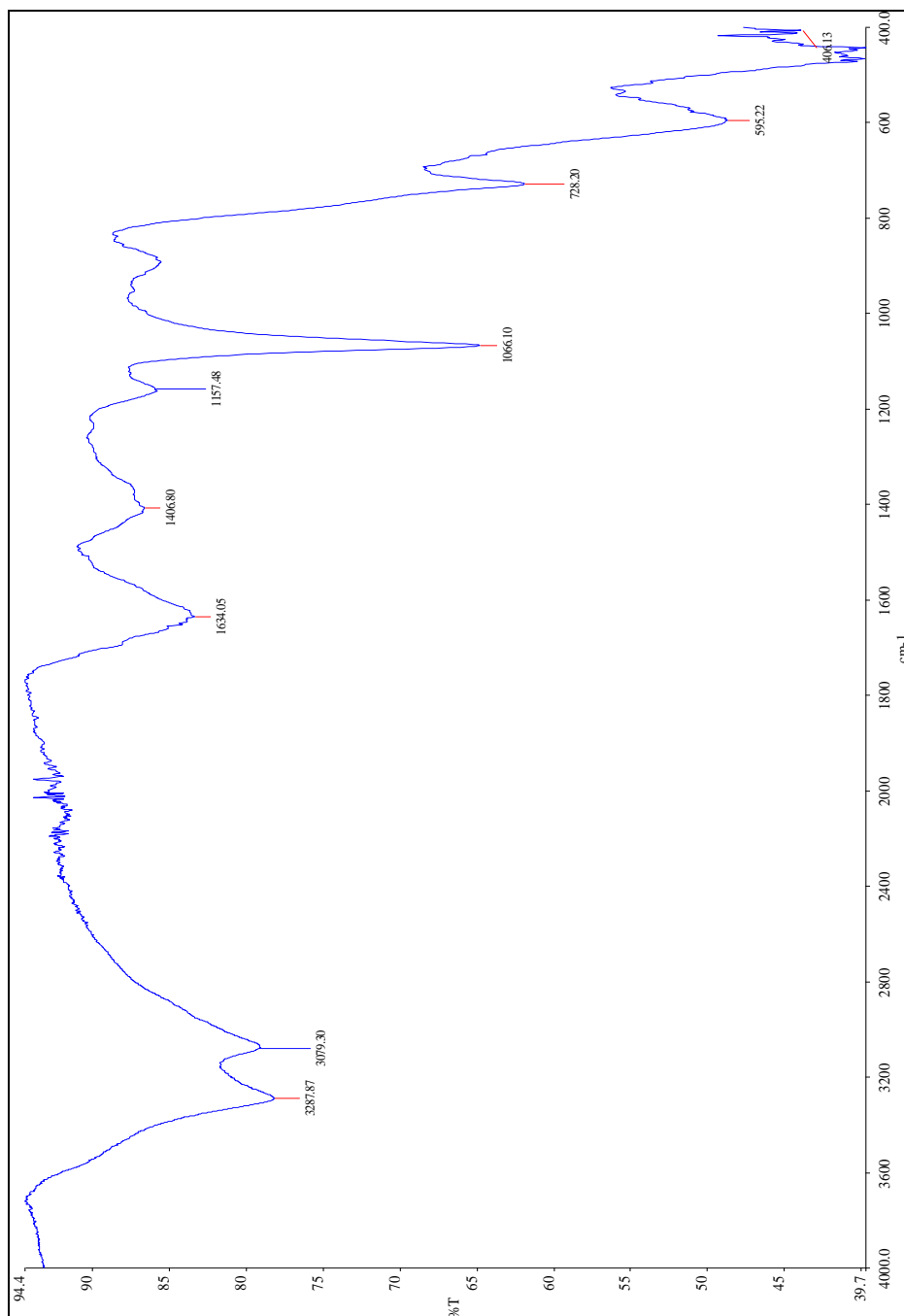


Figure 4.36. The FT-IR spectra of Ru<sub>0.54</sub>Pt<sub>0.46</sub>In<sub>2</sub>O<sub>3</sub> nanoparticles



## 4.10. NPs of $\text{Ru}_{0.54}\text{Pt}_{0.46}\text{In}_2\text{O}_3$

### 4.10.1. SEM analysis of $\text{Ru}_{0.54}\text{Pt}_{0.46}\text{In}_2\text{O}_3$

The surface morphology of  $\text{Ru}_{0.56}\text{Cu}_{0.44}\text{In}_2\text{O}_3$  was investigated by the SEM as shown in Figure 4.37a and Figure 4.37b. From the images, Figure 4.37b shows the formation of nanoparticles for  $\text{Ru}_{0.56}\text{Cu}_{0.44}\text{In}_2\text{O}_3$ . It can be observed from Figure 4.37b that the structure is actually composed of numerous nanosphere that are intercrossed with each other to form amorphous like structure. This is probably due to the polarization of the molecules under the rapidly changing electro-magnetic field of the microwave reactor, which may result in transient, localized high temperatures for the reaction system, leading to fast synthesis with desired morphology. Figure 4.37b shows that the average diameter of nanoparticles less than 100 nm. Real particle size can not be measured because of amorphous structure. It is a well-known fact that the temperature and reaction time are the two important factors in determining the morphology of the nanomaterials. In the conventional method, the reaction time is kept as 3 h, at 400 °C, which resulted in the formation of nanoparticles. But in microwave method, because of rapid heating, which is achieved within the few minutes, due to the suppressed diffusion process, the nano-amorphous would have been formed.

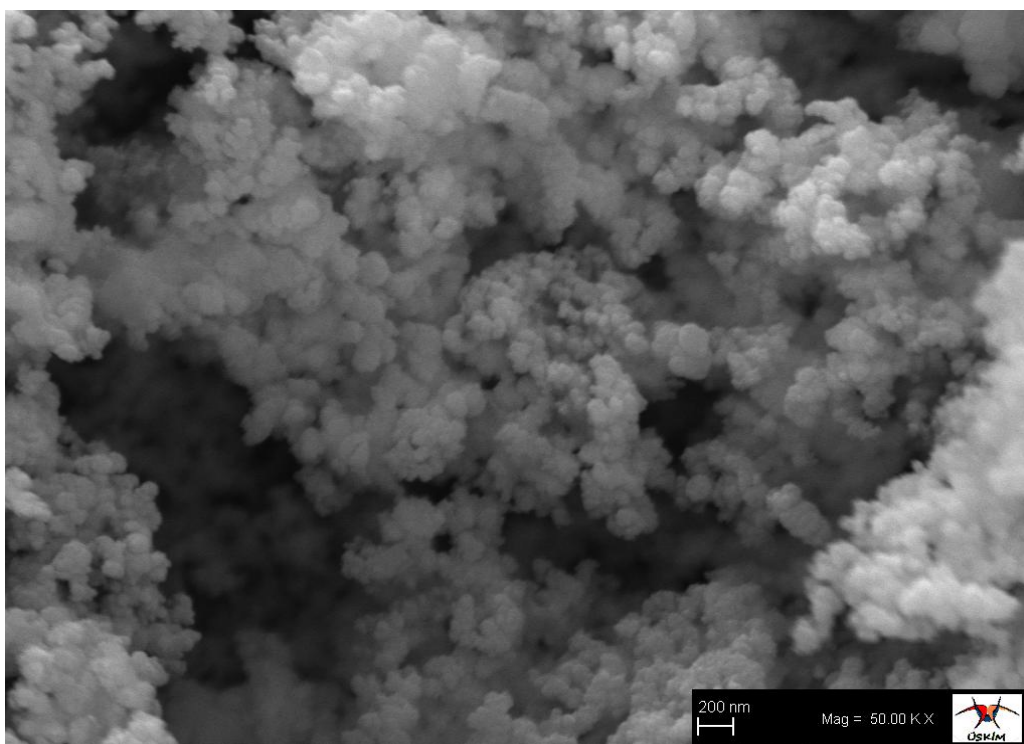


Figure 4.37a. SEM images of  $\text{Ru}_{0.56}\text{Cu}_{0.44}\text{In}_2\text{O}_3$  nanoparticles prepared.

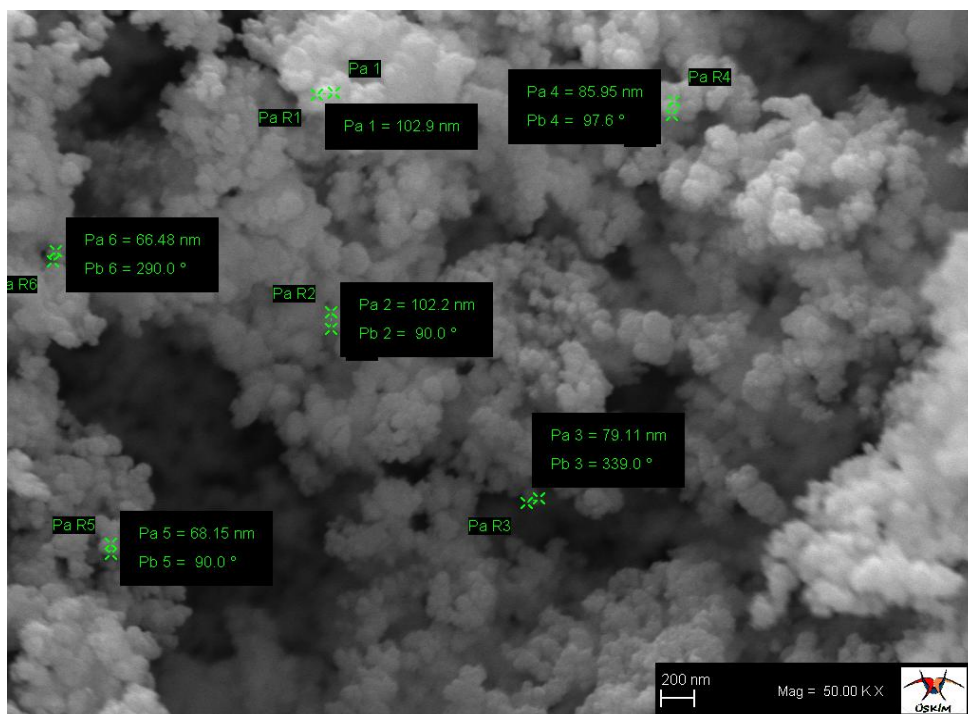


Figure 4.37b. SEM images of  $\text{Ru}_{0.56}\text{Cu}_{0.44}\text{In}_2\text{O}_3$  nanoparticles prepared.

#### 4.10.2. EDX analysis of $\text{Ru}_{0.54}\text{Pt}_{0.46}\text{In}_2\text{O}_3$

The formation of pure  $\text{Ru}_{0.56}\text{Cu}_{0.44}\text{In}_2\text{O}_3$  was confirmed by means of energy dispersive X-ray analysis EDX as shown in Figure 4.38. The EDX result showed the presence of  $\text{Ru}_{0.56}\text{Cu}_{0.44}\text{In}_2\text{O}_3$  by the appearance of Ru, Fe, In and O peaks in the spectrum. The absence of carbon, nitrogen and other impurities are also evidenced from the EDX spectrum. This analysis confirmed that the sample  $\text{Ru}_{0.56}\text{Cu}_{0.44}\text{In}_2\text{O}_3$  prepared by microwave-assisted method. Hence, the result is definitive evidence to suggest that the sample does not contain any other element and are indeed free from other impurities. The peaks at 2.1–2.2 keV in the EDX spectra are due to the gold, which is coated on the samples before recording SEM.

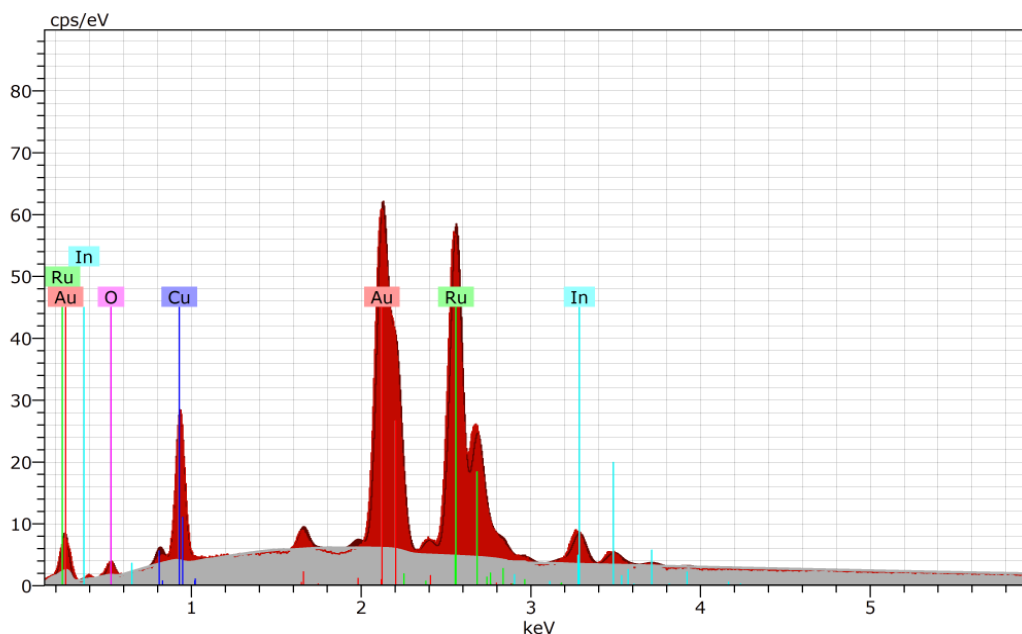


Figure 4.38. EDX spectrum of  $\text{Ru}_{0.56}\text{Cu}_{0.44}\text{In}_2\text{O}_3$  nanoparticles

#### 4.10.3. XRD analysis of $\text{Ru}_{0.54}\text{Pt}_{0.46}\text{In}_2\text{O}_3$

Powder characterization, shaping and conventional sintering the crystalline phase was identified by XRD using the  $\text{Cu-K}\alpha$  radiation with 0.154 nm wavelength at  $2\theta$  angle range from 10 to 70. In order to investigate the crystal structure of the obtained powder material XRD analysis was performed and the resultant pattern of the as-prepared sample is presented in Fig. 1. In agreement with XRD patterns, a crystalline product appeared after 60 min of reaction at 200 °C. As shown in Figure 4.39, XRD can be used to study the phase purity of the obtained  $\text{Ru}_{0.56}\text{Cu}_{0.44}\text{In}_2\text{O}_3$  nanoparticles.

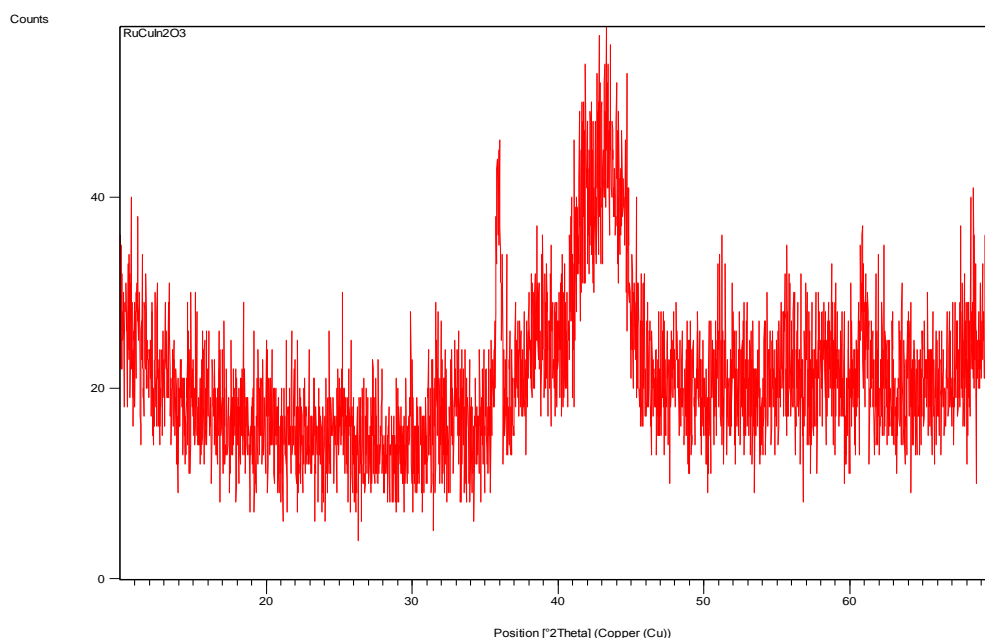


Figure 4.39. X-ray diffraction patterns of the  $\text{Ru}_{0.56}\text{Cu}_{0.44}\text{In}_2\text{O}_3$  nanoparticles

#### 4.10.4. FT-IR analysis of $\text{Ru}_{0.54}\text{Pt}_{0.46}\text{In}_2\text{O}_3$

The FT-IR spectroscopy is the most powerful and useful technique adopted by all the chemists to analyze, confirm and elucidate the structure of compounds and to identify the functional groups present in them. To confirm the formation of  $\text{Ru}_{0.56}\text{Cu}_{0.44}\text{In}_2\text{O}_3$  nanoparticles, the FT-IR spectra of the  $\text{Ru}_{0.56}\text{Cu}_{0.44}\text{In}_2\text{O}_3$  powders synthesized by microwave-assisted method at the ignition temperature of 200 °C, were obtained. Figure 4.40 shows FT-IR spectra of nanoparticles in the range 400–4000  $\text{cm}^{-1}$ . The peaks around 3287 and 1634  $\text{cm}^{-1}$  as other compounds were not observed that show the absence of all kind of water. The absorption bands in the range 400–1000  $\text{cm}^{-1}$  appears due to the formation of metal oxides. However, the intensity of bands very low to explaining modes. The other analysis show  $\text{Ru}_{0.56}\text{Cu}_{0.44}\text{In}_2\text{O}_3$  nanoparticles structure.

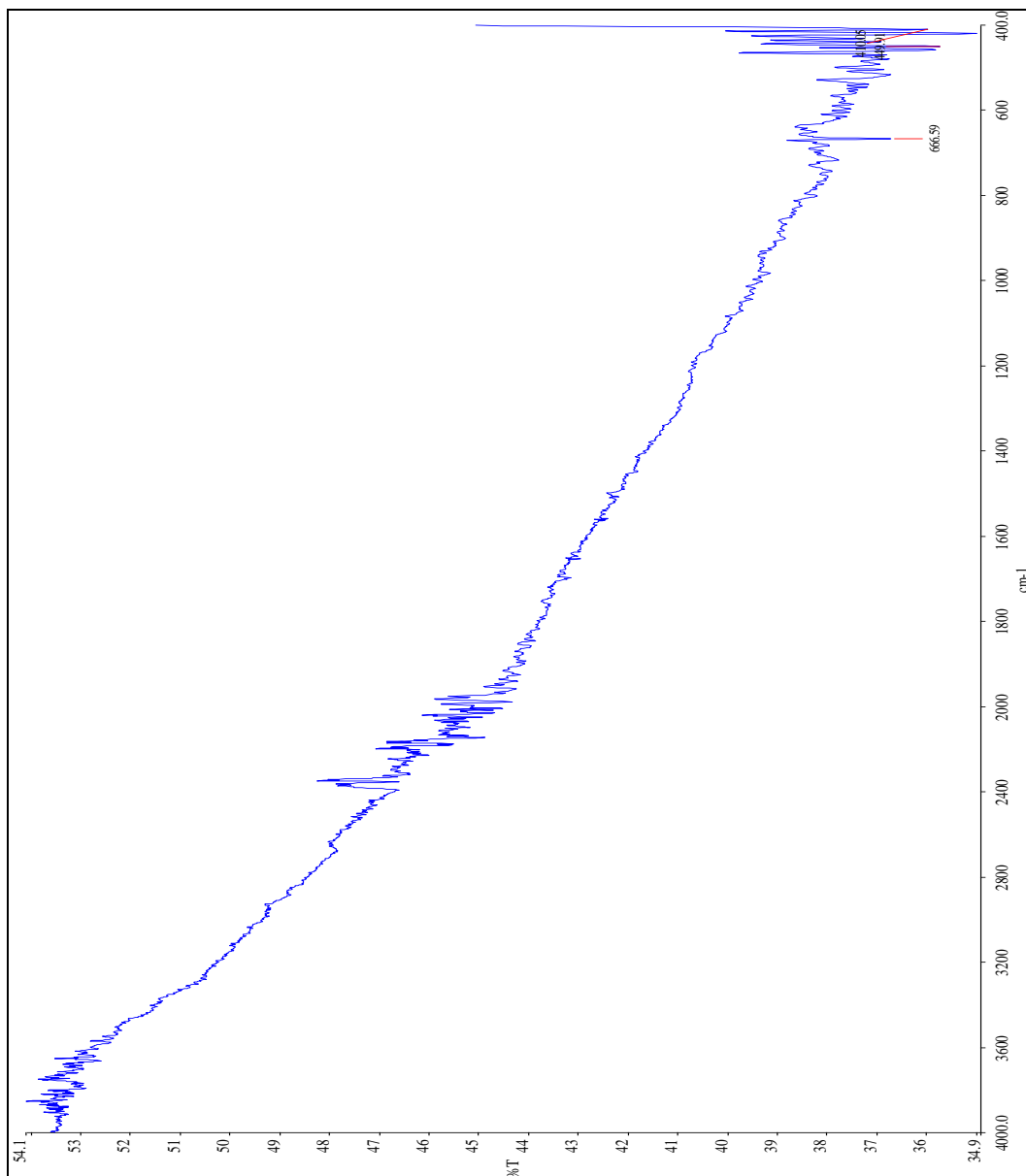


Figure 4.40. The FT-IR spectra of Ru<sub>0.56</sub>Cu<sub>0.44</sub>In<sub>2</sub>O<sub>3</sub> nanoparticles

## 5. CONCLUSION

Three metal composed of nanostructures have been successfully synthesized by a simple and rapid microwave-assisted method using thiourea as the fuel and EG as the surfactant. In the case of homogeneous precipitation, thiourea acts as a precipitant, since thiourea decomposed around 100 °C to produce carbon dioxide, sulphur dioxide and ammonia thereby increasing the pH of the solution at which metal cation precipitation takes place. In summary, we synthesized single phase nanoparticles by a microwave-assisted route without additional high temperature calcination process. In comparison with conventional heating, microwave-assisted combustion method shortens the reaction time. Besides, the effect of microwave power, and reaction time on the particle size of nanoparticles was studied. The heating is not only quick but also uniformly spread through the entire bulk of the reaction mixture. This may result in the formation of nanoparticles structure with narrow distribution of particle size. Therefore, our methodology and experiments may promote the control of desired morphologies of other functional oxide materials. Moreover, the microwave-assisted method is an economical and rapid method for the preparation of nanostructures when compared to the conventional method with respect to energy, time and simplicity.

Microwave irradiation has yielded nanosized cubic phase  $\text{Ru}_{0.62}\text{In}_{0.38}\text{Al}_2\text{O}_3$  and  $\text{Ru}_{0.77}\text{Co}_{0.23}\text{In}_2\text{O}_3$  particles. The mean grain size of the nanoparticles less than 100 nm FT-IR studies confirms the presence of metal–oxygen bond. XRD and SEM of the synthesized nanoparticles show that the as prepared  $\text{Ru}_{0.77}\text{Co}_{0.23}\text{In}_2\text{O}_3$  has high crystallinity and sphere-like shape. The morphology, particle size and microstructure were analyzed using SEM and XRD. The XRD data of  $\text{Ru}_{0.77}\text{Co}_{0.23}\text{In}_2\text{O}_3$  and  $\text{Ru}_{0.92}\text{Pd}_{0.08}\text{In}_2\text{O}_3$  also confirm the formation of single phase structure. Their micrograph pattern shows the crystalline perfection. The crystallite sizes were found in the range of 41-94 nm; FT-IR spectra further supports and confirm the crystalline phase as well as the specific bands to show the modes of vibration in M-O system. Flower shaped  $\text{Ru}_{0.63}\text{Co}_{0.37}\text{Al}_2\text{O}_3$ ,  $\text{Ru}_{0.93}\text{Ni}_{0.07}\text{Al}_2\text{O}_3$  and  $\text{Ru}_{0.54}\text{Cu}_{0.46}\text{Al}_2\text{O}_3$  particles were obtained when aluminum salts, thiourea and EG solution were used. The nanostructures are influenced by microwave irradiation time, reagent concentration and molar ratio of the precursors. High crystalline materials were readily obtained without the need of a post-synthesis treatment. This method can also be perpetrated for the preparation of gram quantity of other metal oxide powders.

SEM micrographs of nanopowders calcined at 200 °C are shown in Figure 1-10. Formation of spherical particles and flower type has been observed for all samples. SEM images show particle diameter in range from 30 to 95 nm.

Similar morphology has also been observed for all other indium doped samples, there are change in morphology when aluminum enters into the nanoparticles lattice, but the particles shape and size also are changed from sphere to flower type  $Ru_xM_{1-x}Al_2O_3$  (M: Co, Cu, Ni).

The SEM results revealed that the morphology of the prepared nanoparticles are nearly spherical in shape with smaller size. It is clear from the SEM images that some nanoparticles are non spherical in shape and some of them have flower shapes.

The synthesized  $Ru_xM_{1-x}In_2O_3$  architectures (M: Co, Ni, Pd, Pt, Cu) were found to be polycrystalline and spherical in shape.

The EDX analysis Fig. 1-10, in set of the nanoparticles indicated that the elements of Ru, Fe, Co, Ni, Cu, Pd, Pt, In and Al existed in the products. The surface treatment of spray gold for elimination of charged effects were responsible for the signals of gold in the EDX analysis of the products. In other words, no impurities like N, S, P, Cl, etc. were detected except for Ru, Fe, Co, Ni, Cu, Pd, Pt, In and Al elements, indicating the nanoparticles were pure.

Obtaining control over the morphology of microparticles with well-defined shapes remained an important goal of modern materials chemistry, since shape-controlled particles with anisotropic nanostructure were promising candidates as active components in a wide range of technological applications, and were model systems for the study of microscale shape-dependent properties. In particular, the shape-controlled synthesis of nanoparticles compounds had attracted intensive interest.

Herein, were ported a microwave-assisted method to synthesize spherical and flower shape nanoparticles via the reaction between three metal salts and thiourea with the addition of the EG.

The use of nanoparticles can improve the pigment performance: in the organic coatings, for instance, nano-pigments enhance the tribological and mechanical properties while maintaining toughness. All synthesized nanoparticles in this study have black colour.

They may be used as black nano-pigments. These nanopigments with particle size in nanoscale may have a massive potential market, because of their high surface area, which assures higher surface coverage, higher number of reflectance points and hence improved scattering. In paint formulations, for example, the small particle size allows uniform dispersion by homogenous mixing with binders, which enhances the mechanical strength of the paint after drying. When properly dispersed, the nanosized pigments exhibit superior effectiveness also in critical abrasive and polishing applications. These synthesized nanoparticles can be used for ink-jet printing. [79]

This microwave-assisted method may be extended to synthesize other hierarchical nanostructures in the future.



## REFERENCES

- [1] Horikoshi, S., and Serpone, N., 2013 *Microwaves in Nanoparticle Synthesis*, First Edition, Research, 1-20 P.
- [2] Dwivedi et al., 2011; Gao et al., 2008; Krystek et al., 2011; Radad et al., 2012.
- [3] Asere, T., G., 2012-2013, Exploring potential environmental applications of selenium nanoparticles. Host University, Research, 1-12 p.
- [4] Daniel, M.-C., and Astruc, D. 2004. *Chem. Rev.*, 104, 293 – 346.
- [5] W., Herbst, K., Hunger, 2004, *Industrial Organic Pigments, Production, Properties, Applications Third, Completely Revised Edition*. Book, 1-4 p.
- [6] Historically nanoparticules/nanopigments. (Access date: 13-11-2013). [http://www.britishmuseum.org/explore/highlight\\_image.aspx?image = k741. Jpg & retpage=20945](http://www.britishmuseum.org/explore/highlight_image.aspx?image = k741. Jpg & retpage=20945)
- [7] Azam, A. 2012. Microwave assisted synthesis and characterization of Co doped Cu ferrite nanoparticles. *Journal of Alloys and Compounds*, 540, 145-153.
- [8] Hu, H., Wang, X., Liu, F., Wang, J., Xu, C. 2011. Rapid microwave-assisted synthesis of graphene nanosheets–zinc sulfide nanocomposites: Optical and photocatalytic properties. *Synthetic Metals*, 161(5): 404-410.
- [9] Definition of Nano Particles and Methods of Nanoparticle Synthesis (Access date: 15-2-2014). [http://www.univie.ac.at/cost531/COST\\_MP0602/WG-eetings/Brno/WGMeeting\\_Brno Liu.pdf](http://www.univie.ac.at/cost531/COST_MP0602/WG-eetings/Brno/WGMeeting_Brno Liu.pdf)
- [10] Asere, T., G., 2012-2013, Exploring potential environmental applications of selenium nanoparticles. Host University, Research, 1-12 p.
- [11] Türke, A., Fischer, W. J., Adler, H. J., Pich, A. 2010. Microwave-assisted synthesis of hybrid colloids for design of conducting films. *Polymer*, 51(21): 4706-4712.

- [12] Kajbafvala, A., Ghorbani, H., Paravar, A., Samberg, J. P., Kajbafvala, E., Sadrnezhaad, S. K. 2012. Effects of morphology on photocatalytic performance of Zinc oxide nanostructures synthesized by rapid microwave irradiation methods. *Superlattices and Microstructures*, 51(4): 512-522.
- [13] Gondal, M. A., Saleh, T. A., Drmosh, Q. A. 2012. Synthesis of nickel oxide nanoparticles using pulsed laser ablation in liquids and their optical characterization. *Applied Surface Science*, 258(18): 6982-6986.
- [14] Gupta, S., Giordano, C., Gradzielski, M., Mehta, S. K. 2013. Microwave-assisted synthesis of small Ru nanoparticles and their role in degradation of congo red. *Journal of colloid and interface science*, 411, 173-181.
- [15] Rejitha, S. G., Krishnan, C. 2013. Synthesis of cadmium-doped copper oxide nanoparticles: Optical and structural characterizations. *Advances in Applied Science Research*, 4(2):103P.
- [16] Figure Nanoparticles in a wide variety of different shapes and sizes (Access date: 19-2-2014). <http://www.sciencedaily.com/releases/2007/07/070709171558.htm>
- [17] Rastogi, P. K., Ganesan, V., Krishnamoorthi, S. 2012. Microwave assisted polymer stabilized synthesis of silver nanoparticles and its application in the degradation of environmental pollutants. *Materials Science and Engineering: B*, 177(6): 456-461.
- [18] Carrillo, A. I., Serrano, E., Luque, R., García-Martínez, J. 2013. Microwave-assisted catalysis by iron oxide nanoparticles on MCM-41: Effect of the support morphology. *Applied Catalysis A: General*, 453, 383-390.
- [19] Mirjalili, B., F., Akbari, A. J. 2011. Nano-TiO<sub>2</sub>: An eco-friendly alternative for the synthesis of quinoxalines, *22*, 753–756.
- [20] Topuz, B. B., Gündüz, G., Mavis, B., Çolak, Ü. 2013. Synthesis and characterization of copper phthalocyanine and tetracarboxamide copper phthalocyanine deposited mica-titania pigments. *Dyes and Pigments*, 96(1): 31-37.
- [21] Jähne, C., Klingeler, R. 2012. Microwave-assisted hydrothermal synthesis of low-temperature LiCoO<sub>2</sub>, *14*, 941-947.

- [22] Structure of Nanoparticles (Access date: 16-2-2014)  
[http://www.mawi.tudarmstadt.de/st/strukturforschung/forschung\\_7/strukturvonnanopartikeln/strukturvonnanopartikeln.en.jsp](http://www.mawi.tudarmstadt.de/st/strukturforschung/forschung_7/strukturvonnanopartikeln/strukturvonnanopartikeln.en.jsp).
- [23] Al-Gaashani, R., Radiman, S., Tabet, N., Daud, A. R. 2011. Effect of microwave power on the morphology and optical property of zinc oxide nano-structures prepared via a microwave-assisted aqueous solution method. *Materials Chemistry and Physics*, 125(3): 846-852.
- [24] Majithia, R. Y. 2013. Microwave-assisted synthesis of II-VI semiconductor micro- and nanoparticles towards sensor applications (Doctoral dissertation, Texas A&M University).
- [25] La Porta, F. A., Ferrer, M. M., de Santana, Y. V., Raubach, C. W., Longo, V. M., Sambrano, J. R., Varela, J. A. 2013. Synthesis of wurtzite ZnS nanoparticles using the microwave assisted solvothermal method. *Journal of Alloys and Compounds*, 556, 153-159.
- [26] Hosseinpour-Mashkani, S. M., Salavati-Niasari, M., Mohandes, F., Venkateswara-Rao, K. 2013. CuInS<sub>2</sub> nanoparticles: Microwave-assisted synthesis, characterization, and photovoltaic measurements. *Materials Science in Semiconductor Processing*, 16(2): 390-402.
- [27] Schematic images of bimetal nanoparticles: alloy structure, core-shell. (Access date: 20-2-2014) <http://www.usask.ca/chemistry/groups/scott/images/bimetallic.jpg>
- [28] Define Pigments (Access date: 26-9-2013)  
<http://www.ihs.com/products/chemical/planning/ceh/inorganic-color.aspx>
- [29] Calogero, G., Yum, J. H., Sinopoli, A., Di Marco, G., Grätzel, M., Nazeeruddin, M. K. 2012. Anthocyanins and betalains as light-harvesting pigments for dye-sensitized solar cells. *Solar Energy*, 86(5): 1563-1575.
- [30] Lang, Arnold R. 2008. *Dyes and pigments NEW RESEARCH*. Nova Science Publishers, Inc. New York. (384 p. 353 p., chapter 3 - 97p.) Respectively.

- [31] Ahmed, L. S., Shama, S. A., Dessouki H. A., Ali A. A., 2011. Low temperature combustion synthesis of  $\text{Co}_x\text{Mg}_{1-x}\text{Al}_2\text{O}_4$  nano pigments using oxalyldihydrazide as a fuel, 125, 326-33.
- [32] Patel, M. A., Bhanvase, B. A., Sonawane, S. H. 2013. Production of cerium zinc molybdate nano pigment by innovative ultrasound assisted approach. *Ultrasonics sonochemistry*, 20(3): 906-913.
- [33] Bahadur, N. M., Furusawa, T., Sato, M., Kurayama, F., Suzuki, N. 2010. Rapid Synthesis, characterization and optical properties of  $\text{TiO}_2$  coated ZnO nanocomposite particles by a novel microwave irradiation method. *Materials Research Bulletin*, 45(10): 1383-1388.
- [34] Wang, J. L., Li, Y. Q., Byon, Y. J., Mei, S. G., Zhang, G. L. 2013. Synthesis and , characterization of  $\text{NiTiO}_3$  yellow nano pigment with high solar radiation reflection efficiency. *Powder Technology*, 235, 303-306.
- [35] Kantar, C., Mert, F., Şaşmaz, S. 2011. Microwave-assisted synthesis and Characterization of phthalocyanines substituted with azo compound containing eugenol moiety. *Journal of Organometallic Chemistry*, 696(18): 3006-3010.
- [36] Kumar, A., Mukasyan, A. S., Wolf, E. E. 2011. Combustion synthesis of Ni, Fe and Cu multi-component catalysts for hydrogen production from ethanol reforming. *Applied Catalysis A: General*, 401(1): 20-28.
- [37] Lill, J. R., Ingle, E. S., Liu, P. S., Pham, V., Sandoval, W. N. 2007. Microwave -assisted proteomics. *Mass spectrometry reviews*, 26(5): 657-671.
- [38] Define Microwave (Access date: 14-2-2014).  
<http://www.oxforddictionaries.com/definition/english/microwave>
- [39] Jiménez-Becerril, J., García-Sosa, I., Rivero, I. A. 2011. Synthesis of basic aluminum sulfate assisted by microwave heating. *Ceramics International*, 37(8): 3627-3630.
- [40] Chen, D., Yi, X., Chen, Z., Zhang, Y., Chen, B., Kang, Z. 2013. Synthesis of  $\text{CoFe}_2\text{O}_4$  Nanoparticles by a Low Temperature Microwave-Assisted Ball-Milling Technique. *International Journal of Applied Ceramic Technology*.

- [41] Gölcü, M., Volkan, K., "The effect of microwave power on the drying time of the egg tray." 2013.
- [42] Kajbafvala, A., Li, M., Bahmanpour, H., Maneshian, M. H., Kauffmann, A. 2013. Nano/ Microstructured Materials: Rapid, Low-Cost, and Eco-Friendly Synthesis Methods. *Journal of Nanoparticles*, 2013. 1P.
- [43] Gude, V. G., Patil, P., Martinez-Guerra, E., Deng, S., Nirmalakhandan, N. 2013. Microwave energy potential for biodiesel production. *Sustainable Chemical Processes*, 1(1): 1-31.27-35 p and 15-18 p. respectively. Research.
- [44] Sharma, D., Sharma, S., Kaith, B. S., Rajput, J., Kaur, M. 2011. Synthesis of ZnO nanoparticles using surfactant free in-air and microwave method. *Applied Surface Science*, 257(22): 9661-9672.
- [45] Santos, T., Valente, M. A., Monteiro, J., Sousa, J., Costa, L. C. 2011. Electromagnetic and thermal history during microwave heating. *Applied Thermal Engineering*, 31(16): 3255-3261.
- [46] Krishnakumar, T., Jayaprakash, R., Pinna, N., Singh, V. N., Mehta, B. R., Phani, A. R. 2009. Microwave-assisted synthesis and characterization of flower shaped zinc oxide nanostructures. *Materials Letters*, 63(2): 242-245.
- [47] WANG, X., ZHENG, J., FU, R., MA, J. 2011. Effect of microwave power and irradiation time on the performance of Pt/C catalysts synthesized by pulse-microwave assisted chemical reduction. *Chinese Journal of Catalysis*, 32(3): 599-605.
- [48] Bardajee, G. R. 2013. Microwave-assisted solvent-free synthesis of fluorescent naphthalimide dyes. *Dyes and Pigments*, 99(1): 52-58.
- [49] Benaskar, F., Patil, N. G., Engels, V., Rebrov, E. V., Meuldijk, J., Hulshof, L. A., Schouten, J. C. 2012. Microwave-assisted Cu-catalyzed Ullmann ether synthesis in a continuous-flow milli-plant. *Chemical Engineering Journal*, 207, 426-439.
- [50] Yu, Y., Zhao, Y., Huang, T., Liu, H. 2010. Microwave-assisted synthesis of palladium nanocubes and nanobars. *Materials Research Bulletin*, 45(2): 159-164.

- [51] Zhu, Z., Zhang, Y\*, Zhang, Y., Liu, H., Zhu, C., Wu, Y., 2013. PEG-directed microwave-assisted hydrothermal synthesis of spherical  $\alpha$ -Ni(OH)<sub>2</sub> and NiO architectures, 39, 2567–2573.
- [52] Farhadi, S., Sepahvand, S. 2010. Microwave-assisted solid-state decomposition of La[Co (CN)<sub>6</sub>] $\cdot$ 5H<sub>2</sub>O precursor: A simple and fast route for the synthesis of single-phase perovskite-type LaCoO<sub>3</sub> nanoparticles. Journal of Alloys and Compounds, 489(2): 586-591.
- [53] Vijayakumar, V., Ponnalagi, K. A., Nagamuthu, S., Muralidharan, G., 2013. Microwave assisted synthesis of Co<sub>3</sub>O<sub>4</sub> nanoparticles for high-performance supercapacitors, 106, 500– 505.
- [54] Köseoğlu\* Y., 2013 A simple microwave-assisted combustion synthesis and structural, optical and magnetic characterization of ZnO nanoplatelets.
- [55] Vereš, J., Lovás, M., Jakabský, Š., Šepelák, V., Hredzák, S. 2012. Characterization of blast furnace sludge and removal of zinc by microwave assisted extraction. Hydrometallurgy, 129, 67-73.
- [56] Raspolli Galletti, A. M., Antonetti, C., Marracci, M., Piccinelli, F., Tellini, B. 2013. Novel microwave-synthesis of Cu nanoparticles in the absence of any stabilizing agent and their antibacterial and antistatic applications. Applied Surface Science, 280, 610-618.
- [57] Bhosale, M. A., Bhatte, K. D., Bhanage, B. M. 2013. A rapid, one pot microwave assisted synthesis of nanosize cuprous oxide. Powder Technology, 235, 516-519.
- [58] Tseng, C. C., Chou, Y. H., Liu, C. M., Liu, Y. M., Ger, M. D., Shu, Y. Y. 2012. Microwave-assisted hydrothermal synthesis of zinc oxide particles starting from chloride precursor. Materials Research Bulletin, 47(1): 96-100.
- [59] Sosnik, A., Gotelli, G., Abraham, G. A. 2011. Microwave-assisted polymer synthesis (MAPS) as a tool in biomaterials science: how new and how powerful. Progress in Polymer Science, 36(8): 1050-1078.

- [60] Khan, A., El-Toni, A. M., Alrokayan, S., Alsalhi, M., Alhoshan, M., Aldwayyan, A.S. 2011. Microwave-assisted synthesis of silver nanoparticles using poly-N isopropylacrylamide/acrylic acid microgel particles. *Colloids and Surfaces A: Physicochemical and Engineering Aspects*, 377(1): 356-360.
- [61] Chatterjee, A., Mishra, S. 2013. Rheological, thermal and mechanical properties of nano-calcium carbonate (CaCO<sub>3</sub>)/Poly (methyl methacrylate) (PMMA) core-shell nanoparticles reinforced polypropylene (PP) composites. *Macromolecular Research*, 21(5): 474-483.
- [62] Ru, J., Hua, Y., Xu, C., Li, J., Li, Y., Wang, D., Zhou, Z. 2013. Microwave-assisted preparation of submicron-sized FeTiO<sub>3</sub> powders. *Ceramics International*.
- [63] Vijayakumar, S., Ponnalagi, K., A., Nagamuthu, S., Muralidharan, G., 2013. Microwave assisted synthesis of Co<sub>3</sub>O<sub>4</sub> nanoparticles for high-performance supercapacitors, 106 (3): 500– 505.
- [64] Li, L., Song, J., Lu, Q., Tan, X. 2014. Synthesis of nano-crystalline Sm<sub>0.5</sub>Sr<sub>0.5</sub>Co (Fe)O<sub>3-δ</sub> perovskite oxides by a microwave-assisted sol-gel combustion process. *Ceramics International*, 40(1 Part A): 1189-1194.
- [65] Karakas, Z. K., Boncukcuoglu, R., Karakas, İ. H., Kocakerim, M. M. 2013. The Investigation of the Removal of the Arsenic from Wastewaters by Using NiFe<sub>2</sub>O<sub>4</sub> Nanoparticles Produced with Microwave Assisted Combustion Method. *Journal of Selcuk University Natural and Applied Science*, 332-338.
- [66] Sutradhar, P., Debnath, N., Saha, M. 2013. Microwave-assisted rapid synthesis of alumina nanoparticles using tea, coffee and triphala extracts. *Advances in Manufacturing*, 1(4): 357-361.
- [67] Sertkol, M., Köseoglu, Y., Baykal, A., Kavas, H., Toprak, M. S. 2010. Synthesis and magnetic characterization of Zn<sub>0.7</sub>Ni<sub>0.3</sub>Fe<sub>2</sub>O<sub>4</sub> nanoparticles via microwave-assisted combustion route. *Journal of magnetism and magnetic materials*, 322(7): 866-871.
- [68] Cui, W., Liu, Y., Liu, L., Hu, J., Liang, Y. 2012. Microwave-assisted synthesis of CdS intercalated K<sub>4</sub>Nb<sub>6</sub>O<sub>17</sub> and its photocatalytic activity for hydrogen production. *Applied Catalysis A: General*, 417, 111-118.

- [69] Wang, Z., Xie, Y., Wang, P., Ma, Y., Jin, S., Liu, X. 2011. Microwave anneal effect on magnetic properties of Ni<sub>0.6</sub>Zn<sub>0.4</sub>Fe<sub>2</sub>O<sub>4</sub> nano-particles prepared by conventional hydrothermal method. *Journal of magnetism and magnetic materials*, 323(23): 3121-3125.
- [70] Hoang, L. H., Van Hai, P., Van Hanh, P., Hai, N. H., Chen, X. B., Yang, I. S. 2011. Microwave-assisted synthesis and characterization of Ti<sub>1-x</sub>V<sub>x</sub>O<sub>2</sub> (x= 0.0–0.10) nanopowders. *Materials Letters*, 65(19): 3047-3050.
- [71] Li, Z.Q., Chen X.T., Xue Z.L., 2013. Microwave-assisted synthesis and photocatalytic properties of flower-like Bi<sub>2</sub>WO<sub>6</sub> and Bi<sub>2</sub>O<sub>3</sub>-Bi<sub>2</sub>WO<sub>6</sub> composite. *Materials Letters*, 394, 69-77.
- [72] Kashani Motlagh, M., M., Youzbashi, A. A., Hashemzadeh, F., Sabaghzadeh, L. 2013. Structural properties of nickel hydroxide/oxyhydroxide and oxide nanoparticles obtained by microwave-assisted oxidation technique. *Powder Technology*, 237, 562-568.
- [73] Ragupathi, C., Kennedy, L. J., Vijaya, J. J., 2013, A new approach: Synthesis, characterization and optical studies of nano-zinc aluminate *Advanced Powder Technology*, accepted proof.
- [74] Azam, A., 2012, Microwave assisted synthesis and characterization of Co doped Cu ferrite nanoparticles, *Journal of Alloys and Compounds* 540, 145–153
- [75] Wang, Z., Xie Y., Wang, P., Ma, Y., Jin, S., Liu, X., 2011, Microwave anneal effect on magnetic properties of Ni<sub>0.6</sub>Zn<sub>0.4</sub>Fe<sub>2</sub>O<sub>4</sub> nano-particles prepared by conventional hydrothermal method, *Journal of Magnetism and Magnetic Materials*, 323, 3121–3125
- [76] Microwave-assisted synthesis and characterization of flower shaped zinc oxide nanostructures, Krishnakumar, T., Jayaprakash, R., Nicola Pinna, V.N., Singh, B.R., Mehta, A.R., *Materials Letters*, 2009, 63, 242-245.



- [77] Li, Z.Q., Chen, X, T., Xue, Z, L, 2013, Microwave-assisted synthesis and photocatalytic properties of flower-like  $\text{Bi}_2\text{WO}_6$  and  $\text{Bi}_2\text{O}_3$ - $\text{Bi}_2\text{WO}_6$  composite *Journal of Colloid and Interface Science*, 394, 69–77
- [78] Yang, Z., Wang, G., Guo, Kang, Y., F., Huang, Y., Bo, D., 2012, Microwave-assisted synthesis and characterization of hierarchically structured calcium fluoride, *Materials Research Bulletin* 47, 3965–3970
- [79] Cavalcante, P.M.T, Dondi, M, Guarini, G, Raimondo, M, Baldi, G, 2009, Colour performance of ceramic nano-pigments, 80, 226-232

## **CURRICULUM VITAE**

### **PERSONAL IDENTITY**

Name, Surname : Othman Abdulrahman HAMAD JUKAL

Date and place of birth : 1 July, 1978, Ranya, Sulaymaniya, Iraq

Marital Status : Single

Telephone : +90 53 4051 6404  
: +964 750 107 35 65  
: +964 770 155 90 56

E-Posta : [Othmansilver@yahoo.com](mailto:Othmansilver@yahoo.com), or belan\_silver@yahoo.com

### **EDUCATION BACKGROUND**

<b>Degree</b>	<b>Place of education</b>	<b>Date of graduate</b>
Baccalaureate	University of Salahaddin, Department of Chemistry	2004
High school	5 Azar High school.	2000

### **WORK EXPERIENCE**

<b>Year</b>	<b>Place</b>	<b>Position</b>
2004-2009	Ministry of Education	Teacher
2009-2010	Koya University	Ass. Chemist
2010-2012	Raparin University	Ass. Chemist